To the Graduate Council:
I am submitting herewith a dissertation written by Gaurav Chauhan entitled "Crowd Control: Regulating the Spatial Organization of Biopolymers and Gene Expression by Macromolecular Crowding." I have examined the final electronic copy of this dissertation for form and content and recommend that it be accepted in partial fulfillment of the requirements for the degree of Doctor of Philosophy, with a major in Chemical and Biomolecular Engineering.

Steven M. Abel, Major Professor

We have read this dissertation
and recommend its acceptance:

Steven M. Abel

Michael L. Simpson

Manolis Doxastakis

Maxim O. Lavrentovich

Eric Boder

Accepted for the Council:

Robert Hinde

Vice Provost and Dean of the Graduate School

(Original signatures are on file with official student records.)

Crowd Control: Regulating the Spatial Organization of Biopolymers and Gene Expression by Macromolecular Crowding

A Dissertation Presented for the

Doctor of Philosophy

Degree

The University of Tennessee, Knoxville

Gaurav Chauhan

May 2022

© by Gaurav Chauhan, 2022.
All Rights Reserved.

Dedicated to my late grandmother Shrimati Javitri Devi

Acknowledgements

I owe my PhD and my scientific career to many people who have contributed immensely to my journey and made me a better researcher and a better person. The pursuit of a career in science lead me to Knoxville, Tennessee, a place I didn't know existed on the map before I applied to the graduate program. The kindness and generosity of people who I met along my path here made me who I am today and I am greatly indebted to them all.

First and foremost, I would like to thank my advisor, Dr.Steven M. Abel for the amazing guidance and mentorship during my PhD. Even though I knew no biology when I started grad school, joining Steve's research group and working on biological problems has been one of the most fruitful decisions I have ever made. I am immensely grateful to Steve for providing me with the freedom to pursue my research ideas and for being available for feedback and direction at a door's knock. I am immensely grateful to Steve for making the PhD a wonderfully cheerful and enriching experience.

I would be extremely remiss if I did not highlight the significant contributions of our collaborator Michael L. Simpson. Mike has been extremely receptive to the insights from the computational work and very patient in explaining the experiments to me. I would like to thank Mike for not only his research inputs, but also for inculcating a strong likeness for the art of storytelling in scientific communications. I am also appeciative of the students in Mike's group who have carried out experiments that have informed and validated some of our computational work. In particular, I

would like to thank Dr.Liz Norred for conducting the experiments as well as for the insightful discussions.

I would also like to thank Drs.Eric Boder, Manolis Doxastakis and Maxim O. Lavrentovich for agreeing to serve on my thesis committee. The research inputs given to me during committee meetings as well as on other occasions have been extremely helpful and I am highly appreciative of that.

I would like to take this opportunity to thank my peers in the Abel group who have helped shape my work. The feedback and support offered by the group members Aaron, Paul, Rob, Bing, Honor, Tom, Nikhil and Hannah has helped me immensely. I would also like to thank the undergraduate researchers in Clayton, Chloe and Victoria, who I had the opportunity to mentor. I would also like to thank them for creating a cheerful lab environment. A lot of the ideas that I have built on in my PhD work have come from the extremely engaging group meetings and active participation of the people in the group.

As I write this acknowledgment section, I am reminded of the wonderful teachers and mentors that lead me to pursuing the PhD degree. In particular, I would like to thank Prof. Prateek Jha at IIT Roorkee for giving me the opportunity to obtain first-hand research experience in his group. That experience in 2015, before joining the doctoral program at UTK, helped me substantially in my career and if not for that experience, it is highly unlikely that I would have pursued the doctoral degree.

I am hugely thankful to my cohort of PhD students in the department for making this place feel like home to me. I would especially like to thank Chris, Jonathan, Nobahar, Rupesh, Payal, Vikram, Umesh, Rahul, Shantanu, Khushboo, Denis, Abhyuday, Ajay and many others for making grad school a thoroughly enjoyable experience.

Last but not the least, I would like to express eternal thanks to my family for being highly supportive of my ambitions and for instilling in me the self-belief to follow through with my goals and dreams.

"Keep the spices cool" - Dr. Steven M. Abel, *circa* 2018

Abstract

The intracellular environment is crowded with macromolecules that can occupy a significant fraction of the cellular volume. This can give rise to attractive depletion interactions that impact the conformations and interactions of biopolymers, as well as their interactions with confining surfaces. We used computer simulations to study the effects of crowding on biologically-inspired models of polymers. We showed that crowding can lead to attractive interactions between two flexible ring polymers, and we further characterized the adsorption of both flexible and semiflexible polymers onto confining surfaces. These results indicate that crowding-induced depletion interactions could play a role in the spatial organization of biopolymers in cells, and they also suggest that macromolecular crowding could be used to alter the spatial organization of cell-free synthetic systems. A major limitation of cell-free expression systems, which are widely used to study gene expression, is the lack of means to achieve spatial control of gene expression components. With a coarse-grained model of DNA plasmids and crowders, we showed that plasmids were uniformly distributed at low levels of crowding but, due to depletion interactions, became strongly adsorbed to confining surfaces at high levels of crowding. These results were experimentally validated by our collaborators using DNA and crowders in cell-sized vesicles. We used reaction kinetic models to study the effect of crowding and confinement on gene expression dynamics and noise, giving insight into experiments. Our work provides insights into the role of crowding and confinement on the spatial organization and dynamics of gene expression in cellular and cell-free systems.

Table of Contents

1 Introduction **1**

1.1 Crowding in biology 1

1.2 Effects of crowding on biomolecular reactions 3

1.3 Cell-free protein synthesis systems 4

1.4 Depletion Potentials 5

1.4.1 Particle-particle interactions 5

1.4.2 Particle-wall interactions 8

1.5 Polymer physics under crowding 12

1.5.1 Crowding with confining surfaces 14

1.6 Thesis Outline 15

2 Crowding-induced interactions of flexible ring polymers **16**

2.1 Introduction 16

2.2 Methods 18

2.3 Results 25

2.4 Discussion 39

3 Adsorption of semiflexible polymers in crowded environments **42**

3.1 Introduction 42

3.2 Methods 45

3.3 Results 47

3.3.1 Interplay between polymer stiffness, volume fraction of crowders, and crowder size . . . 48
3.3.2 Properties of the polymers . . . 51
3.3.3 Adsorption threshold and finite-size effects . . . 56
3.3.4 Adsorption in spherical confinement . . . 60
3.4 Discussion . . . 64

4 Crowding-induced spatial organization of gene expression in cell-sized vesicles 70
4.1 Introduction . . . 70
4.2 Results . . . 73
4.3 Discussion . . . 80
4.4 Methods . . . 83
4.4.1 Coarse-grained simulation of DNA plasmid and crowder in spherical confinement . . . 83
4.4.2 Reaction kinetics model . . . 83
4.4.3 Experimental methods . . . 84

5 Conclusions 87

Vita 109

List of Tables

2.1 Parameters for umbrella sampling along the distance between the center of mass of the polymer and the wall. The biasing potential was $U_{\text{bias}} = \frac{1}{2}k(z_{pw}^0 - z_{pw})^2$. 23

List of Figures

1.1 Two hard spheres of radius R in the presence of penetrable hard spheres of diameter σ. The centers of the two hard spheres are separated by distance r and the surfaces are separated by distance $h = r - 2R$. The effective depletion radius R_d can be defined as $R_d = R + \sigma/2$. Adapted from Tuinier and Lekkerkerker[1]. 6

1.2 A hard sphere of radius R in the presence of penetrable hard spheres of diameter σ. The center of the hard sphere is separated by a distance r from the wall while the surface of hard sphere is separated from the wall by a distance of $h = r - R$. Adapted from Tuinier and Lekkerkerker[1]. 9

1.3 Different size regimes for the particle-polymer interaction with the left most representing the colloid limit, the middle panel representing the equal size regime and the right panel representing the protein limit. Adapted from Tuinier and Lekkerkerker[1]. 11

2.1 Umbrella sampling for polymer-polymer interactions: Histograms of distances between the centers of mass (r_{12}) observed in each sampling window at different crowding fractions (ϕ). 22

2.2 Umbrella sampling for polymer-wall interactions: Histograms of distances between the polymer's center of mass and the wall (z_{pw}) observed in each sampling window at different crowding fractions (ϕ). 24

2.3 A) Radius of gyration of an isolated polymer at different crowding fractions (ϕ). Error bars denote the standard deviation. B) Probability density of the radius of gyration scaled by $\langle R_g(0)\rangle$, the average radius of gyration in uncrowded conditions. Distributions are shown for different crowding fractions. C) Asphericity of the polymer. D) Snapshots of the ring polymer for the most probable value of R_g at different crowding fractions. 26

2.4 For an isolated ring polymer, the probability density of the radius of gyration ($R_g(\phi)$) scaled by the average radius of gyration ($\langle R_g(\phi)\rangle$). Distributions are shown for different crowding fractions (ϕ). 29

2.5 Number of beads of polymer 1 in contact with any bead of polymer 2 (N_{12}) as a function of time for different crowding fractions (ϕ). Inset: Snapshot corresponding to the configuration with the largest value of N_{12} for each crowding fraction. 30

2.6 Potentials of mean force (U) between two polymers as a function of the distance between their centers of mass. For each crowding fraction (ϕ), the distance (r_{12}) is scaled by the average radius of gyration of an isolated polymer ($\langle R_g(\phi)\rangle$). Error bars indicate the standard deviation determined using the bootstrapping procedure described in Methods. 32

2.7 A) Center of mass of a polymer in the z direction (z_{COM}) as a function of time in unbiased simulations. A single trajectory with a polymer starting away from the walls is shown for each crowding fraction (ϕ). B) Snapshot from each trajectory, with walls denoted by the thick black lines at the upper and lower bounds of the box ($z = \pm 15\ \sigma$). To facilitate comparison between different crowding fractions, each snapshot corresponds to the frame in which the polymer was closest to the wall. 34

2.8 A) Radius of gyration of a polymer in the presence of walls at different crowding fractions. B) Asphericity of the polymer. C) Extension of the polymer in the directions parallel to ($R_{\parallel}$) and perpendicular to ($R_{\perp}$) the wall. D) Snapshots of the polymer for the most probable value of R_g at different crowding fractions. The polymer is viewed along the z direction (toward a wall). 36

2.9 Potentials of mean force (U) between a polymer and a wall as function of the distance between them (z_{pw}), for different crowding fractions. . 38

3.1 Average fraction of monomers near a wall, $\langle N_{\text{wall}}/N \rangle$, as a function of the bending stiffness, κ. Two sizes of the crowding particles are shown: $\sigma_c = \sigma_m$ (dashed) and $\sigma_c = 0.8\sigma_m$ (solid). Different volume fractions of the crowding particles (ϕ) are shown. 49

3.2 Probability density of the fraction of monomers near a confining wall. The volume fraction of crowding particles ($\phi = 0.2$, 0.3, 0.4) increases from left to right. The bending stiffness of the polymer ($\kappa = 0$, 5, 15, 50) increases from top to bottom. Simulations were carried out with $\sigma_c = 0.8\sigma_m$. 52

3.3 Snapshots of partially adsorbed semiflexible polymers. Boundary conditions are periodic in the x- and y-directions; confining walls in the z-direction are shown by black lines. The size of the crowders is $\sigma_c = 0.8\sigma_m$. (a) - (c) represent three cases (different values of κ and ϕ) that exhibit partial adsorption of the polymer. Three snapshots are shown for each case. The system is viewed along the y-axis, and the crowding particles are minimized in the visualization to more clearly reveal the polymer. 53

3.4 (a) Mean radius of gyration of the polymer in uncrowded conditions ($R_g(0)$) as a function of bending stiffness (κ). (b),(c) Mean radius of gyration at ϕ (volume fraction of crowders) scaled by the corresponding value in uncrowded conditions ($R_g(\phi)/R_g(0)$). For clarity, smaller and larger values of the bending stiffness are shown separately. The size of the crowders is $\sigma_c = 0.8\sigma_m$. 55

3.5 Mean radius of gyration parallel to the wall ($R_{g,\parallel}$, dashed) and perpendicular to the wall ($R_{g,\perp}$, solid), for various values of the bending stiffness (κ). 57

3.6 Average fraction of monomers near a wall as a function of the crowding fraction (ϕ) for different values of the bending stiffness (κ). Results for three polymer lengths ($N = 50$, 30, and 10) are shown. The size of the crowders is $\sigma_c = 0.8\sigma_m$. 59

3.7 Average fraction of monomers near a wall as a function of the bending stiffness. Solid lines correspond to a flat wall and dashed lines correspond to spherical confinement with a radius of 30σ. The size of the crowders is $\sigma_c = 0.8\sigma_m$. 61

3.8 (a) Critical crowding fraction (ϕ_c) as a function of the bending stiffness (κ) for three polymer lengths. ϕ_c is defined as the crowding fraction at which on average 50% of polymer beads are in contact with a wall. (b) $\Delta\phi_c = \phi_c - \phi_{c,\mathrm{rod}}$ as a function of κ/L for $N = 30$ and 10. Here $L = (N-1)\sigma$ is the contour length of the polymer. 63

3.9 Snapshots of the polymer in spherical confinement with $\phi = 0.4$. Three values of the bending stiffness are shown. The plots below correspond to the same values of κ and show the average fraction of monomers, $N(r)/N$, as a function of the radial distance, r. For each, results are shown for $\phi = 0$ and 0.4. 65

3.10 Average fraction of monomers near the wall in spherical confinement. The range of κ is larger than in previous figures. 66

4.1 A) Schematic of an *E. coli* cell showing spatial organization of DNA and ribosomes. The nucleoid DNA is in the middle of the cell and most ribosomes are excluded from the DNA-rich nucleoid region. B) Homogeneously distributed DNA and ribosomes in a cell-sized vesicle (left) and spatially organized DNA and ribosomes (right). This chapter explores the question: Can crowding lead to spatial organization of DNA and ribosomes in cell-sized vesicles? 72

4.2 A) Schematic of the computational model showing DNA plasmids and spherocylindrical crowders in spherical confinement. Particle-particle interaction potentials are given by the purely repulsive WCA potential U_{ij}, and particle-wall interactions are given by the purely repulsive 9-3 LJ potential U_{iw}. B) Representative snapshots of the plasmid polymer and crowders in spherical confinement (top) along with the radial distribution of the monomers N(r) as a function of radial distance r from the center of sphere (bottom). Different crowding fractions (ϕ) are shown. C) Confocal images of DNA, fluorescent labelled with Pico488, in cell-sized vesicles. The volume fraction ϕ in experiments is estimated from the partial specific volume of Ficoll-70. 75

4.3 A) Confocal images of representative vesicles with fluorescently-labelled ribosomes at different Ficoll-70 concentrations. B) Fraction of fluorescence in the wall region as a function of crowder concentration for DNA and ribosomes. C) Schematic of the two compartment reaction kinetics model of gene expression, where ribosomes can be exchanged between the bulk compartment and the wall-associated compartment. Results of the simulation of the two compartment model showing protein abundance as a function of exchange rate from wall to the bulk compartment (Γ_{wb}). Results for the two different spatial organizations of the DNA are shown. 77

4.4 Protein abundance as a function of radius for different exchange rates of ribosomes. The legend denotes the exchange rates of ribosomes from the wall compartment to the bulk compartment (Γ_{wb}) and the associated slopes for the protein abundance vs radius plots on log-log scale. 78

4.5 A) The plasmid used for cell-free experiments included a T7 promoter, a gene coding for mCherry, and a sequence encoding an untranslated RNA aptamer, Spinach2. B) Fabrication steps for forming vesicle microreactors. Cell-free reagents and Ficoll-70 were placed in an oil phase solution containing phospholipids, sheared into polydisperse vesicles by vortexing, layered onto a balanced aqueous solution, and centrifuged into the solution. (C and D): Representative vesicles demonstrating spatial distribution of mRNA (c) and protein (D) at different crowder concentrations. E) 3-D reconstruction of an individual vesicle showing the spatial distribution of mRNA and protein. F) mRNA and protein abundance as a function of crowder concentration for vesicles with a diameter of 14-16 μm. G) Translation efficiency as a function of crowder concentration for vesicles with a diameter of 14-16 μm. H) Protein abundance as a function of radius for different crowder concentrations. I) The exponent of the protein abundance versus radius scaling as calculated by linear regression. The error bars denote the 95% confidence intervals. 81

Nomenclature

κ	Bending stiffness
ϕ	Volume fraction occupied by crowders
R_g	Radius of gyration
CFPS	Cell-free protein synthesis
PMF	Potential of mean force
WCA	Weeks-Chandler-Andersen

Chapter 1

Introduction

1.1 Crowding in biology

The intracellular environment is not a dilute environment, but is rather highly crowded with macromolecules such as proteins and RNA. Macromolecules within cells can occupy up to 40% of the total cellular volume and crowd the intracellular environment.[2–4] In *E. coli*, the total macromolecular concentration is estimated to be $\sim$ 300-400 mg/mL.[4] Proteins are a major source of intracellular crowding as they account for $\sim$ 55% of the total dry weight, followed by ribosomal RNAs which account for $\sim$ 15% of total dry weight.[5] A large fraction of the protein and RNA is ribosomal,[6] and hence ribosomes make a significant contribution to cellular crowding.[7]

The reported diffusion coefficients in eukaryotes is larger in comparison to prokaryotes,[8] and it has been shown that the cytoplasm of prokaryotic cells is more crowded than that of mammalian cells.[9] It has been proposed that cells maintain their overall macromolecular concentration in a narrow range, a process termed as homeocrowding, for optimal cellular processes.[10] Experimentally, it has been shown that the crowding levels remain the same within the cytoplasm throughout the cell cycle while the crowding levels inside the nucleus change during the cell cycle for HeLa cells.[11]

There has been a growing interest on the role of crowding-induced depletion interactions in biological systems where they have been shown to affect genome organization,[12–15] gene regulation,[3,16] cellular organization,[7,17] protein stability[18] and biochemical reaction equilibria.[19,20] Computer simulations provide the means to mechanistically probe the effects of crowding on biopolymers encountered in biological systems. In this thesis, we have used computer simulations to study the role of crowding on conformations and spatial organization of biopolymers. Since cellular environments are characterized by the presence of confining surfaces such as cell membranes, we have also studied the role of crowding on spatial organization of polymers in the presence of confining surfaces. Crowding is particularly important in the organization and conformation of DNA and other large biopolymers inside cells. Crowding has been shown to compact DNA molecules[21–23] and also cause self-association.[24] It has also been experimentally shown that crowding can lead to aggregation of DNA plasmids[25] and formation of large polynucleosome assemblies that sediment in the presence of crowders.[26] Depletion interactions by non-adsorbing polymeric crowders have been shown to be sufficient to condense semiflexible actin filaments.[27]

The $\sim$2 m long DNA in human cell is constrained in a $\sim$ $200\mu m^3$ nucleus and the $\sim$ $2mm$ long *E. Coli* genome is packaged in nucleoid of $\sim$ $0.5\mu m^3$ size.[28] Depletion interactions, due to the presence of macromolecular crowding, play a major role in the organization of long chromosomal DNA into the compact space inside cells.[13,28–30] It was observed that isolated *E. coli* nucleoids became more compact upon addition of PEG macromolecules.[30] The theory put forward by Odijk[31] and simulations conducted by Shendruk et al.[29] showed how an increase in crowding leads to a continous decrease in size of the model chromosome polymer. While crowding plays a major role in compaction of the chromosome, other factors such as nucleoid-associated proteins in bacteria are also important for the organization of chromosomes.[13,32]

There has been a growing interest in the cell biology community on the formation of membraneless compartments in cells. Some of these compartments are formed as a result of liquid-liquid phase separation (LLPS).[33,34] Weak transient interactions between proteins and RNAs facilitate phase separation.[35] There have been recent studies which have suggested that the formation of phase-separated condensates formed by LLPS is facilitated by crowding.[7,36,37] For instance, Kaur et al.[37] showed that the liquid-liquid coexistence boundary of ribonucleoproteins (RNP) gets lowered by the presence of macromolecular crowders in *in vitro*. It was shown, both *in vivo* and *in vitro*, that crowding by ribosomes in the cytoplasm controlled the formation of phase separated compartments.[7]

Besides being crowded, the cellular environment is also characterized by the presence of confining membranes such as the plasma or nuclear membrane. Crowding can also lead to attractive forces between surfaces and a biomolecule of interest.[17] For instance, DNA plasmids have been shown to preferentially localize near the walls of vesicles.[38,39] Besides the DNA, other polymers such as actin have been shown to partially and completely adsorb to confining surfaces in the presence of macromolecular crowding.[40] Interactions of proteins with surfaces in crowded environments have also been implicated in the enhanced formation of protein fibrils.[41,42]

1.2 Effects of crowding on biomolecular reactions

Crowding inside cells affects biomolecular reaction kinetics and promotes equilibrium to bound states.[3] It has been proposed that any reaction in which reactants exclude more volume than products will be favored in crowded environments.[43] However, the effects of crowding on reactions are more nuanced than the effects of excluded volume alone due to the effects of crowding on diffusion.

Crowding decreases the diffusion coefficients of the reactants because crowder molecules act as obstacles to the diffusion of reactant species.[44] The decrease of a

diffusion coefficient depends on the size of the species, with larger species experiencing more pronounced decrease in their diffusion coefficient. If collision of reactants mostly leads to reaction, then reaction can be termed as diffusion-limited. Since crowding can lead to differential decrease in diffusion of different species, interesting non-trivial effects of crowding on reaction rates have been observed. For instance, transcription-translation reactions showed non-monotonic dependence on crowder concentration and were most efficient at some intermediate crowder concentrations.[45] This is consistent from the simulation work carried out by Matsuda et al.[46] where they used Brownian dynamics simulation and Monte Carlo simulations to observe non-monotonic dependence of mRNA abundance on crowding, with the maximum abundance observed at physiologically relevant crowding levels.

Crowding is also expected to impact the noise properties of transcription and translation. Gene expression is bursty in cells with the production of mRNA and proteins occuring in short bursts separated by periods of no mRNA/protein production. It has been shown that crowding-induced colocalization and exclusion patterns as well as reduced diffusion play a major role in gene expression bursting.[47] Since it is difficult to manipulate crowding in live cells, *in vitro* systems are used to study the effects of crowding on gene expression kinetics and noise.

1.3 Cell-free protein synthesis systems

Cell-free protein synthesis (CFPS) platforms are *in vitro* systems utilized to express proteins using minimal reactants from cell lysates. Cell-free protein synthesis systems facilitate control over physical parameters such as macromolecular crowding, volume of reactants, etc. and are devoid of complicated genetic networks observed in live cells. The cell-free reactants can also be encapsulated inside vesicles to study the effects of confinement and surfaces. Because of these features, CFPS platforms are regularly employed to study gene expression.

However, the current paradigm in cell-free platforms lacks the ability to spatially control the organization of gene expression components to mimic the spatial organization observed in cells. For instance, the DNA-rich nucleoid region and the ribosome rich region are spatially segregated in prokaryotes, even in the absence of a membrane. Hence, a cell-free platform with the ability to spatially organize gene expression components can help to shed light on the role of resource availability and spatial organization on gene expression.

1.4 Depletion Potentials

1.4.1 Particle-particle interactions

Asakura Oosawa's (AO) seminal paper, published in 1954, described attractive forces between two colloidal particles due to the presence of polymeric solutes.[48] They assumed the polymer to be penetrable hard spheres i.e. polymers modeled as spheres had hard sphere interaction with the colloidal particles and no interaction with each other. They calculated the force on the two colloidal particles as a function of the polymer concentration. When the separation between the two particles is less than the diameter of solute particles, the solute particles are excluded from the region between the two particles because of volume exclusion. Hence, there exists an osmotic pressure imbalance that leads to an effective attractive force between two particles.

Another way of thinking about the solute is as "depletants". Due to the presence of the excluded volume interactions, there is a region adjacent to the colloidal particles that is excluded from the solute particles(Figure 1.1). This region is known as the depletion layer. When the depletion layer of the two colloidal particles would overlap, it would increase the volume available for the solute particles and hence increase the overall entropy of the system. Because of this origin of the attractive force, the potential between two colloidal particles due to the presence of solute macromolecules is known as a depletion interaction.

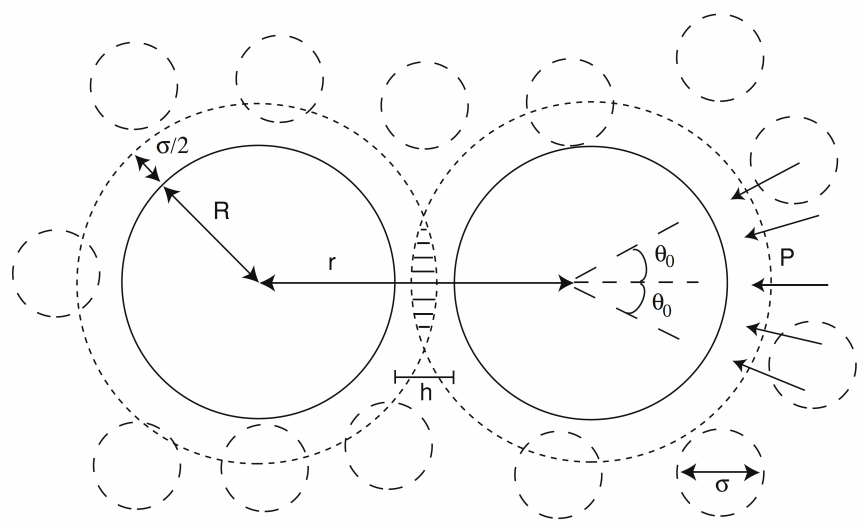


Figure 1.1: Two hard spheres of radius R in the presence of penetrable hard spheres of diameter σ. The centers of the two hard spheres are separated by distance r and the surfaces are separated by distance $h = r - 2R$. The effective depletion radius R_d can be defined as $R_d = R + \sigma/2$. Adapted from Tuinier and Lekkerkerker [1].

The force on the two particles is proportional to the osmotic pressure of the medium (P), which for a dilute and monodisperse solution is given by $P = n_b k_B T$, where k_B is the Boltzmann constant and n_b is the bulk number density of solute particles. It is important to note that this expression for osmotic pressure ($P = n_b k_B T$) is only valid for dilute systems and more sophisticated expressions such as third-order virial expansion ($P = \frac{(\phi_c + 4{\phi_c}^2 + 10{\phi_c}^3)}{\nu_c} k_B T$), scaled particle theory ($P = \frac{(\phi_c + {\phi_c}^2 + {\phi_c}^3)}{\nu_c(1-{\phi_c}^3)} k_B T$) are used to determine osmotic pressures outside of the dilute regime. The total force $K_s(r)$ acting on two spherical particles of radius R that are separated by distance r in a solution of spherical solute particles with diameter σ was shown to be,[1]

$$\frac{K_s(r)}{n_b k_B T} = \begin{cases} -\pi {R_d}^2 \left[1 - (r/2R_d)^2\right], & 2R \leq r < 2R + \sigma \\ 0, & r \geq 2R + \sigma \end{cases} \tag{1.1}$$

where R_d is the effective depletion radius defined as $R_d = R + \sigma/2$. The depletion potential between two particles can then be obtained by integration of the depletion force, and is given by

$$W_s = \begin{cases} -n_b k_B T V_{ov}(r), & 2R \leq r < 2R + \sigma; \\ 0, & r \geq 2R + \sigma, \end{cases} \tag{1.2}$$

with

$$V_{ov}(r) = \frac{4\pi}{3} R_d^3 \left[1 - \frac{3}{4}\frac{r}{R_d} + \frac{1}{16}\left(\frac{r}{R_d}\right)^3\right] \tag{1.3}$$

The overlap volume $V_{ov}(r)$ can also be written as:

$$V_{ov}(r) = \frac{\pi}{6}(\sigma - h)^2(3R + \sigma + h/2) \tag{1.4}$$

Note that, in the limit of $\sigma/2 \ll R$, the depletion potential takes the quadratic form,

$$\frac{W_s}{n_b k_B T} = -\pi R \frac{1}{2}(\sigma - h)^2, \tag{1.5}$$

for $h(= r - 2R) < \sigma$.

1.4.2 Particle-wall interactions

The presence of crowding macromolecules can give rise to attractive particle-wall interactions. The physics behind the particle-wall interactions is the same as particle-particle depletion interactions. There are regions adjacent to the particle and wall that are excluded of penetrable hard spheres (Figure 1.2). The overlap of the depletion layer of the particle and the wall results in excess volume for the solute, thereby increasing the entropy of the system.

The depletion potential between a spherical particle of radius and a wall is given by,

$$\frac{W_s}{n_b k_B T} = \begin{cases} -\frac{1}{3}\pi(\sigma - h)^2(3R + \frac{\sigma}{2} + h), & 0 \leq h < \sigma; \\ 0, & h \geq \sigma, \end{cases} \tag{1.6}$$

For $\sigma \ll R$, this equation simplifies to

$$W_s(h) = \begin{cases} -n_b k_B T \pi R(\sigma - h)^2, & 0 \leq h < \sigma; \\ 0, & h \geq \sigma, \end{cases} \tag{1.7}$$

Hence, for $\sigma \ll R$, the particle-wall interaction (Equation 1.7) is twice that of the particle-particle interaction (Equation 1.5) under same solute concentrations.

Hence, crowding can lead to attractive depletion interactions between two particles and between a particle and a wall. The minimum of the depletion potential occurs when two particles are in contact or in case of particle-wall interactions, when the particle contacts the wall. This is because these configurations result in maximum overlap of the depletion layers. As seen in Equation 1.6 and Equation 1.4, the magnitude of the depletion potential scales linearly with solute concentration in the dilute regime.

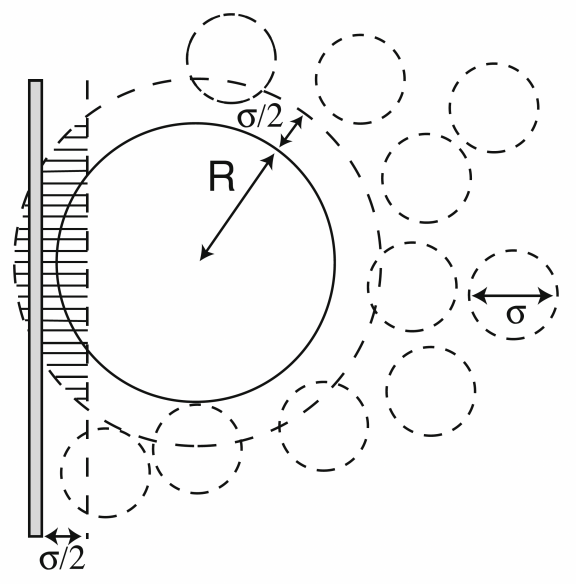


Figure 1.2: A hard sphere of radius R in the presence of penetrable hard spheres of diameter σ. The center of the hard sphere is separated by a distance r from the wall while the surface of hard sphere is separated from the wall by a distance of $h = r - R$. Adapted from Tuinier and Lekkerkerker [1].

Depletion interaction regimes have been characterized based on the size of the depletant (for polymers, characterized by the radius of gyration, R_g) and the size of the particles of interest (characterized by radius R). The relative size of the particle and the polymer is given by the size ratio $q = R_g/R$. Three regimes as shown in Figure 1.3 can be identified based on the size ratio q: $q \lesssim 0.5$ is known as the colloid limit, $q = O(1)$ is known as the equal size limit and $q \gtrsim 2$ is known as the protein limit.

While much of the early work in colloid-polymer mixtures has been done in the colloid limit,[1,49] significant works have also been done in the equal size and protein limit regimes.[50] Previous works have studied and quantified the effective potentials between colloidal potentials in the protein limit via simulations.[51,52] These studies have also given insights into the resultant shape changes of the polymers as a result of the presence of colloidal particles.[52–54] Since the size of macromolecular crowders in cells, such as globular proteins, is similar to the size of proteins in cells, the protein limit is particularly important in biological problems such as protein folding in crowded environments[55] Apart from these three regimes comparing the polymer and colloid size, another relevant length scale in biological systems is the size of the monomers making the polymer and the size of the colloidal particle relative to the monomers. In cellular and cell-free systems, the linear size of macromolecular crowders is often comparable to the cross-sectional diameter of biopolymers such as DNA or actin. The size of globular proteins crowding the intracellular environment is within the 3-6 nm range[56] and comparable to the effective diameters of actin (≈ 6 nm)[40] and dsDNA (≈ 6.6 nm at 60 mM ionic strength).[57,58] Furthermore, synthetic crowders such as dextran 70 and Ficoll 70, widely used in *in vitro* studies, have hydrodynamic radii of ≈ 6.8 nm and ≈ 5 nm, respectively.[59] Hence, understanding the role of crowding on conformations and spatial organization of polymers in this regime is quite relevant for biological systems. In this thesis, we have extensively studied the regime where the size of crowders is of the same order as the size of the monomers making the biopolymer.

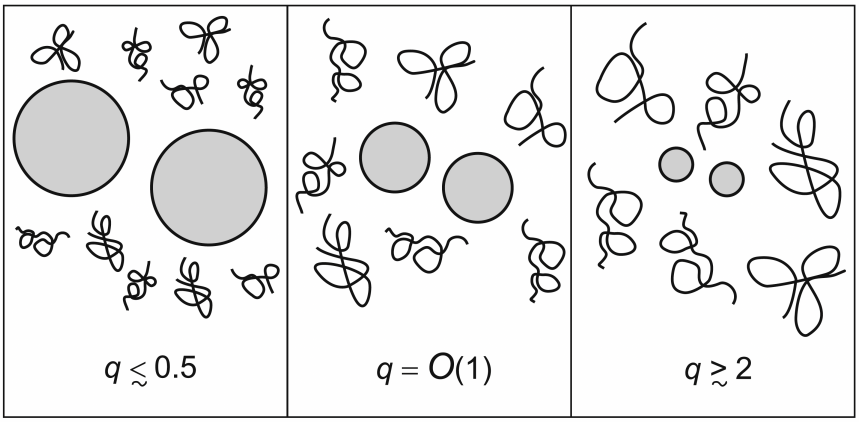


Figure 1.3: Different size regimes for the particle-polymer interaction with the left most representing the colloid limit, the middle panel representing the equal size regime and the right panel representing the protein limit. Adapted from Tuinier and Lekkerkerker[1].

1.5 Polymer physics under crowding

Recently, there has been considerable interest in understanding the impact of crowding on conformations of biopolymers. While it is challenging to analytically study the role of crowding on conformation of polymers, computer simulations have become an important tool. Typically, polymers are coarse-grained into bead-spring chains, with consecutive beads connected by springs. Simulation packages/ custom codes are then used to solve for equations governing the motion of the beads.

In this thesis, we have used Langevin dynamics to simulate polymers and crowders, with the solvent modeled implicitly in the Langevin equation. The dynamics of the ith particle with position $\boldsymbol{r_i}$ and velocity $\boldsymbol{v_i}$ is evolved using the Langevin equation, given by:

$$m\frac{d^2\boldsymbol{r_i}}{dt^2} = -\tau\boldsymbol{v_i} - \nabla_{\boldsymbol{r_i}}U + \boldsymbol{F_i}(t) \tag{1.8}$$

where m and τ are the mass and friction coefficient,respectively, of the ith particle. The first term in the RHS of the equation 1.8 accounts for the frictional drag due to the solvent. The second term is the conservative force acting on the particle due to the total potential U. $\boldsymbol{F_i}(t)$ is the random force acting on the ith particle due to collisions with the solvent molecules and satisfies the fluctuation-dissipation theorem:

$$\langle \boldsymbol{F_i}(t) \cdot \boldsymbol{F_j}(t') \rangle = \delta_{ij} 6 k_B T \tau \delta(t - t') \tag{1.9}$$

The equation 1.9 shows that the random force acting on particle i at time t is not correlated with the random forces on other particles j and is not correlated with random force on the particle i at any other timepoint t'.

In our work, we have used LAMMPS[60] simulation package to carry out Langevin dynamics simulation of polymers in the presence of explicit crowding particles and confining surfaces. The LAMMPS simulation package is used to integrate equations of motion (Equation 1.8) forward in time, and the resulting trajectories are then analyzed to study properties such as size and spatial organization of the polymer.

Typically, radius of gyration, R_g is used as a measure of the size of the bead-spring polymer and is given by,

$$R_g^2 = \frac{1}{N}\sum_{n=1}^{N}(r_i - R_{cm})^2$$

where N is the number of beads, r_i is the position of bead i and R_{cm} is the center of mass of the polymer beads and is given by

$$R_{cm} = \frac{1}{N}\sum_{n=1}^{N} r_i$$

Simulation works have provided considerable insights on polymer physics in crowded environments. In their pioneering work, Kang et al.[61] investigated the effects of spherical crowders on the conformations of a flexible polymer. The authors found that an increase in the volume fraction of crowders resulted in a decrease in the radius of gyration of the flexible polymer. They also found that for the same volume fraction of crowders, the decrease was more prominent for smaller crowder sizes. At sufficiently small crowder sizes, they observed a coil-to-globule transition of the flexible polymer. Other works have studied the problem of flexible polymer in crowded environments in different contexts,[29,62,63] and have shown how crowding by spherical crowders results in compaction of a flexible polymer. The size effect of the polymer and the crowder beads was also explored by a recent work on crowding-induced compaction of a heterogeneous polymer of different sized beads.[63] They showed that clustering of few large monomer beads lead to sharp compaction at small crowding followed by gradual compaction due to clustering of smaller monomer beads at higher crowding.[63]

Some studies have also explored the role of shape of the crowder on conformation of polymers. Chen and Zhao[62] found that a flexible polymeric crowder resulted in more compaction of the probed chain with an increase in length of the polymer crowder. This is in contrast with the observations for a spherical crowder. Larger spherical

crowders result in lesser compaction because the probed chain can be accomodated in the cavity created by larger crowder particles, and hence the probed polymer beads experienced weaker depletion interactions. In contrast, a flexible polymeric crowder induces local bead-bead interactions which do not change with increase in crowder polymer lengths. In addition, the longer crowder polymer can mutually interpenetrate the probed chain and hence induce greater depletion interactions. They also studied conformations of flexible polymer in the presence of rod-like crowders and found a non-monotonous dependence of radius of gyration of the probed polymer with the length of the rod-like crowder. This non-monotonic dependence on rod size can be understood in terms of competition between anisotropy-induced stretching and the crowding-induced depletion potential. Additionally, Kang et al.[64] have shown how a combination of spherical and spherocylindrical crowders can result in non-trivial additive effects on compaction. They also showed how crowding can result in unexpected swelling of sufficiently stiff semiflexible polymers.

1.5.1 Crowding with confining surfaces

Crowding can lead to attractive depletion interactions between a polymer and a wall. Understanding the interactions of polymers with surfaces has been a long-standing problem in the field of polymer physics.[65–67] The effects of crowding on polymer conformations and spatial organization in the presence of surfaces have been probed by many simulation studies.[68–70] Simulations have shown that crowding can lead to adsorption of a polymer chain onto a cylindrical wall.[68] It has been shown that crowding leads to preferential localization of a flexible polymer chain near the walls of spherical confinement and that the attractive interaction between crowder and the polymer impedes polymer adsorption to wall.[70] The role of crowding on the separation of the two arms of chromosome has also been probed by simulation studies.[15]

While there has been considerable work done on understanding the adsorption of flexible polymers to a wall,[71–73] much less is known about the adsorption of

semiflexible polymers.[69,74] Previous simulation works have focused on the problem of adsorption of semiflexible polymer to a wall via an implicit attractive potential and not by explicit crowder particles.[40,69,74–76] Since depletion potentials has been shown to scale non-linearly at high crowder concentrations,[77] explicit crowding particles need to be considered to accurately study the role of bending stiffness on crowding-induced polymer adsorption.

1.6 Thesis Outline

In this thesis, we used computer simulations to understand the role of crowding on spatial organization of biopolymers and gene expression. In Chapter 2, we used Langevin dynamics simulations to study the effects of crowding on polymer-polymer and polymer-wall interactions. While a lot of studies have highlighted the importance of crowding-induced intra polymer interactions, there hasn't been substantial work done on understanding polymer-polymer interactions. A quantitative understanding of the polymer-polymer and polymer-wall interactions is lacking in the literature. We have addressed that gap by calculating the depths of the attractive potential well for both i) polymer-polymer and ii) polymer-wall case. Chapter 2 is adapted from the article *"Crowding induced interactions of ring polymers"* originally published in *Soft Matter* in 2021. Along with that, we have also studied the dependence of persistence lengths on crowding-induced adsorption of semiflexible polymers onto surfaces by considering explicit crowding particles (Chapter 3). This chapter is adapted from the article *"Adsorption of semiflexible polymers in crowded environments"* originally published in *Journal of Chemical Physics* in 2021. Finally, we have used computer simulations to guide experimental efforts towards the design of a cell-free platform capable of spatially organizing gene expression akin to a prokaryotic cell (Chapter 4). By using computational simulations and cell-free experiments, we also study the role of crowding-induced spatial organization on gene expression.

Chapter 2

Crowding-induced interactions of flexible ring polymers

A version of this chapter was originally published by Gaurav Chauhan, Michael L. Simpson and Steven M. Abel: Chauhan, G., Simpson, M. L., & Abel, S. M. (2021). *Crowding-induced interactions of ring polymers. Soft Matter*, 17(1), 16-23.

2.1 Introduction

Macromolecules within cells can occupy up to 40% of the total cellular volume and crowd the intracellular environment.[2,3] The presence of macromolecular crowders can induce attractive depletion interactions between larger objects, an entropically-driven phenomenon first described by Asakura and Oosawa.[78] Crowding-induced depletion interactions have been shown to impact protein stability[18] and biochemical reaction equilibria,[19,20] and there is a growing realization that they play an important role in cellular organization.[7,17] For example, macromolecular crowding impacts the organization of bacterial chromosomes[13–15,79,80] and can lead to phase separation in the cytoplasm.[7,37]

Crowding-induced depletion interactions have been shown to impact biopolymers like DNA in a number of experimental studies. Polymeric crowders can lead to the compaction of both linear DNA and circular DNA plasmids.[22,23] While linear DNA chains collapse with an increase in crowding in bulk conditions, in nanochannels, they can exhibit depletion-induced elongation.[81] Crowding can also lead to aggregation of DNA plasmids,[25] and polynucleosomes that are soluble in uncrowded solutions form large assemblies and sediment in the presence of crowders.[26]

Computer simulations have been an important tool for understanding the effects of crowding on conformations of biopolymers. Shendruk et al.[29] showed that crowding-induced depletion interactions can lead to the collapse of a model chromosome polymer, causing a coil-to-globule transition. Kang et al.[61] carried out simulations of a linear polymer for different sizes of crowding particles. They found that crowding decreased the radius of gyration of the polymer and that smaller crowding particles resulted in a larger decrease at the same volume fraction of crowders. Additionally, polydispersity in the size of crowding particles has been shown to swell sufficiently stiff polymer chains,[64] and flexible polymeric crowders result in larger compaction of a polymer chain than hard spheres at the same crowding fraction.[62]

The presence of surfaces such as cell membranes can be of consequence to biopolymers because crowders can induce depletion attractions between a polymer and a surface. Simulations have shown that crowding can induce adsorption of a polymer chain onto a cylindrical wall,[68] that a model DNA chain in spherical confinement preferentially resides near the boundary at high levels of crowding,[70] and that depletion interactions are responsible for separation of two arms of a model chromosome or two ring polymers under strong cylindrical confinement.[15,82] However, these studies did not quantify the magnitude of the effective interactions, which is important for understanding the relative importance of interactions in the bulk versus at the surface.

In parallel with the previous studies, there has been a growing body of work on gene expression in synthetic, cell-free platforms.[83] Recent studies have used synthetic,

monodisperse crowding molecules to study the impact of crowding on expression from DNA plasmids.[38,47,84] Interestingly, crowding can lead to spatially heterogeneous regions of gene expression,[47,84] and confining the crowded systems to cell-sized vesicles caused DNA to localize near the inner surfaces.[38,39] The physical reasons for the spatial organization remain unclear.

Taken together, a variety of experimental and simulation studies highlight the importance of crowding-induced depletion interactions between biopolymers in cellular and cell-free systems. However, in most instances, a detailed quantitative understanding of the depletion interactions is lacking. In this work, we help to address this gap by using computer simulations to characterize effective interactions in a model that captures key physical features of DNA plasmids and crowding particles. We focus particularly on characterizing depletion interactions in the context of cell-free gene expression platforms, but our results are relevant in other biological and non-biological contexts as well.

2.2 Methods

The ring polymer was modeled as a self-avoiding flexible chain consisting of 50 beads. The adjacent beads of the polymer were connected by the finitely extensible nonlinear elastic (FENE) bond potential,[85] given by

$$U_{\mathrm{FENE}} = -\frac{1}{2} K {R_0}^2 \ln\left[1 - \left(\frac{r}{R_0}\right)^2\right],$$

where r is the center-to-center distance between two adjacent beads. The maximum distance between two beads connected via a FENE bond (R_0) was chosen to be 2σ with spring constant $K = 15\epsilon/\sigma^2$. In this work, σ and ϵ set the length and energy units respectively.

Crowder particles were modeled as purely repulsive particles of radius R_c. All particles (polymer beads and crowders) interacted via the short-ranged and purely

repulsive Weeks-Chandler-Andersen (WCA) potential,[86]

$$U_{ij} = \begin{cases} 4\epsilon_{ij}\left[\left(\frac{\sigma_{ij}}{r_{ij}}\right)^{12} - \left(\frac{\sigma_{ij}}{r_{ij}}\right)^{6}\right] + \epsilon_{ij} & r_{ij} < 2^{1/6}\sigma_{ij} \\ 0 & r_{ij} \geq 2^{1/6}\sigma_{ij} \end{cases}$$

where r_{ij} is the center-to-center distance between particles i and j. The strength parameter was the same for all pairs, $\epsilon_{ij} = \epsilon = k_{\mathrm{B}}T$. Further, $\sigma_{ij} = R_i + R_j$, where R_i and R_j denote the radius of particles i and j respectively. The sizes (σ_{ii}) of polymer beads and crowder particles were chosen to be 1.5σ and 0.6σ, respectively, because the Kuhn length of DNA is larger than the size of typical crowding molecules. The level of crowding was controlled by the number of crowding particles (N_c), with the volume occupied defined as $V_c = N_c 4\pi {R_c}^3/3$. We refer to the volume fraction of the crowding particles ($\phi = V_c/V$) as the *crowding fraction*.

The size of the system without walls was $30\sigma \times 30\sigma \times 30\sigma$, with periodic boundaries in all dimensions. For the system with walls, we imposed repulsive walls in one dimension (z) and periodic boundaries in the other dimensions (x and y). This system was 30σ in the z direction and 25σ in the x and y directions. Particles interacted with the walls via the 9-3 Lennard-Jones wall potential at the lower and upper boundaries in the z direction,[87]

$$U_{iw} = \begin{cases} \epsilon_{iw}\left[\frac{2}{15}\left(\frac{\sigma_{iw}}{r_{iw}}\right)^{9} - \left(\frac{\sigma_{iw}}{r_{iw}}\right)^{3}\right] + (\frac{10}{9})^{1/2}\epsilon_{iw} & r_{iw} < (\frac{2}{5})^{1/6}\sigma_{iw} \\ 0 & r_{iw} \geq (\frac{2}{5})^{1/6}\sigma_{iw} \end{cases}$$

where r_{iw} is the distance between the particle and the wall surface. The strength factor for wall-particle interactions was the same for all particles, $\epsilon_{iw} = \epsilon = k_{\mathrm{B}}T$. The length parameter σ_{iw} was specified by the relation $(2/5)^{1/6}\sigma_{iw} = \sigma_{ii}/2$. With this condition, a particle experienced a repulsive force when the distance between the wall and the particle was less than the particle radius.

The Langevin equation was integrated forward in time using the velocity-Verlet algorithm in the LAMMPS simulation package.[60,88] The timestep for integration was 0.005τ, where τ is the natural unit of time. The friction coefficient for component k was chosen to be $\tau_k = 0.2\frac{\sigma_{kk}}{\sigma_{mm}}\tau^{-1}$ with σ_{mm} and σ_{kk} being the diameter for polymer beads and component k respectively. Resulting trajectories were visualized using OVITO.[89]

Umbrella Sampling

We employed umbrella sampling and the Weighted Histogram Analysis Method (WHAM) to determine the potential of mean force (PMF) as a function of the distance between the centers of mass of two polymers (r_{12}). We sampled along the coordinate r_{12} via a harmonic bias potential using the COLVARS module in LAMMPS.[90] Distances and the strength of the biasing potential were chosen to obtain good overlap of histograms generated in adjacent windows (see Supplementary Information). WHAM was then used to determine an unbiased potential.[91,92] Because the reaction coordinate r_{12} is a nonlinear function of the Cartesian coordinates defining the state of the system, an additional term ($2k_{\mathrm{B}}T\ln r_{12}$) was added to the potential obtained using WHAM to give the PMF, $U(r_{12})$. The additional term accounts for the r_{12}-dependent size of configuration space.[93]

Umbrella sampling for polymer-polymer interactions

We performed umbrella sampling along the distance between the centers of mass of two ring polymers. For $\phi \geq 0.2$, we sampled from a distance of 3σ to a distance of 13σ with a step size of 0.5σ between the centers of the biasing potentials. For $\phi = 0$ and 0.1, we sampled until 15σ. The simulation box was periodic in all dimensions with box size of $30\sigma \times 30\sigma \times 30\sigma$ for all crowding fractions for $\phi \geq 0.2$. For $\phi = 0$ and 0.1, the box size was $40\sigma \times 40\sigma \times 40\sigma$. In the bias potential $U_{\mathrm{bias}} = \frac{1}{2}k(r_{12}^0 - r_{12})^2$, the force constant k was set to ϵ/σ^2.

For each window considered, simulations were run for a total of 5×10^7 timesteps, with timestep $\Delta = 0.005\tau$. The production run for each window was obtained after 7.5125×10^6 equilibration timesteps. Histograms of the distances sampled in each window are shown in Fig. S2 below. In the Weighted Histogram Analysis Method (WHAM), we used a bin width of 0.1σ and a convergence tolerance of 10^{-6} for the iterations.

Umbrella sampling for polymer-wall interactions

We also calculated the PMF as a function of the distance in the z direction between a wall and the center of mass of the ring polymer (z_{pw}) using same procedure as above. Because the size of accessible configuration space remains constant with increasing z_{pw}, no correction term was required in this case.

We performed umbrella sampling along the distance between the center of mass of a ring polymer and a fixed wall. The simulation box was 30σ in the z direction (normal to the wall) and 25σ in the x and y directions. Table 2.1 provides the parameter values used for the umbrella sampling for different crowding fractions. We limited our umbrella sampling to crowding fractions $\phi \leq 0.25$.

For each window considered, simulations were run for a total of 5×10^7 timesteps, with timestep $\Delta = 0.005\tau$. The production run for each window was obtained after 1.5×10^7 equilibration timesteps. Histograms of the distances sampled in each window are shown in Fig. S3 below. In WHAM, we used a bin width of 0.1σ and a convergence tolerance of 10^{-6} for the iterations.

For the umbrella potentials, larger force constants were used to study the polymer-wall interactions compared with the polymer-polymer case. This was due to the strong effective interactions between the polymer and wall at small distances. Using the strong biasing potential, we obtained good sampling of distances for the entire range of z_{pw}, as shown in Fig. S3.

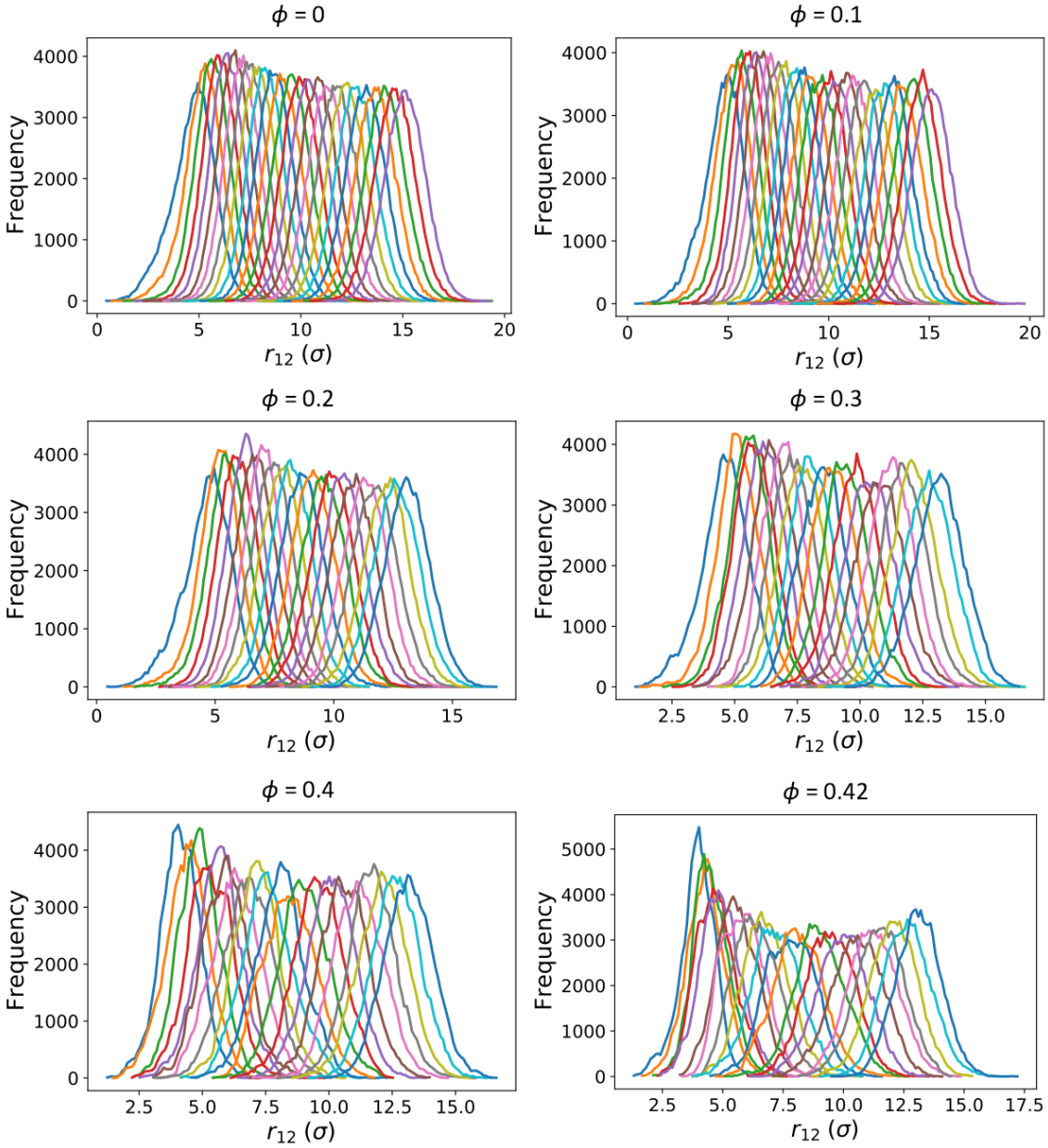


Figure 2.1: Umbrella sampling for polymer-polymer interactions: Histograms of distances between the centers of mass (r_{12}) observed in each sampling window at different crowding fractions (ϕ).

Table 2.1: Parameters for umbrella sampling along the distance between the center of mass of the polymer and the wall. The biasing potential was $U_{\text{bias}} = \frac{1}{2}k(z^0_{pw} - z_{pw})^2$.

$\phi = 0.0$

$z^0_{pw}(\sigma)$	k (ϵ/σ^2)
0.75	20.00
1.00	20.00
1.50	20.00
2.00	20.00
2.50	20.00
3.00	20.00
3.50	20.00
4.00	20.00
4.50	20.00
5.00	20.00
5.50	20.00
6.00	20.00
6.50	20.00
7.00	20.00
7.50	20.00
8.00	20.00
8.50	20.00
9.00	20.00
9.50	20.00
10.00	20.00
10.50	20.00
11.00	20.00
11.50	20.00
12.00	20.00
12.50	20.00
13.00	20.00

$\phi = 0.1$

$z^0_{pw}(\sigma)$	k (ϵ/σ^2)
0.75	10.00
1.00	10.00
1.50	10.00
2.00	10.00
2.50	10.00
3.00	10.00
3.50	10.00
4.00	10.00
4.50	10.00
5.00	10.00
5.50	10.00
6.00	10.00
6.50	10.00
7.00	10.00
7.50	10.00
8.00	10.00
8.50	10.00
9.00	10.00
9.50	10.00
10.00	10.00
10.50	10.00
11.00	10.00
11.50	10.00
12.00	10.00
12.50	10.00
13.00	10.00

$\phi = 0.2$

$z^0_{pw}(\sigma)$	k (ϵ/σ^2)
0.75	25.00
1.00	25.00
1.50	15.00
2.00	15.00
2.50	15.00
3.00	15.00
3.50	15.00
4.00	15.00
4.50	15.00
5.00	15.00
5.50	15.00
6.00	15.00
6.50	15.00
7.00	15.00
7.50	15.00
8.00	15.00
8.50	15.00
9.00	15.00
9.50	15.00
10.00	15.00
10.50	15.00
11.00	15.00
11.50	15.00
12.00	15.00
12.50	15.00
13.00	15.00

$\phi = 0.25$

$z^0_{pw}(\sigma)$	k (ϵ/σ^2)
0.75	25.00
1.00	25.00
1.25	25.00
1.50	15.00
2.00	15.00
2.50	15.00
3.00	15.00
3.50	15.00
4.00	15.00
4.50	15.00
5.00	15.00
5.50	15.00
6.00	15.00
6.50	15.00
7.00	15.00
7.50	15.00
8.00	15.00
8.50	15.00
9.00	15.00
9.50	15.00
10.00	15.00
10.50	15.00
11.00	15.00
11.50	15.00
12.00	15.00
12.50	15.00
13.00	15.00

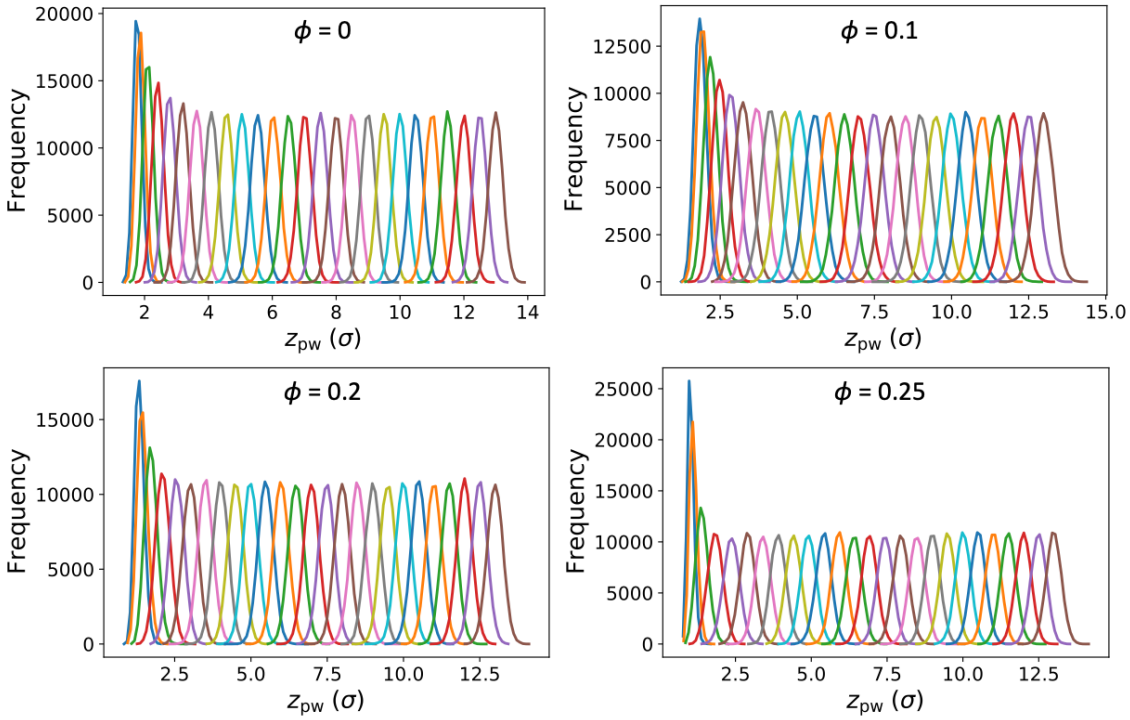


Figure 2.2: Umbrella sampling for polymer-wall interactions: Histograms of distances between the polymer's center of mass and the wall (z_{pw}) observed in each sampling window at different crowding fractions (ϕ).

The statistical errors in the PMFs were calculated using a Monte Carlo bootstrap analysis method.[92] For each time series corresponding to a different umbrella potential, we first calculated the correlation time (τ_c) by determining the time it took for the autocorrelation function to decay by a factor of e. Each original time series consisted of t_f data points. 50 new bootstrapped distributions, with a total of t_f/τ_c data points, were generated at random (with replacement) from the probability distribution of the simulated trajectory at each distance. 50 PMFs were calculated from the bootstrapped data sets, which were then used to calculate the mean and standard deviation of the PMF.

2.3 Results

Crowding causes compaction of an isolated ring polymer

We first considered a single ring polymer in a simulation box with periodic boundaries in all dimensions. No walls were present, and the volume fraction occupied by crowding particles (ϕ) ranged from no crowding (ϕ=0) to highly crowded (ϕ=0.42). Figure 2.3A shows the radius of gyration (R_g) of the polymer as a function of the crowding fraction. The average radius of gyration decreased with an increase in crowding, with a pronounced decrease seen at the largest crowding fractions ($\phi = 0.4$ and 0.42). Figure 2.3B shows the full distributions of R_g for each crowding fraction. The distributions shift to smaller values with increasing ϕ and have a qualitatively different shape at $\phi = 0.4$ and 0.42, where they are less symmetric. Figure 2.4 shows that at these crowding levels, the mode of the distribution shifts to the left of the mean.

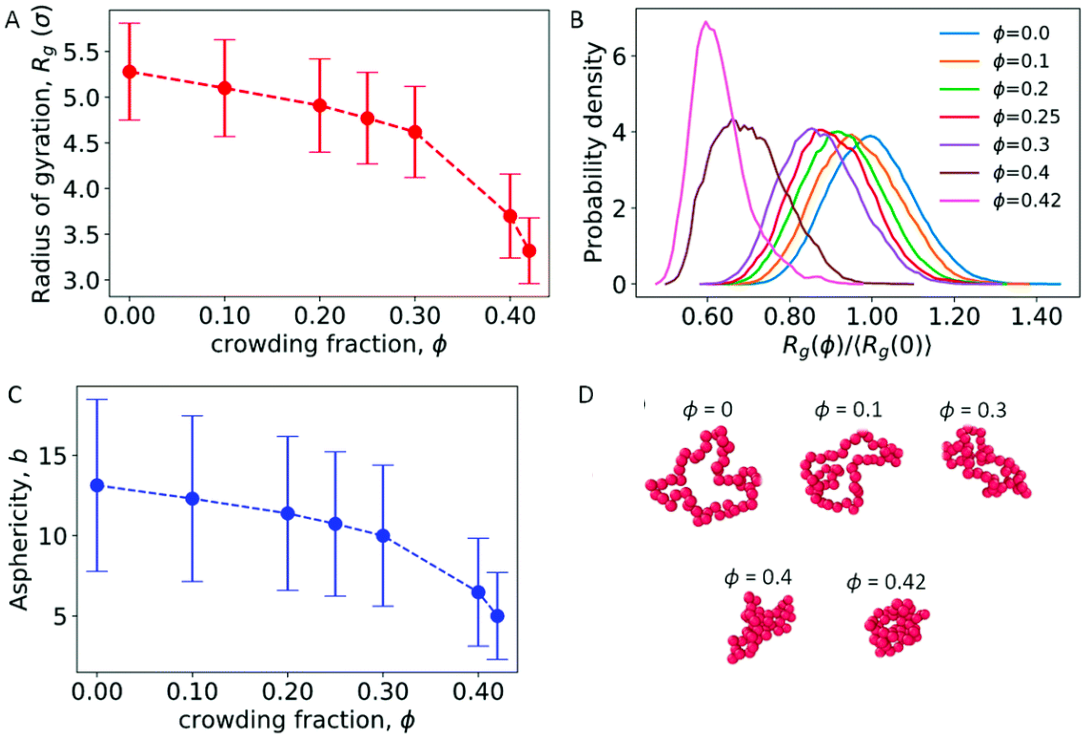


Figure 2.3: A) Radius of gyration of an isolated polymer at different crowding fractions (ϕ). Error bars denote the standard deviation. B) Probability density of the radius of gyration scaled by $\langle R_g(0)\rangle$, the average radius of gyration in uncrowded conditions. Distributions are shown for different crowding fractions. C) Asphericity of the polymer. D) Snapshots of the ring polymer for the most probable value of R_g at different crowding fractions.

We also calculated the asphericity (b) of the polymer, $b = \lambda_1 - \frac{1}{2}(\lambda_2 + \lambda_3)$, where $\lambda_1 \geq \lambda_2 \geq \lambda_3$ are the eigenvalues of the gyration tensor,[94,95]

$$S_{ij} = \frac{1}{N}\sum_{k=1}^{N}(r_{k,i} - r_{cm,i})(r_{k,j} - r_{cm,j})\,.$$

Here, $N = 50$ is the number of beads in the polymer, $r_{k,i}$ is the i^{th} coordinate of the position of the k^{th} particle, and $r_{cm,i}$ is the corresponding component of the center of mass. The asphericity is zero for a sphere and non-zero for non-spherical shapes, with larger values indicating larger deviations from sphericity. Figure 2.3C shows that the average asphericity also decreases with an increase in crowding.

Figure 2.3D shows snapshots of the ring polymer at various crowding fractions. For each case, a representative snapshot was chosen from the most probable bin in Fig. 2.3B. By inspection, the snapshots illustrate the decreasing size and asphericity at higher crowding fractions.

Taken together, these results show that increased crowding causes a decrease in the characteristic size ($\langle R_g \rangle$) and in the asphericity ($\langle b \rangle$) of a ring polymer. Figures 2.3B and 2.4 further demonstrate a qualitative change in the distribution of R_g at large values of ϕ. These results indicate that the ring polymer adopts conformations that are more compact and globule-like as crowding increases. This effect arises due to crowding-induced depletion interactions between beads of the polymer and is consistent with previous work on linear polymers.[61]

Crowding promotes interactions between two polymers

In the absence of crowding particles, two ring polymers are expected to experience an effective repulsion when they approach one another due to the entropic penalty arising from reduced conformational degrees of freedom.[96] In Fig. 2.3, we characterized changes in the size and shape of a single ring polymer due to crowding-induced depletion interactions between its segments. Based on this, we hypothesized

that crowding could also induce attraction between two otherwise purely repulsive polymers.

We simulated two polymers in a box with periodic boundaries and characterized N_{12}, the number of beads of polymer 1 within the WCA cutoff distance ($2^{1/6}\sigma_{mm}$) of any bead of polymer 2. Figure 2.5A shows N_{12} as a function of time. When the two polymers were in contact, larger crowding fractions resulted in a longer duration of contact and an increase in the number of beads in contact (N_{12}). The larger values of N_{12} are not attributable to an effect of slower diffusion alone, suggesting that there was a crowding-induced reduction in the effective repulsion between the two polymers. The effect was most pronounced at large crowding fractions ($\phi = 0.4$ and 0.42). Inset snapshots show the conformations of the two polymers at the maximum value of N_{12} in each figure. At low levels of crowding, the polymers stayed relatively expanded with small numbers of beads in contact. At higher levels of crowding, the polymers made more extensive contacts and were closer together in more compact conformations.

To quantify the strength of the effective interaction between the two polymers, we used umbrella sampling to calculate the potential of mean force (PMF) as a function of the distance between the centers of mass of the two polymers (r_{12}). Figure 2.6 shows the resulting PMFs at different crowding fractions. As expected, the PMFs are flat at large distances, indicating that the polymers did not interact when sufficiently far away from one another. For reference, we set the PMFs to zero at the largest value of r_{12} considered (15σ for $\phi = 0.0$ and 0.1, and 13σ for larger crowding fractions). This was in the regime in which the two polymers did not interact. When not in contact, the two polymers were more compact at higher crowding fractions, which was analogous to the single-polymer results in Fig. 1b. In Fig. 2.6, we present the PMFs in terms of the characteristic polymer size by scaling the distance (r_{12}) by the average radius of gyration for each crowding fraction.

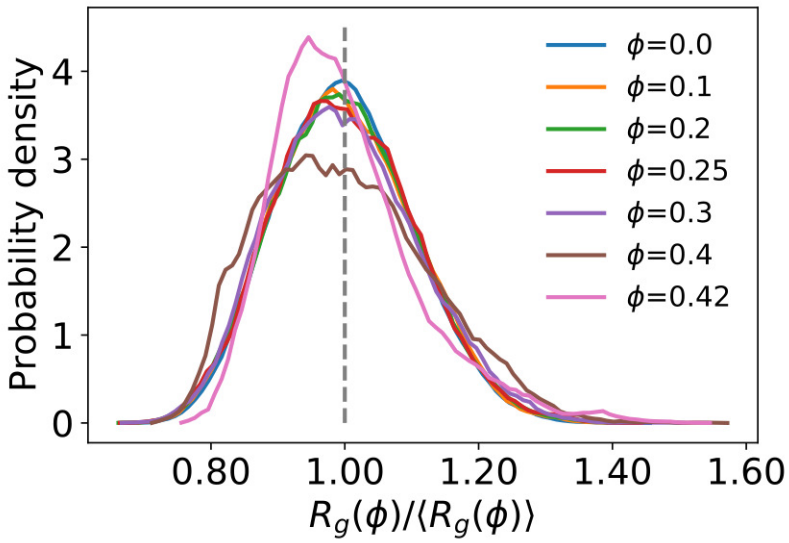


Figure 2.4: For an isolated ring polymer, the probability density of the radius of gyration ($R_g(\phi)$) scaled by the average radius of gyration ($\langle R_g(\phi)\rangle$). Distributions are shown for different crowding fractions (ϕ).

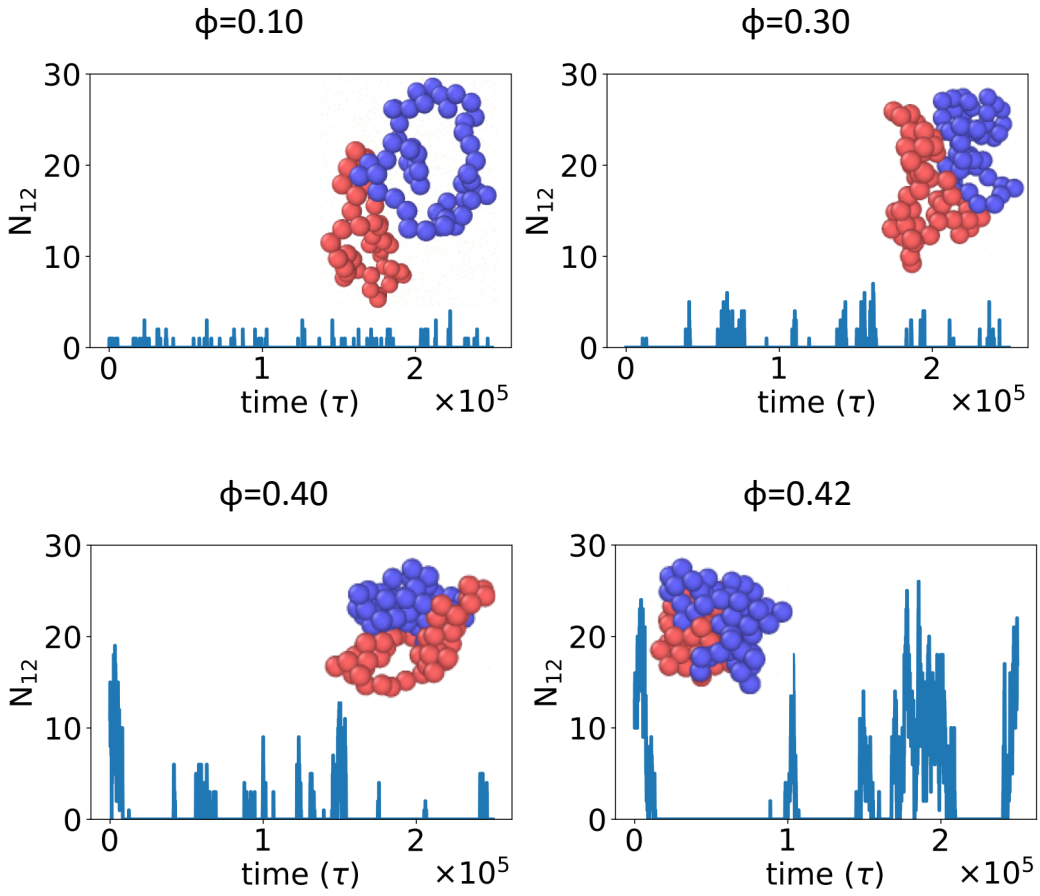


Figure 2.5: Number of beads of polymer 1 in contact with any bead of polymer 2 (N_{12}) as a function of time for different crowding fractions (ϕ). Inset: Snapshot corresponding to the configuration with the largest value of N_{12} for each crowding fraction.

For the uncrowded system ($\phi = 0$) in Fig. 2.6, the PMF indicates a purely repulsive interaction, with the repulsive part of the potential ($dU/dr_{12} < 0$) emerging when the centers of mass of the polymers are slightly farther apart than $2\langle R_g \rangle$. The PMFs associated with crowding fractions $\phi = 0.1$, 0.2, and 0.3 exhibit similar monotonic behavior, indicating purely repulsive interactions. However, the magnitude of the PMF is modestly smaller for $\phi = 0.3$. This indicates a smaller energetic penalty to bring two polymers into contact at higher crowding fractions, which is consistent with the larger number of beads in contact (N_{12}) observed in Fig. 2.5. For $\phi = 0.4$, in contrast with smaller values of ϕ, the PMF exhibited a small attractive minimum ($U_{\text{min}} = -0.64\ k_{\text{B}}T$) at $r_{12} = 1.65\langle R_g \rangle = 6.10\sigma$. The behavior at smaller values of r_{12} was repulsive. For $\phi = 0.42$, the PMF exhibited a deeper minimum ($U_{\text{min}} = -2.59\ k_{\text{B}}T$) at $r_{12} = 1.27\langle R_g \rangle = 4.20\sigma$.

These results highlight the role of depletion interactions in shaping the effective interactions of two ring polymers. In the absence of crowding, there is an effective repulsion between the two polymers at short distances due to the decreased conformational entropy of the polymers. Depletion interactions due to crowding can offset the loss of conformational entropy. This leads to enhanced contact between the polymers due to a smaller effective repulsive potential ($\phi \leq 0.3$) that becomes attractive at large crowding fractions ($\phi = 0.4$ and 0.42).

Crowding leads to polymer adsorption at a wall

Biopolymers commonly encounter extended surfaces in both cellular and cell-free environments. Crowding-induced depletion interactions can influence the effective interaction between a polymer and a surface. To characterize this effect, we simulated a single ring polymer in the presence of repulsive walls.

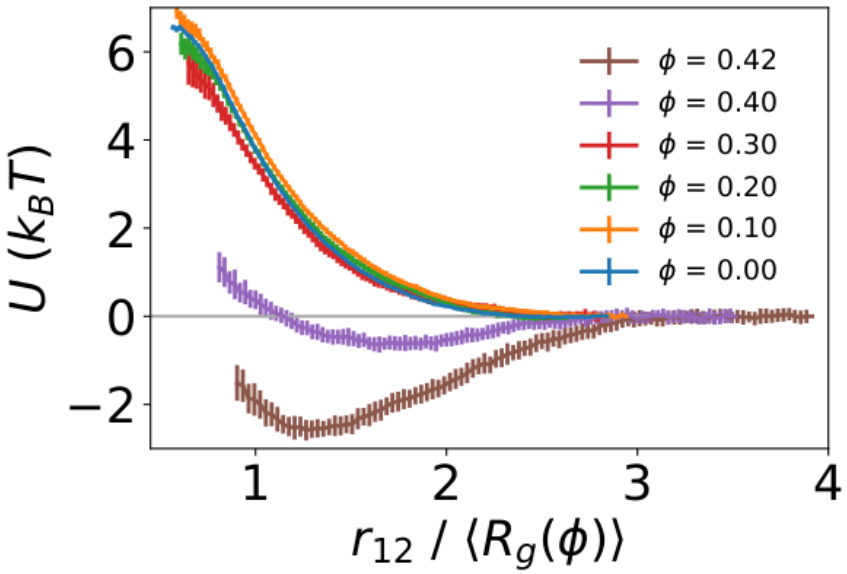


Figure 2.6: Potentials of mean force (U) between two polymers as a function of the distance between their centers of mass. For each crowding fraction (ϕ), the distance (r_{12}) is scaled by the average radius of gyration of an isolated polymer ($\langle R_g(\phi)\rangle$). Error bars indicate the standard deviation determined using the bootstrapping procedure described in Methods.

We first simulated a ring polymer in a simulation box with walls located at $z = \pm 15\sigma$. Figure 2.7A shows the time-dependent position of the center of mass of the polymer in the z direction when the polymer started near the center. At $\phi = 0.1$, the polymer remained within the bulk of the simulation box, with the center of mass remaining separated from the wall. This is consistent with an effective repulsion that the polymer is expected to experience near the wall due to reduced conformational entropy.

However, at $\phi = 0.2$, qualitatively different behavior emerged. Here, the center of mass of the polymer was more likely to reside close to a wall for an extended period of time. At larger crowding fractions ($\phi = 0.3$ and 0.4), the polymer became strongly associated with one of the walls for the duration of the simulation. The behavior for $\phi \geq 0.2$ is consistent with the polymer experiencing an effective attraction to the wall, with the strength of the attraction increasing with larger crowding fractions.

Figure 2.7B shows snapshots of the polymer in the presence of walls at different crowding fractions (viewed from the side). To facilitate comparison, each snapshot corresponds to the polymer configuration that was closest to the wall in Fig. 2.7A. At $\phi = 0.2$, the polymer appears to be partially adsorbed to the surface. In conjunction with the time-dependence of the center of mass, this suggests that the polymer was transiently adsorbed with parts of the polymer in contact with the wall. Because only part of the polymer was in contact, the center of mass remained farther from the wall than the polymer configurations seen at $\phi = 0.3$ and 0.4. At these crowding fractions, the polymer is strongly adsorbed, with almost all of the polymer beads in contact with the wall.

To further characterize the conformations of the polymer, Figs. 2.8A and 2.8B show the radius of gyration (R_g) and asphericity (b) of the polymer. With a wall present, both quantities increased for $\phi \geq 0.25$. This is in contrast with the behavior of an isolated polymer in the bulk (Fig. 2.3), which became more compacted and spherical at these crowding fractions.

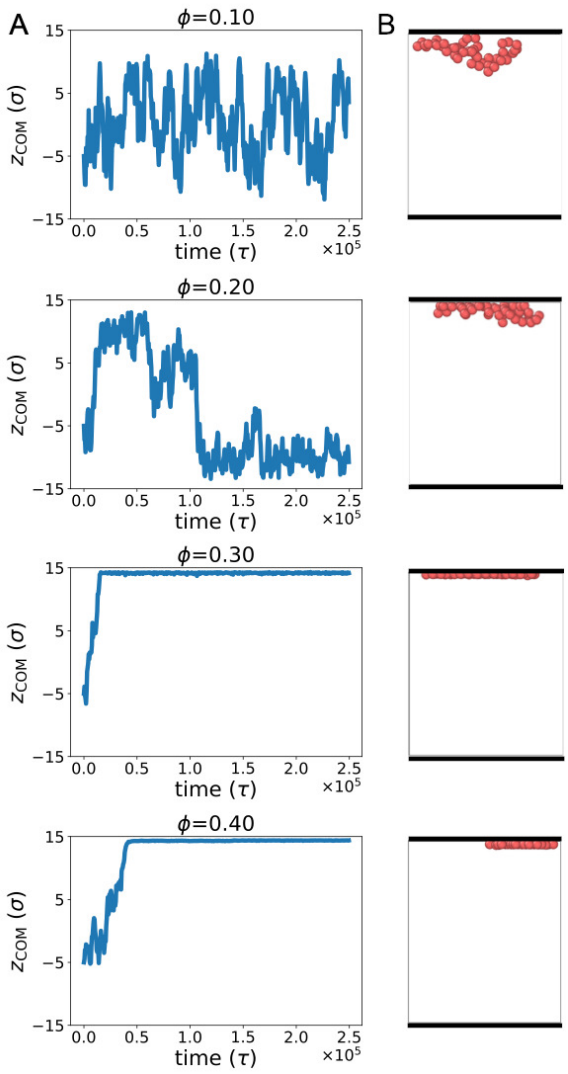


Figure 2.7: A) Center of mass of a polymer in the z direction (z_{COM}) as a function of time in unbiased simulations. A single trajectory with a polymer starting away from the walls is shown for each crowding fraction (ϕ). B) Snapshot from each trajectory, with walls denoted by the thick black lines at the upper and lower bounds of the box ($z = \pm 15\ \sigma$). To facilitate comparison between different crowding fractions, each snapshot corresponds to the frame in which the polymer was closest to the wall.

Snapshots from Fig. 2.7B suggested a flattening of the polymer against the wall at higher crowding fractions, so we investigated a measure of the extension of the polymer in the directions parallel to and perpendicular to the wall:[97]

$$R_{\parallel}^2 = \lambda_1 \sin^2\theta_1 + \lambda_2 \sin^2\theta_2 + \lambda_3 \sin^2\theta_3,$$
$$R_{\perp}^2 = \lambda_1 \cos^2\theta_1 + \lambda_2 \cos^2\theta_2 + \lambda_3 \cos^2\theta_3.$$

Here, θ_i is the angle between the eigenvector corresponding to eigenvalue λ_i of the gyration tensor and the z axis, which is normal to the wall. Figure 2.8C shows that for $\phi \geq 0.25$, the polymer became extended in the directions parallel to the wall and contracted in the direction perpendicular to the wall.

In this regime, the presence of a wall leads to a flattening of the polymer against the wall, resulting in conformations that are extended in the x and y dimensions relative to the z dimension (Figs. 2.8C and 2.8D). This leads to the increase in the average radius of gyration and asphericity and the decrease in the average value of $R_{\perp}$. This demonstrates that crowding can lead to markedly different conformations of the polymer in the presence and absence of a confining wall.

We also observed modest decreases in the average radius of gyration and the average value of $R_{\parallel}$ between $\phi = 0.3$ and 0.4. However, the average asphericty was relatively constant in this range. This was due to the polymer remaining flattened against the wall but becoming more compact in two dimensions due to depletion interactions between different parts of the polymer. Thus, at high crowding fractions, the degree of crowding can impact the quasi-two-dimensional conformations of the strongly adsorbed polymer.

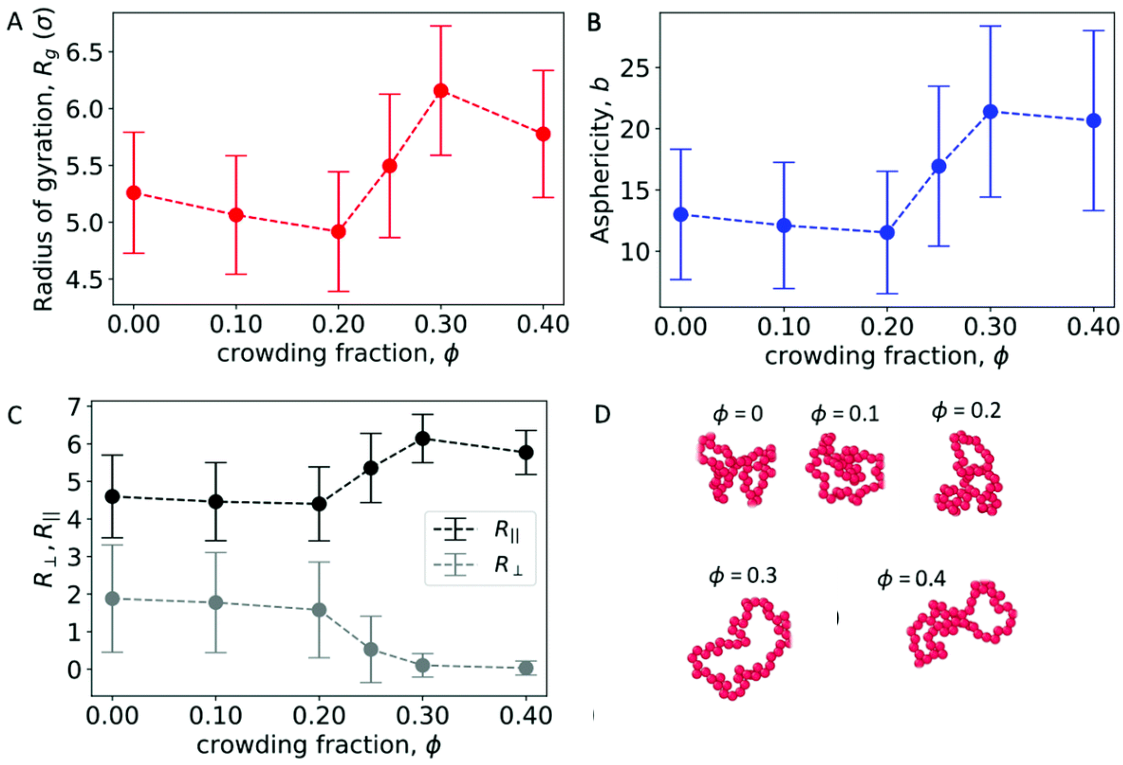


Figure 2.8: A) Radius of gyration of a polymer in the presence of walls at different crowding fractions. B) Asphericity of the polymer. C) Extension of the polymer in the directions parallel to ($R_{||}$) and perpendicular to ($R_\perp$) the wall. D) Snapshots of the polymer for the most probable value of R_g at different crowding fractions. The polymer is viewed along the z direction (toward a wall).

To quantify the strength of the effective interaction between the ring polymer and the wall, we determined the PMF as a function of the distance between the center of mass of the polymer and the position of the wall in the z direction (z_{pw}). Figure 2.9 shows the PMFs for various crowding fractions. We considered crowding fractions $\phi \leq 0.25$ because of challenges associated with obtaining adequate, equilibrated sampling at larger values of ϕ, where the polymer strongly adsorbs to the wall. At $\phi = 0$ and 0.1, the PMFs are strictly repulsive at small distances. At $\phi = 0.2$, there is a shallow attractive well ($U_{\text{min}} = -1.21\ k_{\text{B}}T$) with a minimum at $z_{\text{min}} = 4.3\sigma$. This is consistent with the typical location of the center of mass of the polymer being close to the wall, as observed in Fig. 2.7. The effective repulsion at small values of z_{pw} indicates that depletion interactions do not offset further loss of conformational entropy associated with more monomers being in contact with the wall.

Increasing the crowding fraction further resulted in stronger attraction to the wall. For $\phi = 0.25$, the well depth was $-10.59\ k_{\text{B}}T$. This is notably larger than the depth of the attractive well between two polymers in the bulk at the largest crowding fraction considered ($\phi = 0.42$). The location of the minimum for $\phi = 0.25$ was $z_{\text{min}} = 1.2\sigma$, which is closer to the wall than the minimum for $\phi = 0.2$. This is consistent with increased crowding driving the polymer from a partially adsorbed state at intermediate crowding fractions to a strongly adsorbed state at larger crowding fractions. When strongly adsorbed, the polymer nearly completely flattens against the wall, as shown in Fig. 2.8. We anticipate that larger crowding fractions would result in PMFs with even deeper attractive wells.

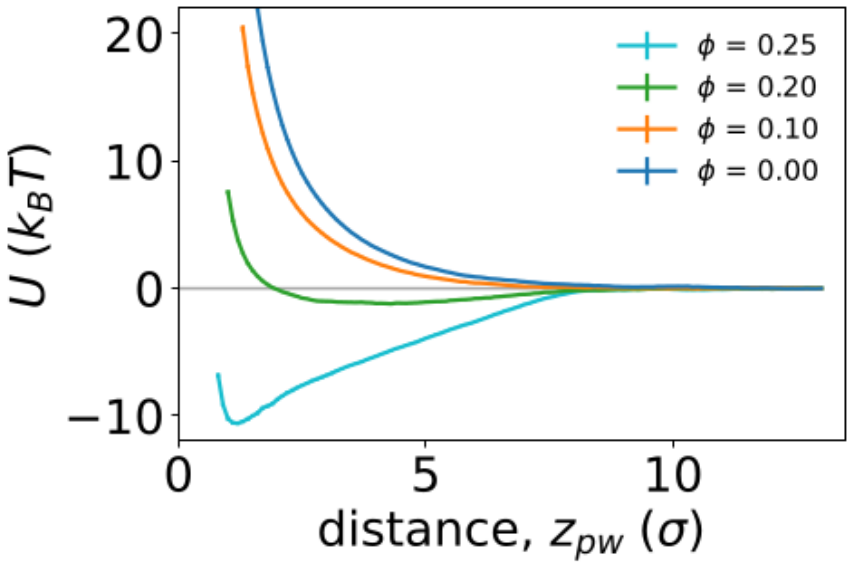


Figure 2.9: Potentials of mean force (U) between a polymer and a wall as function of the distance between them (z_{pw}), for different crowding fractions.

2.4 Discussion

Crowding-induced depletion interactions have been long studied in the context of soft matter systems, especially those comprised of colloids and polymers. The impacts of depletion interactions in cellular environments, which are crowded with macromolecules, have been increasingly appreciated.[7,17,37] Additionally, cell-free experiments incorporating biological components and synthetic crowders have become a new way to study the impact of crowding on biological systems.[47,84]

In this work, we studied a simple model of a ring polymer, monodisperse crowding particles, and a static wall. All components of the system interacted only via short-ranged repulsive interactions. We neglected specific energetic interactions that can play important roles in the organization of biomolecules, and the static wall provided an approximation of dynamic membrane surfaces in the cell. Instead, our focus was on characterizing the magnitude and consequences of depletion interactions as they would apply to a variety of biological systems. We focused on exploring the strength of polymer-polymer and polymer-wall attraction, which was motivated by recent experiments in cell-free systems.[38,47,84] While we studied a specific crowder size in this work, based on crowding-induced compaction of linear polymers,[61] we expect that decreasing the crowder size would increase the magnitude of attractive interactions. However, it would not impact the qualitative features.

We first studied the conformations of isolated ring polymers without a wall present. We observed that crowding generated depletion interactions between segments of the same polymer, leading to compaction of the polymers (Fig. 2.3). Our results are consistent with studies that observed the effects of depletion interactions on the compaction of linear polymers[29,61] and penetrable ellipsoids.[53] The collapse of a polymer with crowding may have important consequences in biology. It has been attributed as a major factor in the condensation of chromosomes in prokaryotes.[98] Additionally, macromolecular crowding improves the encapsulation of polymers in lipid vesicles, which has been attributed to polymer condensation due to crowding.[99]

This is of particular consequence to synthetic cell-free systems encapsulated in vesicles.

We further studied how crowding impacts the effective interactions between two polymers and between a polymer and a surface. We first showed that crowding can lead to enhanced interactions between two ring polymers, and that at sufficiently high crowding fractions ($\phi \approx 0.4$), an effective attraction between polymers emerged (Fig. 2.6). Attraction between polymers can result in aggregation and phase separation, and the impact of crowding-induced depletion interactions on phase separation in biological systems is a topic of intense current interest.[100] Our work helps to contextualize the magnitude of depletion interactions between ring polymers like DNA plasmids.

We also showed that crowding can induce adsorption of a ring polymer to a wall, with an effective attraction emerging at lower crowding fractions ($\phi \approx 0.2$). Between $\phi = 0.2$ and 0.3, the polymer transitioned from partially adsorbed to fully adsorbed, with nearly all of the monomers in direct contact with the wall. In this regime, the polymer adopted a flattened conformation that was extended in the lateral dimensions. We characterized the strength of the attraction to the wall for $\phi = 0.2$ and 0.25 by the depth of the minimum in the potential of mean force. The polymer-wall interactions for $\phi = 0.25$ exhibited a deeper minimum than those observed for polymer-polymer interactions, indicating a significantly stronger interaction.

The markedly different conformations of ring polymers in the bulk versus adsorbed at the wall have the potential to influence the interactions of the polymer with other molecules. Transcriptional machinery is less likely to be able to access compacted conformations of DNA plasmids, potentially impacting the dynamics of gene expression. Tsuji and Yoshikawa[101] showed that different conformations of the widely studied bacteriophage T4 DNA lead to significantly different behavior of transcription. They observed that high concentrations of Mg^{2+} ions caused DNA to adsorb at the surface of cell-sized lipid vesicles, leading to extended conformations of the DNA. The extended conformations exhibited transcription similar to DNA

coils in aqueous solutions. In contrast, collapsed DNA obtained via addition of the polycation spermine showed no transcriptional activity.

Our work suggests that crowding could be used in much the same way to influence the conformations of DNA, hence impacting gene expression. In a crowded environment, it is also possible that an effective polymer-polymer attraction could impact gene expression by causing aggregation of DNA. It highlights crowding as a potential variable with which to control the spatial organization and conformations of DNA, as well as dynamics of gene expression. This control is possible in both cellular and cell-free environments. Indeed, our results suggest a possible mechanism to explain recent cell-free experiments in which crowding modulated the spatial organization of biopolymers. In systems with large volumes, there was evidence of spatially localized transcription that emerged with increasing crowding,[47,84] which could potentially arise due to attractive depletion interactions. In systems confined in small vesicles, crowding induced localization at the walls,[38] which is consistent with the strong attraction we found for polymer-wall interactions.

Our results show that crowding can impact the conformations of individual ring polymers, enhance interactions between two polymers, and strongly promote interactions with surfaces. It has implications for understanding the role of entropic interactions in shaping the behavior of biopolymers in both cellular and cell-free systems. Interesting directions for future investigation include the effects of polydisperse crowders, flexible membrane surfaces, and additional species differentially impacted by depletion interactions.

Chapter 3

Adsorption of semiflexible polymers in crowded environments

A version of this chapter was originally published by Gaurav Chauhan, Michael L. Simpson and Steven M. Abel: Chauhan, G., Simpson, M. L., & Abel, S. M. (2021). *J. Chem. Phys.* 155, 034904

3.1 Introduction

Asakura and Oosawa's seminal paper on depletion interactions, published in 1954, describes how attractive depletion forces arise between objects due to the presence of smaller solute particles.[48] Depletion interactions have been studied widely in the context of colloid-polymer and other soft matter systems, and many outstanding questions remain to be addressed.[1,49] More recently, there has been growing interest in the roles of depletion interactions in biological systems, where they have been suggested to play a role in cellular organization,[17] genome organization,[12–15] gene regulation,[3,16,84] and controlling intracellular phase separation.[7,37]

The interiors of cells contain large concentrations of macromolecules that can occupy up to 40% of the total cellular volume.[2] The cellular environment is replete

with semiflexible polymers such as DNA, actin, microtubules, etc., which have a wide range of persistence lengths. These polymers are often in the presence of surfaces such as the plasma or nuclear membrane. The abundance of macromolecules can result in attractive depletion interactions between biopolymers and surfaces,[17] which can lead to adsorption of the polymers. Understanding the effects of crowding on properties of semiflexible polymers and their interactions with surfaces will help shed light on the role of depletion interactions in organizing cellular systems.

Crowding-induced depletion interactions have been shown to impact the conformations of both flexible and semiflexible biopolymers. For flexible polymers, crowding can cause a coil-to-globule transition,[61] induce collapse of model chromosomes,[29] and lead to attraction between ring polymers.[102] For semiflexible polymers, which have an inherent bending stiffness, experiments have shown that actin filaments undergo condensation upon addition of non-adsorbing polymeric crowders.[27] Simulations have also shown that polydispersity of crowder sizes and shapes can unexpectedly swell polymers of intermediate bending stiffness.[64]

Crowding can also lead to the adsorption of biopolymers onto surfaces. DNA plasmids have been shown to preferentially localize near the walls of crowded cell-sized vesicles,[38,39] and by tuning the concentration of depletants, Welch et al. observed actin filaments in both partially and fully adsorbed states.[40] Interactions of proteins with surfaces in crowded environments have also been shown to enhance the formation of protein fibrils.[41,42] For flexible ring polymers, the magnitude of crowding-induced attraction to a wall was shown to be notably stronger than the magnitude of polymer-polymer attraction, and an effective polymer-wall attraction emerged at a lower volume fraction of crowding particles.[102]

Understanding interactions of polymers with surfaces has been a long-standing problem of interest in polymer physics.[65–67] While polymer adsorption has been studied extensively for flexible polymers,[71–73] much less is known about the adsorption of semiflexible polymers.[67,69] To characterize adsorption, theories and simulations must account for internal degrees of freedom of the polymer, and stiffer polymers lose

less conformational entropy upon adsorption. As a consequence, when there is explicit attraction between a semiflexible polymer and a flat wall, adsorption is promoted by a larger bending stiffness and the critical strength of attraction required for adsorption decreases with increasing stiffness.[40,69,74–76,103] Milchev and Binder[69] recently showed that the conformations of partially adsorbed chains are not well-described by the wormlike chain model and that adsorption does not lead to the expected 2-dimensional decay of the orientational correlation function over an intermediate but broad range of the bending stiffness. Additionally, for semiflexible polymers, the curvature of the surface can impact the adsorption behavior due to an energetic bending penalty experienced by polymers when adsorbed to a curved surface.[95,104–106]

Over the past two decades, there have been a number of theoretical and computational studies aimed at characterizing the relationship between the persistence length (l_p) of a semiflexible polymer and the adsorption threshold, ϵ_c, of a short-ranged attractive adsorption potential between a polymer bead and a wall.[69,104,107,108] Potentials studied have typically been a square well characterized by depth ϵ or another short-ranged attractive potential between a polymer bead and a wall. A well-established result is the relation

$$\epsilon_c \propto k_B T/(l_p^{1/3} l^{2/3}) \propto l_p^{-1/3} \, , \tag{3.1}$$

where l is the range of the adsorption potential. The quantity $l_d = l_p^{1/3} l^{2/3}$ is the Odijk deflection length.[109] A number of elegant theoretical and scaling arguments have been provided to justify this result, which holds for $l \ll l_p$ in the thermodynamic limit. More recently, Kampmann and Kierfeld analyzed the adsorption threshold for polymers of finite length and carefully established scaling relations for adsorption data of finite semiflexible polymers, which can deviate from Eqn. 3.1.[110]

In this paper, we use computer simulations to study crowding-induced interactions of linear semiflexible polymers with surfaces. Previous works studying the adsorption of semiflexible polymers have typically used generic, short-ranged attractive potentials

between polymer beads and a surface. In contrast with these works, we explicitly simulate crowding particles and their effect on a bead-spring model of a semiflexible polymer. This allows us to capture features missing from simpler approaches, including (i) details of crowding-induced interactions between polymer beads and walls that may not be reflected in simple potentials and (ii) crowding-induced interactions between different segments of the same polymer. Additionally, it is challenging to determine a quantitative relation between the properties of the crowders (size, volume fraction, etc.) and the strength of the depletion interaction, especially at higher concentrations where the depletion interaction may not scale linearly with the concentration of crowders.

In the following, we explore how polymer adsorption is impacted by the bending stiffness of the polymers and the volume fraction and size of the crowders. We characterize properties of the polymers and show that the shape of the system and curvature of the surface can impact the adsorption. Taken together, our work sheds light on the role of crowding in the spatial organization of semiflexible polymers in cellular and cell-free environments.

3.2 Methods

We studied effects of crowding on a semiflexible polymer in the presence of a surface using Langevin dynamics simulations. The polymer was modeled as a linear, semiflexible chain consisting of $N = 50$ beads. Adjacent beads were connected via the finitely extensible nonlinear elastic (FENE) bond potential,

$$U_{\mathrm{FENE}} = -\frac{1}{2} K {R_0}^2 \ln\left[1 - \left(\frac{r}{R_0}\right)^2\right],$$

where r is the center-to-center distance between two adjacent beads. The diameter of each bead was $\sigma_m = \sigma$, the maximum distance between two connected beads was $R_0 = 1.5\sigma$, and the spring constant was $K = 15\epsilon/\sigma^2$. σ and ϵ set the length and

energy units, and we report lengths and energies in terms of them. The persistence length of the polymer was controlled by changing the bending stiffness, κ, of the bending potential,

$$U_{\text{angle}} = \kappa(1 + \cos\theta) \ ,$$

where θ is the angle formed by three consecutive beads of the semiflexible polymer. The persistence length (l_p) denotes the length scale over which tangent correlations decay along the polymer chain. The theoretical relationship between the bending stiffness and the persistence length in d spatial dimensions is $l_p = 2\kappa/(d-1)$.[104,111,112]

Crowding particles ("crowders") were modeled as purely repulsive particles of diameter σ_c. We considered two sizes, $\sigma_c = 0.8\sigma$ and σ. The volume fraction of crowders, $\phi = N_c(4/3)\pi(\sigma_c/2)^3/V_{\text{box}}$, was controlled by changing the number of crowder particles in the simulation box of volume V_{box}. We refer to ϕ as the crowding fraction. All particles (polymer beads and crowders) interacted via the short-ranged and purely repulsive Weeks-Chandler-Andersen (WCA) potential,[86]

$$U_{ij} = \begin{cases} 4\epsilon_{ij}\left[\left(\frac{\sigma_{ij}}{r_{ij}}\right)^{12} - \left(\frac{\sigma_{ij}}{r_{ij}}\right)^{6}\right] + \epsilon_{ij} & r_{ij} < 2^{1/6}\sigma_{ij} \\ 0 & r_{ij} \geq 2^{1/6}\sigma_{ij} \ , \end{cases}$$

where r_{ij} is the center-to-center distance between particles i and j. The strength parameter was the same for all pairs, $\epsilon_{ij} = \epsilon = k_{\text{B}}T$. Further, $\sigma_{ij} = (\sigma_i + \sigma_j)/2$, where σ_i and σ_j denote the diameter of particles i and j, respectively.

We simulated a single polymer with many crowders in the presence of confining surfaces, which were represented by the purely repulsive 9-3 Lennard-Jones potential,

$$U_{iw} = \begin{cases} \epsilon_{iw}\left[\frac{2}{15}\left(\frac{\sigma_{iw}}{r_{iw}}\right)^{9} - \left(\frac{\sigma_{iw}}{r_{iw}}\right)^{3}\right] + (\frac{10}{9})^{1/2}\epsilon_{iw} & r_{iw} < (\frac{2}{5})^{1/6}\sigma_{iw} \\ 0 & r_{iw} \geq (\frac{2}{5})^{1/6}\sigma_{iw} \end{cases}$$

Here, r_{iw} is the closest distance between the particle and the wall, the strength factor for wall-particle interactions was the same for all particles ($\epsilon_{iw} = \epsilon = k_{\mathrm{B}}T$), and the length parameter σ_{iw} was specified by $(2/5)^{1/6}\sigma_{iw} = \sigma_{ii}/2$. To simulate a flat wall, we used a repulsive wall in the z-direction with periodic boundaries in the x- and y-directions. The dimensions of the simulation box were 50σ in the x- and y-dimensions and 40σ in the z-dimension. We also studied shorter polymers ($N = 10$ and 30) to assess finite-length effects. For computational efficiency, we used smaller system sizes for the shorter polymers ($30\sigma \times 30\sigma \times 30\sigma$ and $12\sigma \times 12\sigma \times 12\sigma$, respectively). We also simulated polymers in spherical confinement with a radius of 30σ using the above potential.

The Langevin equation was integrated forward in time using the velocity-Verlet algorithm in the LAMMPS simulation package.[60,88] The timestep for integration was 0.005τ, where τ is the natural unit of time. The total number of timesteps was typically 4.95×10^7, with data sampled after an initial equilibration time of 2×10^7 timesteps. For systems at large crowding fractions ($\phi = 0.4$), we ran simulations for an additional 5×10^7 timesteps, for a total sampling time of 7.95×10^7 timesteps. Averages of dynamical variables were calculated by time averaging along each trajectory. Resulting trajectories were visualized using OVITO.[89]

3.3 Results

In cellular and cell-free systems, the linear size of macromolecular crowders is often comparable to the cross-sectional diameter of biopolymers such as DNA or actin. Widely-used synthetic crowders such as dextran 70 and Ficoll 70 have hydrodynamic radii of $\approx$ 6.8 nm and $\approx$ 5 nm, respectively.[59] These sizes, which can be varied with molecular weight, are similar to the effective diameters of actin ($\approx$ 6 nm)[40] and dsDNA ($\approx$ 6.6 nm at 60 mM ionic strength).[57] As such, we simulated crowder sizes that were comparable to the size of a bead of the polymer chain.

3.3.1 Interplay between polymer stiffness, volume fraction of crowders, and crowder size

As a measure of association of the polymer with the wall, we characterized the number of polymer beads within distance σ of a wall (N_{wall}). Figure 3.1 shows $\langle N_{\text{wall}}/N \rangle$, the average fraction of polymer beads in close proximity to a wall, as a function of bending stiffness (κ) for various crowding fractions (ϕ). When $\phi = 0$, there are no depletion interactions, and the polymer interacts with the walls only via short-ranged repulsive interactions between its beads and the wall. In this regime, $\langle N_{\text{wall}}/N \rangle$ remains close to zero for all κ.

When crowders were present, we first considered the case in which the crowding particles were the same size as the monomer beads ($\sigma_c = \sigma_m$, dashed lines in Fig. 3.1). For a flexible chain ($\kappa = 0$), the average fraction of monomers near the wall remained close to zero for all crowding fractions up to $\phi = 0.4$. Thus, the flexible chains did not experience an appreciable crowding-induced attraction to the wall. Physically, there is a reduction in the conformational entropy of the polymer when it is close to the wall. In the absence of crowders, this leads to an effective repulsion between the center of mass of the polymer and the wall as well as a reduction in the density of monomers near the wall.[102] Our results indicate that when $\kappa = 0$ and $\sigma_c = \sigma_m$, depletion effects do not overcome the loss of entropy resulting from the association of the polymer with a wall. That is, when the polymer is in close contact with the wall, the entropic gains by crowding particles due to a larger effective volume do not offset the loss of conformational entropy of the polymer.

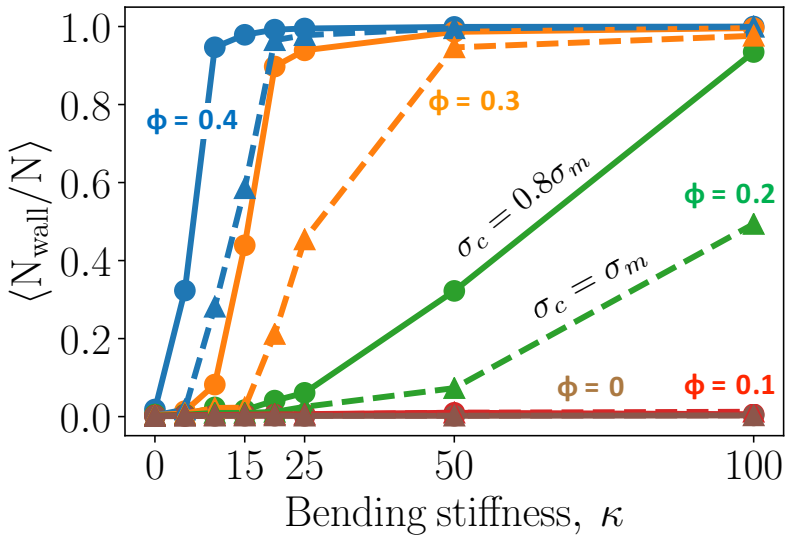


Figure 3.1: Average fraction of monomers near a wall, $\langle N_{\text{wall}}/N \rangle$, as a function of the bending stiffness, κ. Two sizes of the crowding particles are shown: $\sigma_c = \sigma_m$ (dashed) and $\sigma_c = 0.8\sigma_m$ (solid). Different volume fractions of the crowding particles (ϕ) are shown.

Even though there was no crowding-induced adsorption for flexible polymers at these conditions, we observed that increasing the bending stiffness resulted in association with a wall when $\phi \geq 0.2$. For $\phi = 0.2$, weak adsorption emerged at $\kappa = 50$ and 100. In this regime, the adsorption is characterized by partial contact with the wall. The contact is transient, being characterized by intermittent excursions away from the wall. For $\phi = 0.3$ and 0.4, we observed a transition to strong adsorption ($\langle N_{\text{wall}}/N \rangle \approx 1$) with increasing κ. The transition occurs at smaller values of κ for the larger crowding fraction. When the polymer was strongly adsorbed, we did not observe excursions of the center of mass away from the wall during the timescale of the simulations.

Previous work has shown that smaller crowding particles can induce considerable compaction of flexible polymers[61] and strong attraction of a flexible ring polymer to a wall.[102] We studied the effect of crowder size on polymer adsorption by considering smaller crowding particles with $\sigma_c = 0.8\sigma_m$ (Fig. 3.1, solid lines). Note that the volume of each particle is roughly half that of the previous case. The smaller crowding particles promote stronger adsorption than the larger particles at the same volume fraction (ϕ) and polymer stiffness (κ). This is reflected by (i) the transition to strong adsorption ($\langle N_{\text{wall}}/N \rangle \approx 1$) at smaller values of κ and (ii) the larger fraction of monomers close to a wall in the weak and moderate adsorption regimes. Thus, the strength of the depletion interactions increased with a decrease in crowder size at fixed volume fraction, which is consistent with previous work.[61,102] In the rest of the paper, we focus on the smaller crowding particle with $\sigma_c = 0.8\sigma_m$.

Figure 3.2 further explores the contact of the polymer with the wall. It shows the full distribution of contact fractions for different ϕ and κ. There is a prominent peak at $N_{\text{wall}}/N = 0$ for cases without adsorption (e.g., $\phi = 0.2$, $\kappa = 0$), indicating that the polymer rarely contacts the wall in these cases. Analysis of trajectories with $\phi \leq 0.1$ produced similar results with a prominent peak at 0. For $\phi = 0.2$, adsorption occurs at sufficiently large values of κ. In Fig. 3.2, the first hint of this transition can be seen at $\kappa = 15$, where the peak at $N_{\text{wall}}/N = 0$ is slightly lower than for smaller

values of κ, indicating a slight increase in the weight of configurations in which the polymer is in contact with a wall. For $\kappa = 50$, this feature is more prominent, and a broad distribution of contact fractions can be observed, including configurations in which the polymer is fully in contact. This is reflective of partial adsorption, in which fluctuations are prominent: The polymer is commonly not associated with the wall, but when it is, it exhibits a broad distribution of the number of monomers in contact. Similar behavior is observed at $\phi = 0.3$ with $\kappa = 15$ and at $\phi = 0.4$ with $\kappa = 5$, also indicating weak, partial adsorption. For crowding fractions of $\phi = 0.3$ and 0.4, the probability distribution is peaked at $N_{\text{wall}}/N = 1$ for the stiffest polymers, indicating strong adsorption in which the polymer is typically in complete contact with the wall.

3.3.2 Properties of the polymers

The distributions of weakly adsorbed polymers in Fig. 3.2 indicate a broad distribution of the fraction of monomers in contact with the wall. Figure 3.3 shows representative snapshots of the polymer in the partially adsorbed states. Conformations of partially adsorbed polymers are often described using the terminology of trains, tails, and loops.[40,110] Trains are continuous adsorbed segments of the polymer, tails are non-adsorbed end segments of the polymer, and loops are non-adsorbed segments between two trains. Examples for $\phi = 0.2$, 0.3, and 0.4 are shown; as the crowding fraction increases, a smaller bending stiffness is needed for the polymer to adsorb to the wall. Three snapshots are shown for $\phi = 0.2$ and $\kappa = 50$. In each, there is a single train along with one or two tails. Because the polymer is relatively stiff, it would be energetically costly for a loop to form (due to high local curvature). Hence, monomers not in contact with the wall tend to be located at the tails of the polymer. As the crowding fraction increases, the presence of tails decreases and eventually, in the limit of strong adsorption, the polymer is completely in contact with the wall as a single train.

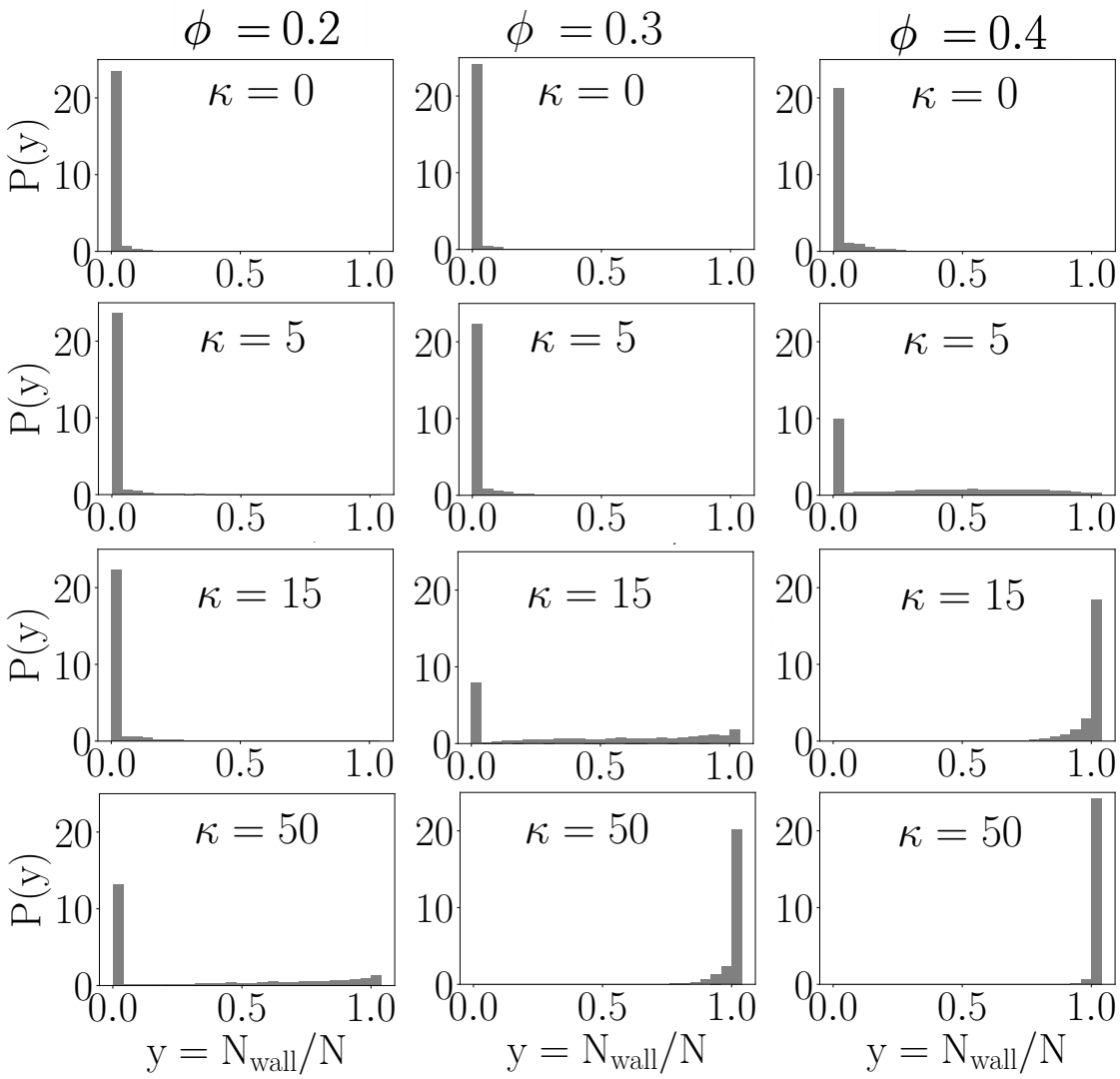


Figure 3.2: Probability density of the fraction of monomers near a confining wall. The volume fraction of crowding particles (ϕ = 0.2, 0.3, 0.4) increases from left to right. The bending stiffness of the polymer (κ = 0, 5, 15, 50) increases from top to bottom. Simulations were carried out with $\sigma_c = 0.8\sigma_m$.

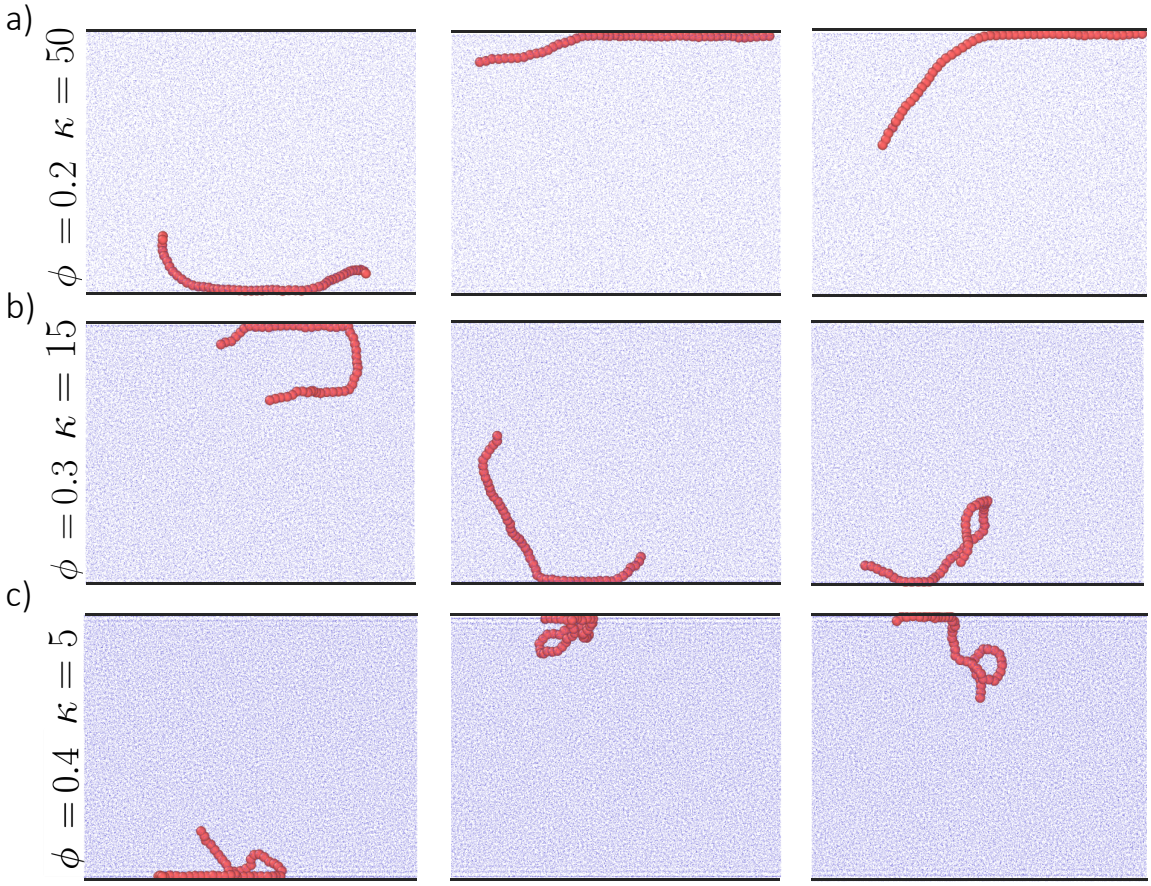


Figure 3.3: Snapshots of partially adsorbed semiflexible polymers. Boundary conditions are periodic in the x- and y-directions; confining walls in the z-direction are shown by black lines. The size of the crowders is $\sigma_c = 0.8\sigma_m$. (a) - (c) represent three cases (different values of κ and ϕ) that exhibit partial adsorption of the polymer. Three snapshots are shown for each case. The system is viewed along the y-axis, and the crowding particles are minimized in the visualization to more clearly reveal the polymer.

Similar behavior was observed for $\phi = 0.3$ and $\kappa = 15$, in which the adsorbed polymer adopted conformations with trains and tails but no loops. However, a greater degree of flexibility is evident in the tails compared with the previous case. For $\phi = 0.4$ and $\kappa = 5$, the partially adsorbed polymer formed trains, tails and loops. In this regime, the polymer is sufficiently flexible so that the energetic penalty associated with forming loops is offset by entropic gains.

The effects of crowding on the polymer are further illuminated by the radius of gyration of the polymer. Figure 3.4a shows the radius of gyration as a function of bending stiffness in uncrowded ($\phi = 0$) conditions. Figures 3.4b and 3.4c show, for different κ, how the radius of gyration varies as a function of the crowding fraction ($R_g(\phi)$) in relation to the corresponding value in uncrowded conditions ($R_g(0)$). For the purely flexible polymer chain ($\kappa = 0$), the radius of gyration decreases with an increase in crowding, which is consistent with previous work on flexible polymers.[61] The decrease is less pronounced for the semiflexible polymer with $\kappa = 5$ in the regime without adsorption ($\phi \leq 0.3$), and no decrease is evident for stiffer polymers. A notable feature is that at sufficiently large values of ϕ, there is an increase in R_g. The largest relative increase in size is observed for intermediate values of the stiffness ($\kappa = 10$ and 15), with a nearly 20% increase in R_g at $\phi = 0.4$. These increases occur in regimes in which the polymer adsorbs to the wall and flattens against it. The increase is considerably smaller for $\kappa = 50$ and especially $\kappa = 100$ because these polymers are relatively extended even in the bulk.

To further characterize the shape of the polymer, we calculated the radius of gyration parallel to the wall ($R_{g,\parallel}$) and perpendicular to the wall ($R_{g,\perp}$), using

$$R_{g,\parallel}^2 = \frac{1}{N}\sum_{i=1}^{N}\left((x_i - x_{\mathrm{COM}})^2 + (y_i - y_{\mathrm{COM}})^2\right) ,$$

$$R_{g,\perp}^2 = \frac{1}{N}\sum_{i=1}^{N}(z_i - z_{\mathrm{COM}})^2 .$$

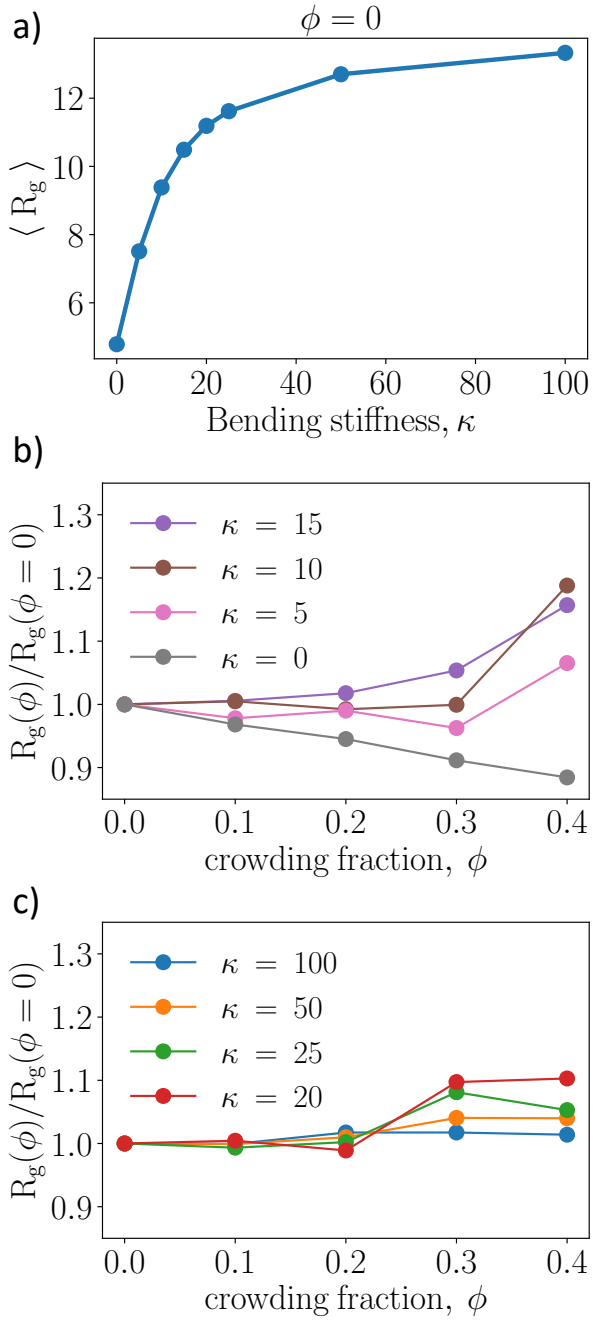


Figure 3.4: (a) Mean radius of gyration of the polymer in uncrowded conditions ($R_g(0)$) as a function of bending stiffness (κ). (b),(c) Mean radius of gyration at ϕ (volume fraction of crowders) scaled by the corresponding value in uncrowded conditions ($R_g(\phi)/R_g(0)$). For clarity, smaller and larger values of the bending stiffness are shown separately. The size of the crowders is $\sigma_c = 0.8\sigma_m$.

Figure 3.5 shows the average values of $R_{g,\parallel}$ and $R_{g,\perp}$ as a function of the crowding fraction. For the flexible polymer ($\kappa = 0$), the behavior of each reflects the decrease seen in R_g, indicating that crowding leads to a compaction in directions both parallel and perpendicular to the wall.

For $\kappa \geq 5$, $R_{g,\parallel}$ increases when the polymer is adsorbed to the wall. Small increases are seen for partially adsorbed polymers (e.g., $\kappa = 5$ and $\phi = 0.4$). Larger increases are seen for fully adsorbed polymers, although the relative increase in $R_{g,\parallel}$ is less for large values of κ. When $R_{g,\parallel}$ increases, there is a concomitant decrease in $R_{g\perp}$, with the value approaching zero for strongly adsorbed polymers. These results are consistent with the polymer flattening against the wall (decreasing $R_{g\perp}$) and increasing its size in the directions parallel to the wall (increasing $R_{g,\parallel}$). The relative increase in the parallel direction is largest for smaller values of κ because the polymer can adopt more compact conformations when not adsorbed. In contrast, in the limit of a rigid-rod polymer ($\kappa \to \infty$), R_g would remain constant upon adsorption and changes in $R_{g,\perp}$ and $R_{g,\parallel}$ would reflect the change in the orientational degrees of freedom only.

3.3.3 Adsorption threshold and finite-size effects

Equation 3.1 relates the critical adsorption strength to the persistence length of semiflexible polymers, with $\epsilon_c \propto l_p^{-1/3}$ (recall that $l_p \propto \kappa$). However, finite-size effects associated with polymers of finite length may impact the scaling. Kampmann and Kierfeld provided extensive analysis of the adsorption threshold for polymers of finite length.[110] Given the length of polymer considered above and the fact that we considered persistence lengths exceeding the contour length, we sought to analyze our simulation data in the context of this work. To this end, we considered shorter polymers with $N = 10$ and 30 in addition to our previous results with $N = 50$.

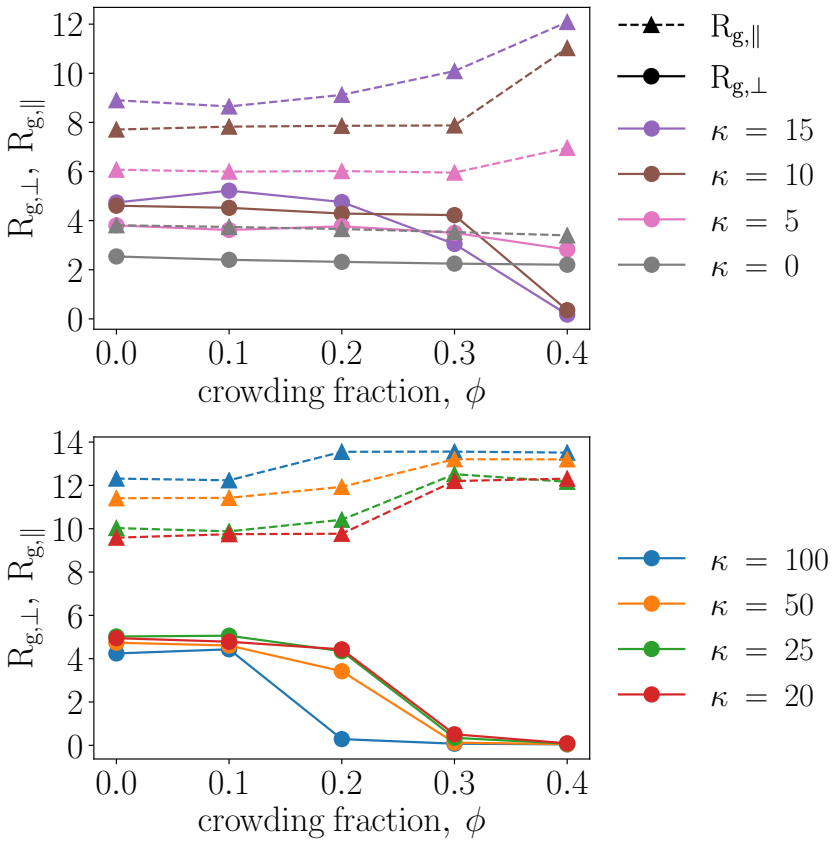


Figure 3.5: Mean radius of gyration parallel to the wall ($R_{g,\parallel}$, dashed) and perpendicular to the wall ($R_{g,\perp}$, solid), for various values of the bending stiffness (κ).

Figure 3.6 shows the results of these simulations. The average fraction of adsorbed beads is plotted as a function of the crowding fraction. For each value of κ, we determined the critical value of the crowding fraction, ϕ_c, as the crowding fraction at which $\langle N_{\text{wall}}/N \rangle = 1/2$. In contrast with previous theoretical and computational work, we do not have direct access to the potential strength, so we use ϕ as a proxy. In the limit of dilute crowding, Asakura-Oosawa (AO) and related theories predict that the minimum of the depletion potential is $u_{\text{min}} \propto -k_B T \phi$.[48,77] However, at larger values of the crowding fraction, a nonlinear relation between ϕ and u_{min} is expected, which complicates attempts to find a scaling relationship between ϕ_c and l_p.[77]

As before, we observe that stiffer polymers adsorb at smaller values of ϕ. The adsorption transition is also broader for shorter polymer lengths and is quite pronounced for the case with $N = 10$. These results are consistent with broadening seen in recent results of Milchev and Binder, who studied much longer tethered polymers that interacted with a wall via a short-ranged attractive potential.[69,107]

Figure 3.8a shows ϕ_c plotted as a function of κ for the three polymer lengths. The results with $N = 50$ appear consistent with a scaling of $\phi_c \propto \kappa^{-1/3}$, whereas the results for $N = 30$ and 10 are clearly not consistent. In the rigid rod limit (not shown on the figure), the longest polymer's adsorption threshold is the smallest of the three. For $\kappa = 10^4$, $\phi_c = 0.075$, 0.081, and 0.143 for $N = 50$, 30, and 10, respectively. Note that each polymer length was simulated in a different box size, which can affect their adsorption threshold and hence limit direct comparison of the values of ϕ_c between polymer lengths.

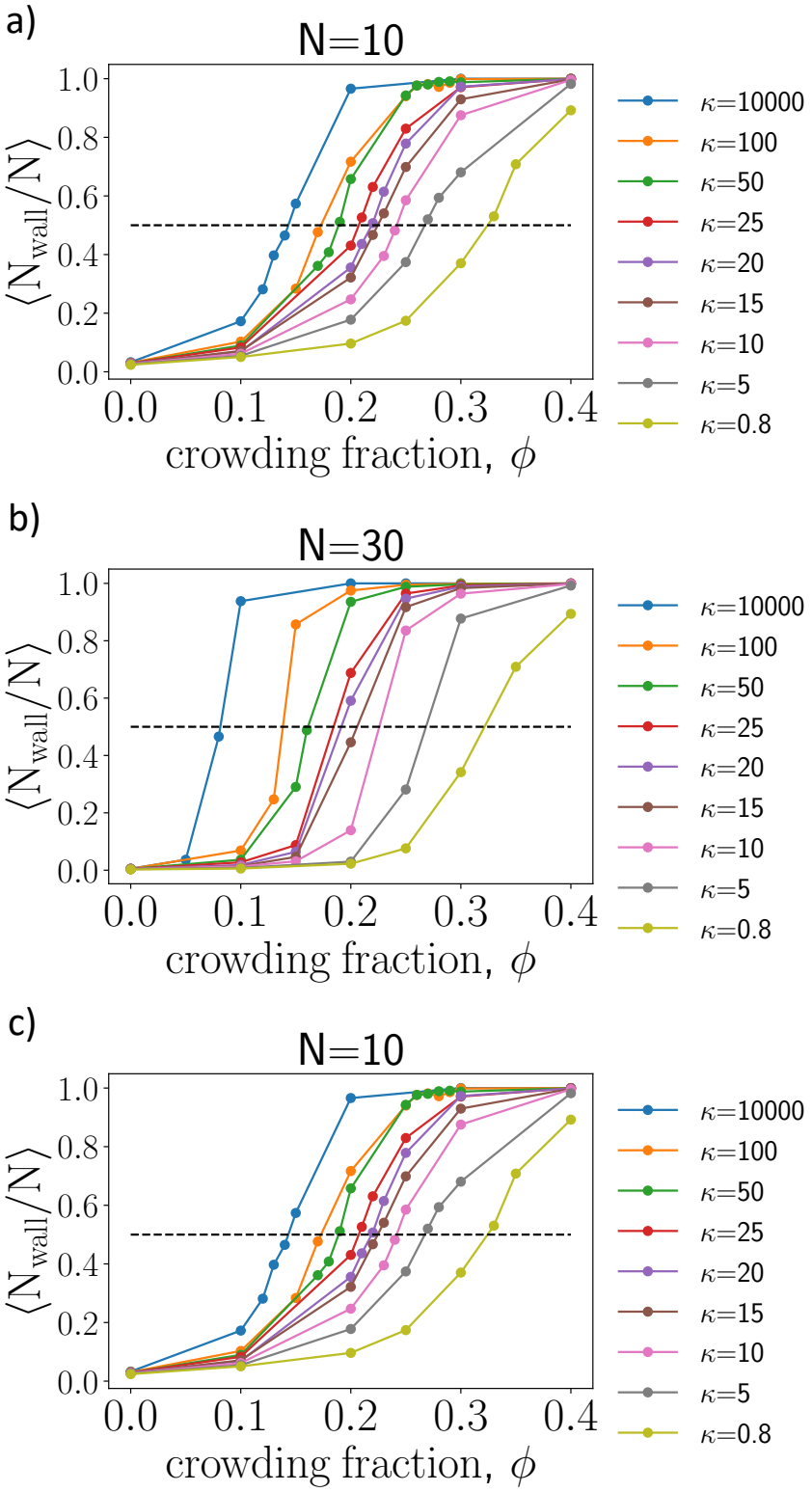


Figure 3.6: Average fraction of monomers near a wall as a function of the crowding fraction (ϕ) for different values of the bending stiffness (κ). Results for three polymer lengths ($N = 50$, 30, and 10) are shown. The size of the crowders is $\sigma_c = 0.8\sigma_m$.

Following Kampmann and Kierfeld, we analyzed $\Delta\phi_c = \phi_c - \phi_{c,\mathrm{rod}}$ for $N = 30$ and 10. We used ϕ_c obtained for $\kappa = 10^4$ as an estimate for $\phi_{c,\mathrm{rod}}$ and plotted $\Delta\phi_c$ as a function of κ/L, where L is the contour length of the polymer. These results are shown in Fig. 3.8b. In the regime in which $L < l_p$, the scaling behavior is expected to depend on the relation of the deflection length l_d to L. Although we do not know the range of our depletion interaction exactly, using $l \sim \sigma_c$ suggests that that $l_d \sim L$, placing us near the transition between two regimes. Based on the simulation results, at large values of κ/L, the results appear to be close to the scaling predicted for $L < l_d$, where $\Delta\phi_c \propto (\kappa/L)^{-1/2}$. The alternative scaling of $(\kappa/L)^{-1/3}$ is expected when $l_d < L < l_p$. Test: $l_d \lesssim L$ for $\kappa = 100$ and $N = 10$

3.3.4 Adsorption in spherical confinement

Confining semiflexible polymers in small regions can significantly impact their conformations,[113] but even modestly confined systems can have an impact because the bending energy of the adsorbed polymer, imposed by curvature of the surface, can compete with depletion interactions. We carried out simulations of a semiflexible polymer with crowding in a spherical domain with a diameter of 60σ. For comparison, the volume is about 13% larger than that of the cuboid in the previous sections, and the ratio of the surface area to volume is twice as large.

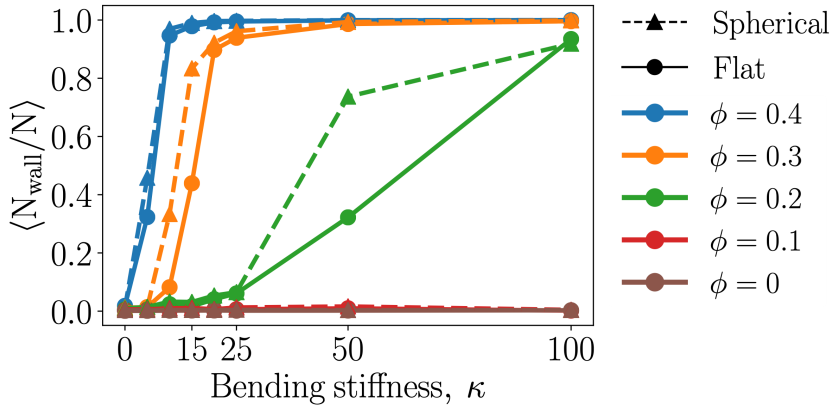


Figure 3.7: Average fraction of monomers near a wall as a function of the bending stiffness. Solid lines correspond to a flat wall and dashed lines correspond to spherical confinement with a radius of 30σ. The size of the crowders is $\sigma_c = 0.8\sigma_m$.

Figure 3.7 shows the average fraction of monomers near the spherically confining wall as a function of κ for various crowding fractions. Like the previous case with flat walls, contact of the polymer with the wall is promoted by larger values of both the crowding fraction and bending stiffness. In contrast with the previous case, the transition to strong adsorption occurs at smaller values of the bending stiffness. This is evident in the regions in which the polymer is partially adsorbed, where the fraction of monomers near the wall is larger for the spherically confined case than for case with flat walls. These differences are likely primarily because of the increased surface area to volume ratio, and hence the larger effective volume near the wall in the spherically confined case.

Figure 3.9 shows representative snapshots of the polymer in spherical confinement for different values of κ at $\phi = 0.4$. There is no adsorption at $\kappa = 0$, partial adsorption at $\kappa = 5$, and strong adsorption at $\kappa = 15$. The partially adsorbed polymer has a train with two tails that extend into the interior of the sphere. The strongly adsorbed polymer follows the contour of the sphere. The plots in Fig. 3.9 show the corresponding time-averaged distribution of the fraction of polymer beads as a function of the radial distance, r. For comparison, the results for the uncrowded system are also shown. For the uncrowded system, the fraction of monomers first increases with increasing radial distance because the volume grows with increasing r ($\propto r^2 dr$). The fraction of monomers decreases close to the wall because there is an effective repulsion between the wall and the center of mass of the polymer that arises due to the wall restricting conformations of the polymer. For $\phi = 0.4$, the polymer does not adsorb to the wall at $\kappa = 0$, but the distribution is shifted slightly toward larger values of r. This indicates that the polymer resides slightly closer to the wall on average. The effect of crowding is likely to make the effective interaction between the polymer and wall less repulsive.[102] A strong enhancement of the bead density is observed near the wall for $\kappa = 5$ (partial adsorption) and $\kappa = 15$ (strong adsorption). Like before, the adsorption of stiffer polymers is promoted because they lose less conformational entropy than their flexible counterpart upon adsorption.

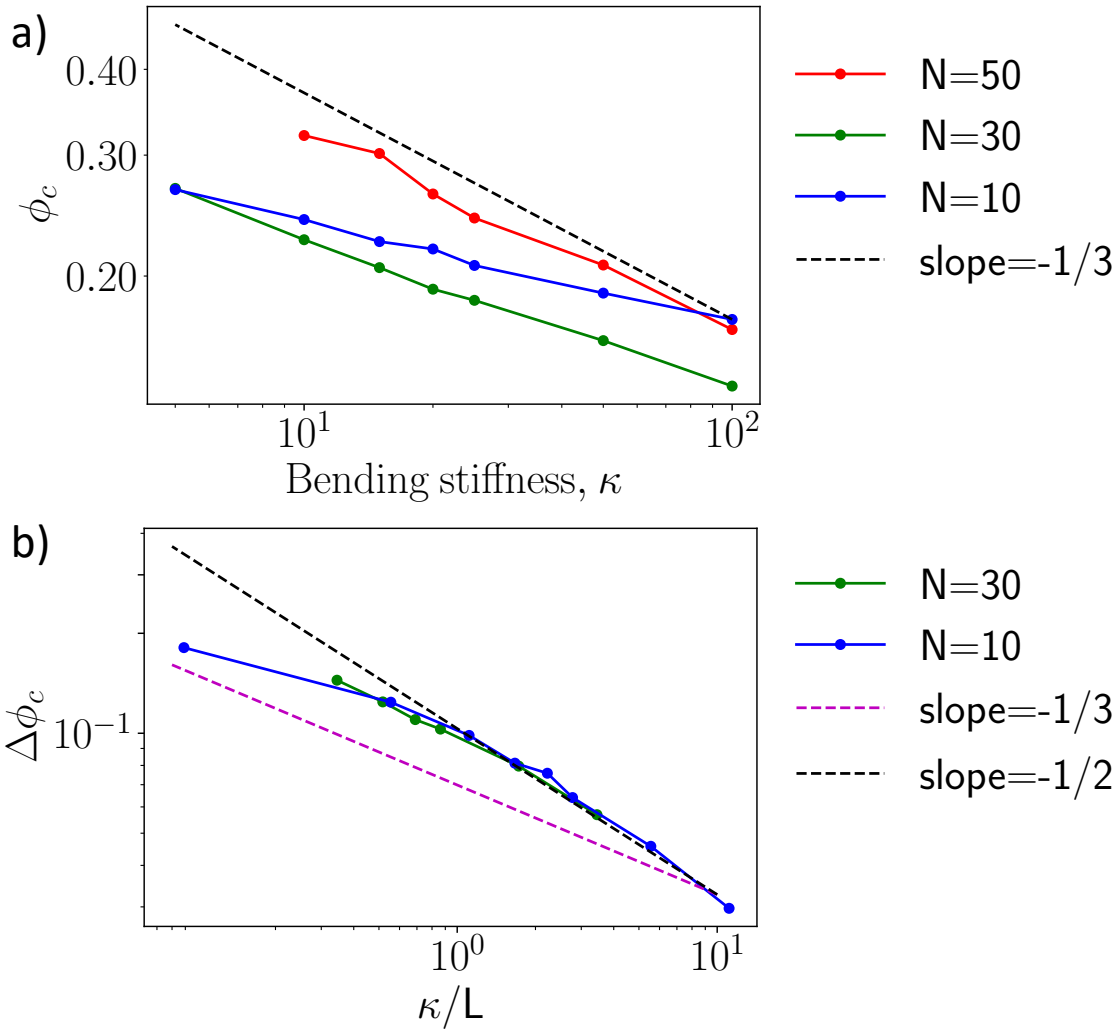


Figure 3.8: (a) Critical crowding fraction (ϕ_c) as a function of the bending stiffness (κ) for three polymer lengths. ϕ_c is defined as the crowding fraction at which on average 50% of polymer beads are in contact with a wall. (b) $\Delta\phi_c = \phi_c - \phi_{c,\text{rod}}$ as a function of κ/L for $N = 30$ and 10. Here $L = (N-1)\sigma$ is the contour length of the polymer.

The adsorption of a semiflexible polymer to a flat surface is promoted by increasing κ. Adsorption to a curved surface, however, introduces an additional competing energy contribution: the energetic penalty associated with bending an adsorbed semiflexible polymer along the contour of the surface. This suggests that adsorption should be suppressed at sufficiently large values of the bending stiffness.

To explore this, we carried out simulations at larger values of κ for the polymer in spherical confinement. Figure 3.10 shows the fraction of polymer beads near the wall for bending stiffness up to $\kappa = 2000$. There was no adsorption for $\phi \leq 0.1$ over the extended range of κ, but there were regimes of strong adsorption for $\phi = 0.2$, 0.3, and 0.4. For $\phi = 0.2$, this regime emerged for $\kappa > 100$. However, when κ was sufficiently large ($\kappa = 2000$), we observed another regime in which the polymer was not adsorbed. In contrast, the cases with $\phi = 0.3$ and 0.4 remained strongly adsorbed at $\kappa = 2000$. The case with $\phi = 0.2$ generates the weakest depletion interactions of the three cases. The non-adsorbed regime at high κ emerged due to the bending energy penalty imposed by being in close proximity to the curved wall. At $\phi = 0.3$ and 0.4, the depletion interactions were still sufficiently strong to promote adsorption, highlighting the interplay between crowding-induced depletion interactions and curvature of the surface.

3.4 Discussion

The adsorption of semiflexible polymers is a problem of fundamental interest that is relevant to cellular and cell-free biological systems, where macromolecular crowding can lead to depletion interactions that affect biopolymers such as DNA and actin. In this work, we used computer simulations to study the crowding-induced adsorption of a bead-spring model of a semiflexible polymer. Unlike most previous works on the adsorption of semiflexible polymers, we explicitly accounted for crowding particles, which were modeled as purely repulsive particles.

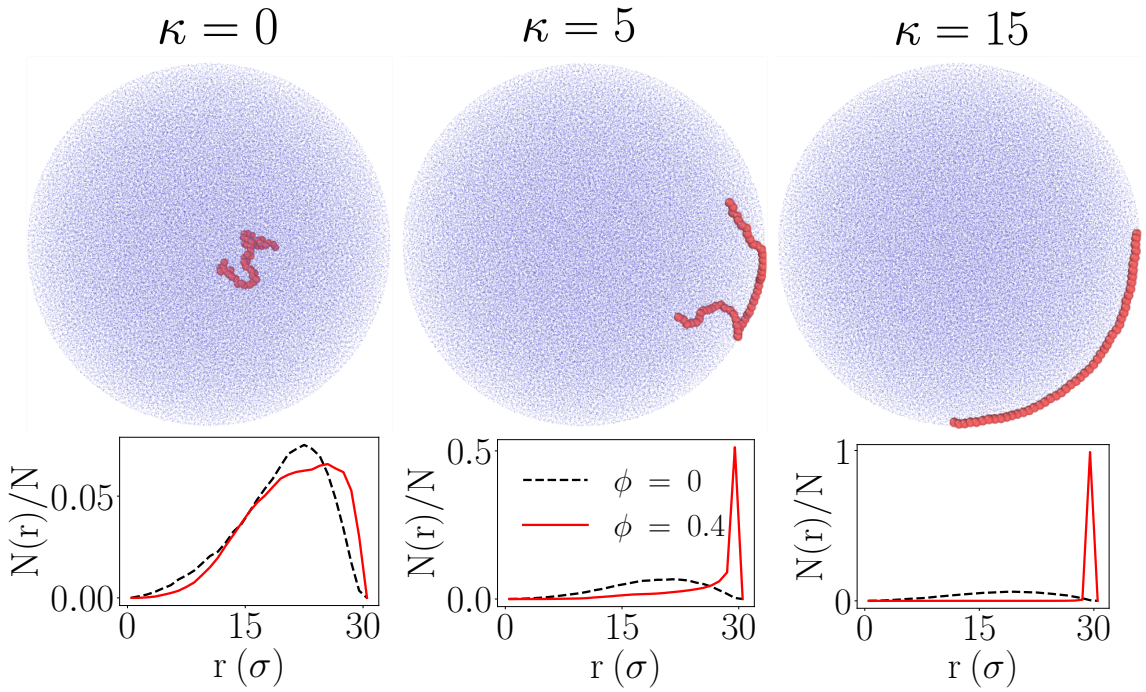


Figure 3.9: Snapshots of the polymer in spherical confinement with $\phi = 0.4$. Three values of the bending stiffness are shown. The plots below correspond to the same values of κ and show the average fraction of monomers, $N(r)/N$, as a function of the radial distance, r. For each, results are shown for $\phi = 0$ and 0.4.

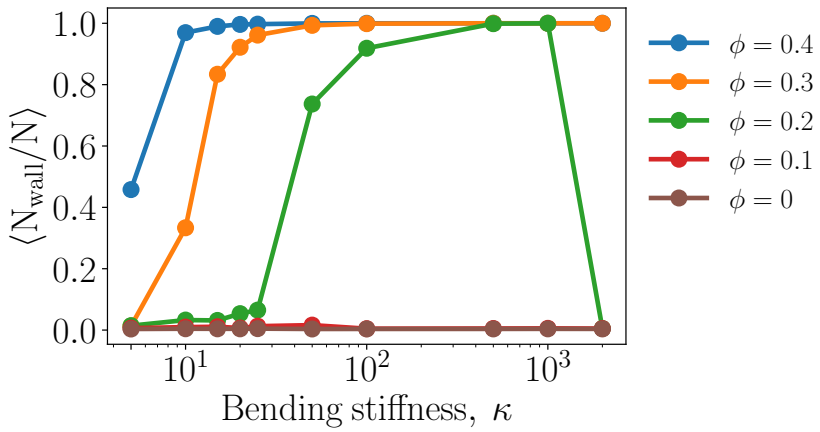


Figure 3.10: Average fraction of monomers near the wall in spherical confinement. The range of κ is larger than in previous figures.

Figure 3.1 demonstrates that polymer adsorption to a flat surface is promoted by stiffer polymers, smaller crowding particles, and larger volume fractions of crowders. With increasing bending stiffness (κ), we observed transitions from non-adsorbed states to partially and then fully adsorbed states. The transitions occurred at smaller values of κ as the volume fraction of crowders (ϕ) increased. Smaller crowding particles enhanced the effective polymer-wall attraction at the same volume fraction, shifting the adsorption transition to smaller values of the polymer stiffness. The transitions were accompanied by changes in the radius of gyration (Figs. 3.4 and 3.5) demonstrating that the polymer flattened against the wall while increasing in size in directions parallel to the wall.

Physically, adsorption of a polymer due to crowding results from an increase in the entropy of the crowders (due to an increase in the accessible volume) that exceeds the loss of entropy associated with the polymer. Semiflexible polymers are more likely than flexible polymers to adsorb to a wall because the conformational entropy of a polymer depends on its persistence length and stiffer polymers experience a smaller loss of conformational entropy upon adsorption.[40,69,74,103] Additionally, the strength of depletion interactions increases with increasing concentration of depletants.[48] Our results showed that crowding-induced polymer adsorption was promoted by larger values of κ and ϕ, which is consistent with these physical underpinnings of depletion interactions and polymer adsorption.

For partially adsorbed polymers, the bending rigidity of the polymer impacted the conformations of the polymer. Loops were observed when partial adsorption occurred at smaller values of κ, but not when the polymer was partially adsorbed at larger values. In this regime, only one or both ends of the polymer were not in contact with the wall. We also showed that curved surfaces, such as those observed in cells and vesicles, can give rise to behavior in which the number of monomers in contact changes nonmonotonically with κ, indicating a desorption transition at large κ. In this regime, the energetic cost of bending the polymer competes with the crowding- and stiffness-dependent depletion interactions.

Figure 3.8 shows the relation between the threshold crowding fraction for adsorption (ϕ_c) and the bending stiffness of the polymer for different polymer lengths. Asakura-Oosawa theory predicts that $u_{\min} \propto -\phi$, but it is formally valid only in the limit of dilute crowding ($\phi \ll 1$) and small crowders ($\sigma_c \ll \sigma_m$). Neither of these conditions is satisfied in this study, and theory and simulations predict nonlinear relationships between ϕ and $u_{\min}$ in crowded conditions.[77] However, the scaling relationships in Fig. 3.8 appear consistent with existing theory when κ is large (and ϕ is small), suggesting a linear relationship between ϕ and $u_{\min}$ in this regime. Given the computational constraints of simulating large numbers of crowding particles, it is challenging to assess the nonlinear effects when ϕ is larger. However, the results hint at nontrivial effects associated with explicit crowders: There is no adsorption for $\phi \leq 0.4$ for $N = 50$ when κ is small. In this regime, we expect adsorption to be suppressed by crowding-induced attractions between different segments of the polymer, which also cause a decrease in the radius of gyration. It is also interesting that the shorter polymers do not exhibit a regime of scaling consistent with $\phi_c \propto \kappa^{-1/3}$, even at smaller values of κ. These will be interesting topics to study in the future and may help to shed insight into the role of crowding on polymer adsorption.

In this work, we considered monodisperse crowding particles and static walls. In reality, cellular environments are crowded with macromolecules of different shapes and sizes, which can can give rise to unexpected effects on the shapes of semiflexible polymers[64] and can affect the depletion interaction experienced by polymers.[21,62] Additionally, cell membranes are deformable, and adsorption of a semiflexible polymer can lead to an interplay between the shapes of the membrane and polymer due to competing bending energies.[95] In the future, it would be interesting to study the effect of crowder polydispersity and membrane flexibility on the adsorption of semiflexible polymers in crowded environments.

The cellular environment is replete with biopolymers that have a variety of persistence lengths. Our work sheds light on how crowding and the presence of surfaces – both features of cells – affect the spatial organization of biopolymers

through their interactions with surfaces. In the context of cell-free systems, our work provides guidance on how crowding can be used to rationally organize components with different persistence lengths.

Chapter 4

Crowding-induced spatial organization of gene expression in cell-sized vesicles

This work was carried out by Gaurav Chauhan, S. Elizabeth Norred, Patrick M. Caveney, Rosemary M. Dabbs, C. Patrick Collier, Steven M. Abel and Michael L. Simpson. GC and SMA designed the computer simulations which were performed by GC. SEN, PMC, CPC and MLS designed the experiments, which were performed by SEN and RMD. GC and SEN wrote MATLAB and python scripts for image segmentation, data extraction, and data analysis. GC, SEN, CPC, SMA and MLS analyzed the data and wrote the manuscript which is adapted in this chapter here.

4.1 Introduction

Gene expression is self-organized in both eukaryotic and prokaryotic cells.[114–116] Despite the lack of a nuclear membrane, many prokaryotes such as *E. coli* show spatial organization of gene expression where different components localize in different

microenvironments. Superresolution microscopy in *E. coli* shows that the DNA-rich nucleoid region is localized in the midcell whereas most ribosomes are spatially segregated from the nucleoid region and are localized at the endcap poles (Figure 4.1).[114] This spatial segregation creates different expression behavior inside and on the nucleoid periphery. In *E. coli*, the actively transcribing genes are relocated to the nucleoid periphery closer to the pool of ribosomes.[116] It has also been speculated that the chromosome template provides a means to spatially organize gene expression in prokaryotes, since transcripts often remain localized near their origin.[115] Understanding the role of spatial organization on gene expression in cells is important but remains difficult to study due to the inherent challenges in manipulating spatial organization in live cells.

Cell-free protein synthesis platforms provide a simpler experimental system to study gene expression because of their open nature and the ability to manipulate the physical environments. Cell-free systems have hence been extensively used to understand cellular behavior and specifically study gene expression.[47,84] A major limitation of cell-free systems is the inability to mimic the spatial organization observed in cells. Cell-free systems have been shown to spatially self-organize in some systems and can mimic some physical features of cells.[47,117] However, more closely mimicking cell-like spatial organization of gene expression components in cell-free systems has remained elusive.

The intracellular environment is crowded with macromolecules such as ribosomes and proteins, and the high volume fraction occupied by crowding molecules (30-40%) can result in attractive depletion interactions between molecules as well as between biomolecules and a confining surface.[17] Crowding-induced depletion interactions have been attributed to play a major role in the compaction of chromosome[13] as well as on cellular organization.[17] Gene expression kinetics has been studied using cell-free systems and crowding has been shown to induce spatial correlations on transcription and also affect gene expression noise.[47,84] Simulation studies have shown that crowding

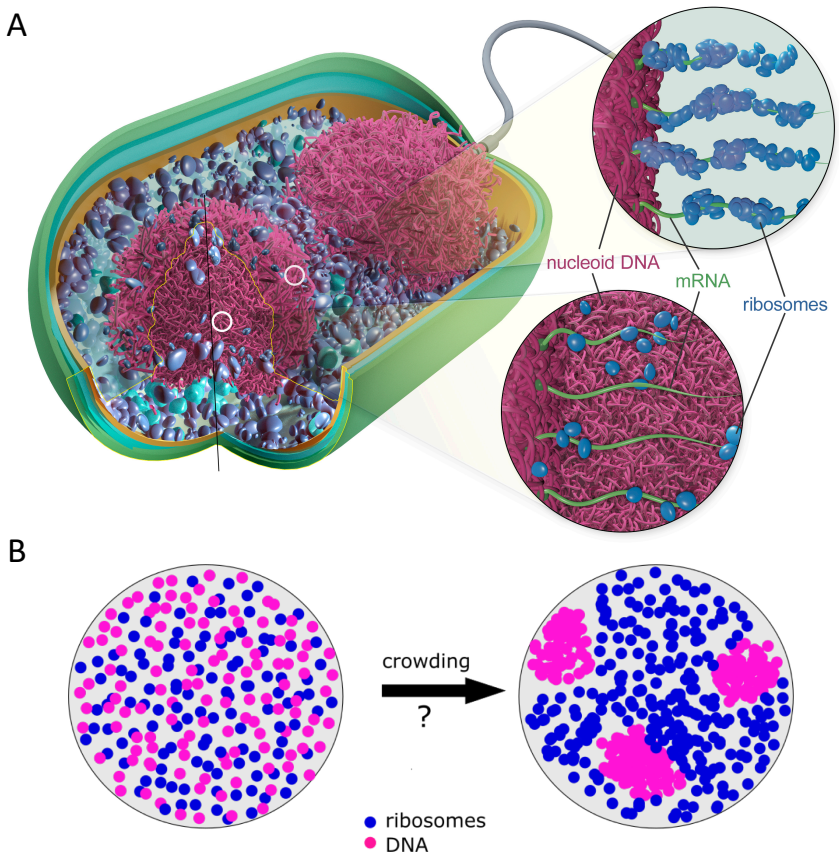


Figure 4.1: A) Schematic of an *E. coli* cell showing spatial organization of DNA and ribosomes. The nucleoid DNA is in the middle of the cell and most ribosomes are excluded from the DNA-rich nucleoid region. B) Homogeneously distributed DNA and ribosomes in a cell-sized vesicle (left) and spatially organized DNA and ribosomes (right). This chapter explores the question: Can crowding lead to spatial organization of DNA and ribosomes in cell-sized vesicles?

can lead to attractive depletion interactions between two polymers, and between a polymer and a wall.[102,118]

In this work, we demonstrate, using computer simulations and cell-free experiments, how crowding in cell-relevant confinement in vesicles can be used to control spatial organization of gene expression akin to prokaryotic cells (Figure 4.1). To understand self-organization in crowded and confined environments, we first used computer simulations to study the spatial organization of model DNA plasmids in the presence of macromolecular crowder in spherical confinement. These simulations guided imaging experiments of fluorescently-labelled DNA and ribosomes in cell-sized vesicles and showed that crowding in vesicles can lead to the spatial segregation of DNA and ribosomes. We then used a two compartment reaction kinetics model to study the effects of crowding-induced segregation of DNA and ribosomes on protein abundance. The effects of this spatial segregation on gene expression were then studied using a dual mRNA/protein reporter assay at different concentrations of the macromolecular crowder Ficoll-70. Our work here would help to understand the role of crowding and cell-sized confinement on spatial organization of gene expression components and the resultant effects on gene expression.

4.2 Results

We used Langevin dynamics computer simulations to guide experimental efforts to control the spatial organization of DNA and ribosomes in vesicles using macromolecular crowding. We utilized a coarse-grained description of the system, with the DNA plasmids modeled as a semiflexible ring polymer. The macromolecular crowder Ficoll-70 was modeled as a purely repulsive spherocylindrical particle[119,120] as shown in Figure 4.2. In this model, all components interacted via the purely repulsive Weeks-Chandler-Andersen (WCA) potential (U_{ij} in Figure 4.1), thereby accounting for the volume excluded by constituents of the system. The effect of confinement was incorporated by using a confining sphere with purely repulsive walls (Figure

4.1). Interactions with the spherical wall were modeled using the purely repulsive 9-3 Lennard-Jones potential (U_{iw} in Figure 4.1) as described in previous works.[102,118] We studied the effect of crowding on equilibrium properties of the model plasmid by varying the number of crowding particles (N_c) in the system. The volume fraction occupied by crowders is $\phi = N_c \times V_c/V_{sphere}$ where V_c and V_{sphere} are the volume of a crowding particle and the confining sphere, respectively.

The simulations revealed that the spatial distribution of the model DNA plasmid is sensitive to the level of crowding (Figure 4.2B). At low crowding fraction (ϕ <2.5%), the polymer density was depleted near the confining surface since that would result in lowering of the conformational entropy of the polymer. The polymer instead localized away from the confining surface and in the bulk of the sphere at low crowding. As crowding is increased further, the attractive depletion interactions between the polymer and the wall became strong enough to compensate for the loss of conformational entropy of the polymer near the wall and the polymer became partially adsorbed (ϕ=5%) and fully adsorbed (ϕ=10%) to the confining surface as can also be seen from the radial distributions (Figure 4.2B). At high crowding, the polymer adsorbed to the walls of the confining surface resulting in an increase in volume accessible to crowders and thereby increasing the overall entropy of the system.

Next, we fluorescently imaged DNA by separately encapsulating plasmid DNA in vesicles crowded with Ficoll-70. Briefly, polydisperse vesicles, containing the DNA plasmids with the Pico488 dye, were fabricated using a shearing method adapted from Nishimura et al.[121]. We observed that the DNA plasmids remained uniformly distributed at low levels of crowding (Ficoll-70 concentration of 0 and 10 mg/mL) and preferentially localized near the walls of the vesicles at high crowding (Figure 4.2C). This is consistent with the simulation predictions in Figure 4.2B, where crowding-induced depletion interactions due to spherocylindrical crowder resulted in adsorption of model DNA plasmid to the confining surface.

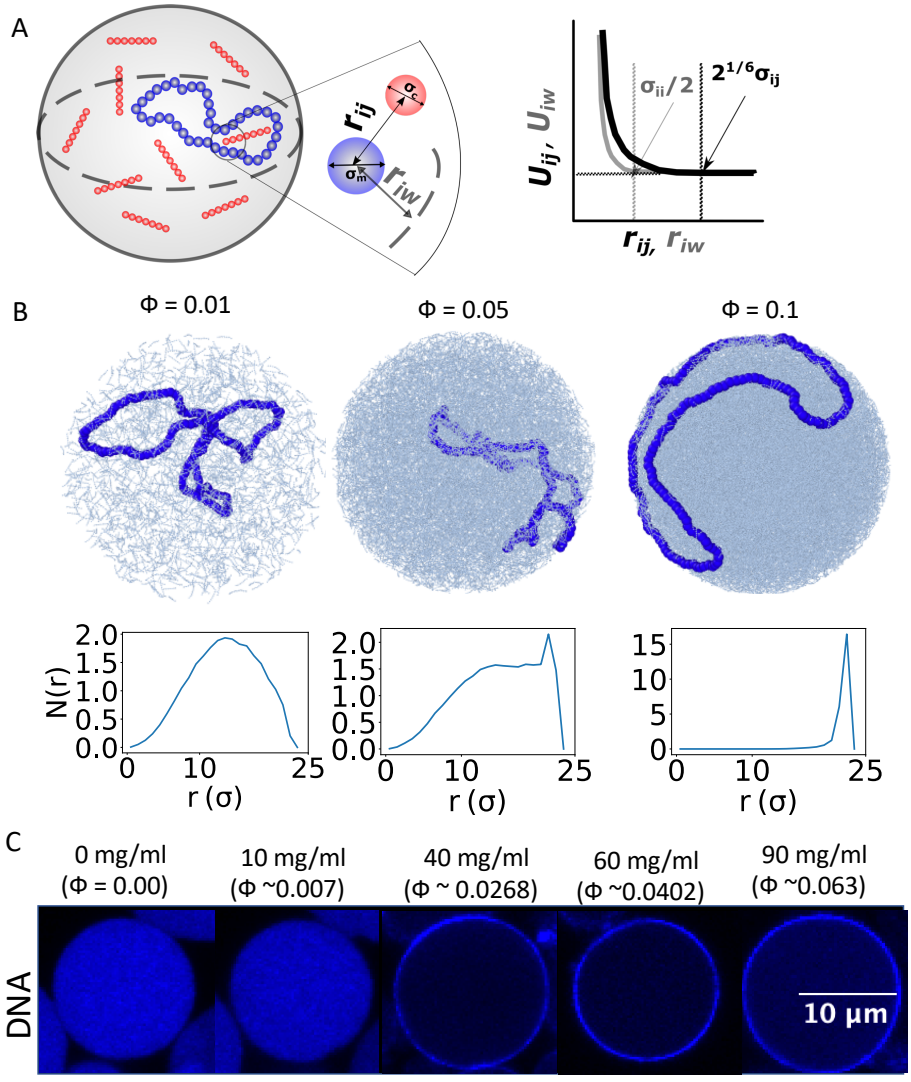


Figure 4.2: A) Schematic of the computational model showing DNA plasmids and spherocylindrical crowders in spherical confinement. Particle-particle interaction potentials are given by the purely repulsive WCA potential U_{ij}, and particle-wall interactions are given by the purely repulsive 9-3 LJ potential U_{iw}. B) Representative snapshots of the plasmid polymer and crowders in spherical confinement (top) along with the radial distribution of the monomers N(r) as a function of radial distance r from the center of sphere (bottom). Different crowding fractions (ϕ) are shown. C) Confocal images of DNA, fluorescent labelled with Pico488, in cell-sized vesicles. The volume fraction ϕ in experiments is estimated from the partial specific volume of Ficoll-70.

Since gene expression is sensitive to the spatial organization of the ribosomes, we next imaged fluorescently-labelled ribosomes separately in cell-sized vesicles at different crowder concentrations. Ribosomes remained uniformly distributed in vesicles at all crowding levels (Figure 4.3A). Figure 4.3B plots and compares the fraction of fluorescence near vesicle walls for both ribosomes and DNA. We observed that ribosomes and DNA show different spatial organization at high crowding: most ribosomes remain in bulk whereas the DNA gets spatially localized near the vesicle membrane.

Next, we used a two compartment reaction kinetics model to study the effects of crowding-induced spatial organization on gene expression (Figure 4.3C). The vesicle was divided into a bulk and a wall-associated compartment. The DNA was either uniformly distributed across the vesicle or localized in the wall-associated compartment while the ribosomes were uniformly distributed. Consistent with a previous study in prokaryotic cells and mRNA imaging experiments here, mRNA was assumed to colocalize with the DNA in our simulations. Crowding also results in substantial decrease in the diffusion coefficients of the reactants,[44] and hence the exchange rate of ribosomes between the compartments was decreased to account for the effects of crowding on diffusion. The localization of DNA to the wall at sufficiently low exchange rate resulted in lower protein abundance as compared to the uniform distribution since most ribosomes in bulk are spatially segregated from the mRNAs in the wall (Figure 4.3D). As the exchange rate was slowed further, there was even fewer ribosomes capable of translating in the wall compartment. In the limiting case of no exchange between the two compartments, only the ribosomes in the wall-associated compartments contributed to the protein production and hence protein abundance scaled as R^2 instead of the expected R^3 scaling (Figure 4.4).

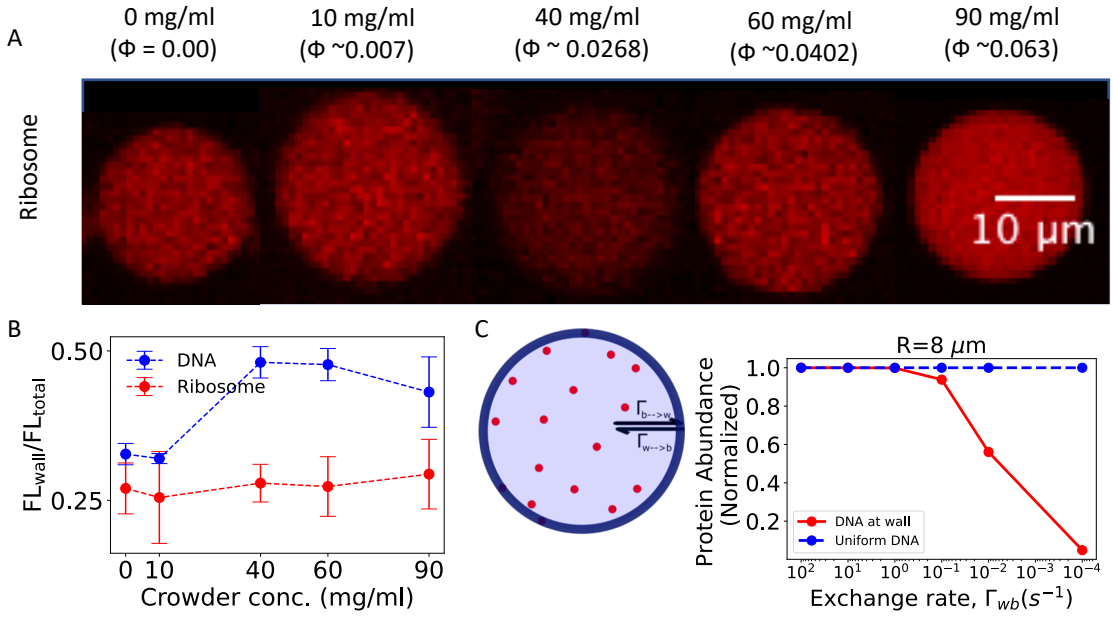


Figure 4.3: A) Confocal images of representative vesicles with fluorescently-labelled ribosomes at different Ficoll-70 concentrations. B) Fraction of fluorescence in the wall region as a function of crowder concentration for DNA and ribosomes. C) Schematic of the two compartment reaction kinetics model of gene expression, where ribosomes can be exchanged between the bulk compartment and the wall-associated compartment. Results of the simulation of the two compartment model showing protein abundance as a function of exchange rate from wall to the bulk compartment (Γ_{wb}). Results for the two different spatial organizations of the DNA are shown.

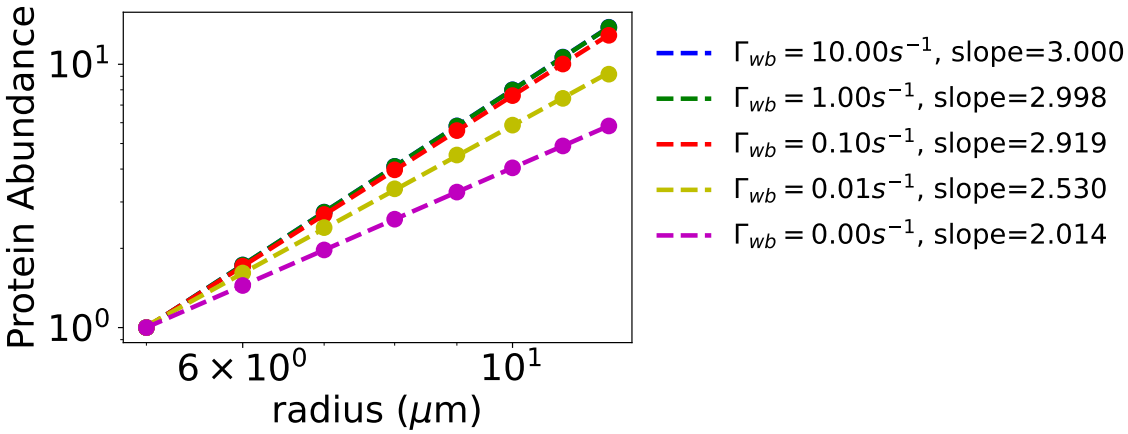


Figure 4.4: Protein abundance as a function of radius for different exchange rates of ribosomes. The legend denotes the exchange rates of ribosomes from the wall compartment to the bulk compartment (Γ_{wb}) and the associated slopes for the protein abundance vs radius plots on log-log scale.

We then studied gene expression in crowded vesicles by tracking transcription and translation using a coupled mRNA/protein reporter technique described in previous works.[84,122–124] Briefly, the RNA aptamer Spinach2[125] was inserted downstream of a gene coding for a red fluorescent protein, mCherry[126] (Figure 4.5A). Spinach2 fluoresces in the green range upon hybridization with the fluorophore DFHBI-1T. The Spinach2 fluorescence intensity was indicative of the mRNA populations, while the mCherry fluorescence intensity was indicative of the protein population. Ficoll-70 at concentrations from 0-90 mg/mL was added to the cell-free protein synthesis (CFPS) reactions. Polydisperse vesicles containing the CFPS reactants were fabricated using a shearing method adapted from Nishimura et al.[121] (Figure 4.5B). The mean mRNA and expressed protein populations were inferred from the mean Spinach2 and mCherry fluorescence levels measured across the population of vesicles.

We observed that, similar to DNA, the mRNA was uniformly distributed throughout the vesicle at low crowding and localized near the vesicle walls at high crowding (Figure 4.5C). In contrast, protein was distributed throughout the vesicle at all crowding levels (Figure 4.5D). Figure 4.5D shows the three dimensional reconstruction of an individual vesicle showing the spatial distribution of mRNA and protein. Next, we compared the protein and mRNA abundance across different crowding fractions by inferring mean Spinach2 and mCherry fluorescence across the population of vesicles in the 14-16 μm diameter range (Figure 4.5F). The mRNA abundance first decreased with an increase in crowding, showed minimum at 40 mg/mL crowder concentration and then increased with an increase in crowding. In comparison to the mRNA, protein abundance decreased dramatically at high crowding levels. This is consistent with the simulation predictions in Figure 4.3C) where the two compartment reaction kinetics model showed that spatial segregation and slow diffusion would result in a decrease in protein abundance.

Next, we quantified translation efficiency, defined as protein abundance for a unit mRNA abundance, and observed that the translation efficiency decreased at high crowder concentrations (Figure 4.5G). Consistent with previous studies,[45] we also

observed maximum protein abundance at intermediate crowding (10 mg/mL Ficoll-70 concentration). We then characterized the size dependence of vesicles of radius R on protein abundance P ($P \propto R^m$) with scaling exponent m given by the slope of the protein abundance vs radius plots on log-log scale (Figure 4.5H). We observed the scaling exponent to be close to 3 for crowder concentrations of 0, 10, 40, 60 mg/mL, as observed before for the PURE system.[127] In contrast, we observed an anomalous scaling exponent close to 2 for the crowder concentration of 90 mg/mL (Figure 4.5I). This is consistent with the model predictions and can be explained by the observation that with slow diffusion and spatial organization of DNA at the wall, most of the translation is carried out by ribosomes near the walls of the vesicle. Hence, we are able to spatially segregate DNA and ribosomes at high crowding and obtain low efficiency translation. In contrast, the colocalizatipn of DNA and ribosomes throughout the vesicle at low crowding results in high efficiency translation.

4.3 Discussion

Cell-free systems are an important platform for studying mechanisms in living systems and for standalone applications, such as sensors and in manufacturing of therapeutics.[128] Because of the open nature of the platform and the ability to manipulate the system, cell-free systems are also used to study cellular mechanisms such as the role of macromolecular crowding on gene expression bursting.[47,84] A major limitation of the current state-of-the-art in cell-free synthetic biology is the inability to spatially organize biological components and mimic spatial organization observed in live cells. In this work, we used macromolecular crowding in cell-sized vesicles to spatially organize gene expression. This organization of gene expression components is conceptually similar to how they are organized in bacterial cells including *E. coli* and *B. Subtilis*.

We first used Langevin dynamics computer simulations to show that crowding by Ficoll-70 can lead to the adsorption of a model DNA plasmid to the walls of

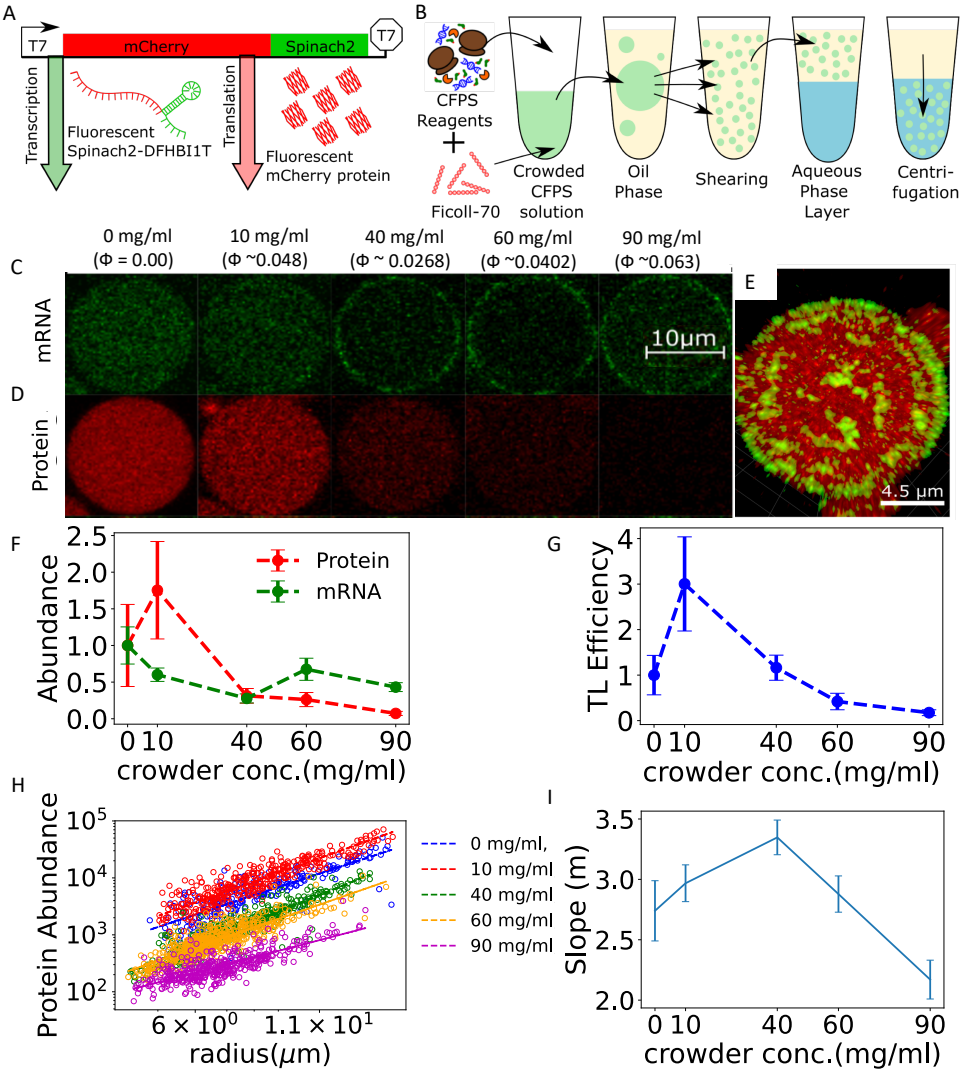


Figure 4.5: A) The plasmid used for cell-free experiments included a T7 promoter, a gene coding for mCherry, and a sequence encoding an untranslated RNA aptamer, Spinach2. B) Fabrication steps for forming vesicle microreactors. Cell-free reagents and Ficoll-70 were placed in an oil phase solution containing phospholipids, sheared into polydisperse vesicles by vortexing, layered onto a balanced aqueous solution, and centrifuged into the solution. (C and D): Representative vesicles demonstrating spatial distribution of mRNA (c) and protein (D) at different crowder concentrations. E) 3-D reconstruction of an individual vesicle showing the spatial distribution of mRNA and protein. F) mRNA and protein abundance as a function of crowder concentration for vesicles with a diameter of 14-16 μm. G) Translation efficiency as a function of crowder concentration for vesicles with a diameter of 14-16 μm. H) Protein abundance as a function of radius for different crowder concentrations. I) The exponent of the protein abundance versus radius scaling as calculated by linear regression. The error bars denote the 95% confidence intervals.

the spherical confinement. Next, we imaged DNA and ribosomes to observe their spatial distribution at different concentrations of Ficoll-70. The DNA was uniformly distributed at low levels of crowding but became localized near the vesicle walls at high crowding. In contrast, ribosomes remained uniformly distributed at all crowding levels. This spatial organization is akin to the DNA-ribosome segregation observed in bacterial cells like *E. coli*. The resultant effect of crowding on gene expression was monitored by dual mRNA/protein fluorescence reporters. The concentration of Ficoll-70 affected mRNA and protein expression, and at high levels of crowding, lead to a decrease in translational efficiency. This result is consistent with predictions of computer simulations, which accounted for the spatial segregation of DNA and ribosomes, along with decreased diffusion coefficients at high levels of crowding.

The cell-free results reported here have important consequences for understanding spatial organization of gene expression in bacteria. Our cell-free results help to shed light on the role of spatial organization and resource availability on gene expression. Depending on the degree of DNA-ribosome segregation observed in bacteria, different localization patterns of transcription are observed. For instance, E. coli has significant DNA-ribosome segregation and transcription occurs predominantly at the nucleoid periphery (close to the ribosome-rich region). In contrast, C. crescentus does not exhibit DNA-ribosome segregation and transcription occurs throughout the nucleoid2. Based on our work, we can speculate that access to ribosomes is an important factor in spatially organizing transcription in the prokaryotic nucleoid.

The realization of an artificial cell has been a long-standing goal of the synthetic biology community. Our work here demonstrates a cell-free platform that can mimic the gene expression spatial organization observed in cells. We hope our work here will contribute to future efforts towards the design of an artificial cell and more advanced experimental cell-free platforms to probe the effects of spatial organization on gene expression.

4.4 Methods

4.4.1 Coarse-grained simulation of DNA plasmid and crowder in spherical confinement

We carried out Langevin dynamics simulation of a model DNA plasmid and crowder molecules in spherical confinement. The DNA plasmid was modeled as a semiflexible ring polymer of 184 beads with size of each bead of the polymer chosen to be 7 nm (1 σ). Adjacent beads of the polymer were connected via the FENE potential while the stiffness of the polymer was maintained by using a cosine bending potential. Since the reported shape of the Ficoll-70 molecule is spherocylindrical with an aspect ratio of 7:1,[119,120] we modeled the crowder molecule as an oligomer of 7 beads with a very stiff bending potential, to give it a spherocylindrical shape. The size of each bead in the 7-mer oligomer was chosen to be 28 Å (0.4 σ) with the end-to-end length of 196 Å. The volume fraction of crowders in the confined sphere of radius R = 23 σ was $\phi = N_{oligomers} \times 7 \times (0.2)^3/R^3$. All particles (crowders and polymer beads) interacted via the short-ranged and purely repulsive Weeks-Chandler-Andersen (WCA) potential, and particles interacted with the confining surface via the purely repulsive 9-3 Lennard-Jones potential. The Langevin equation was integrated forward in time using the velocity-Verlet algorithm in LAMMPS and the resulting trajectories were visualized using OVITO.

4.4.2 Reaction kinetics model

We developed a two compartment reaction kinetics model to study the role of spatial organization and diffusion on protein abundance. As shown in Figure 4.3 C, vesicle was divided into two compartments: a wall-associated and a bulk compartment. The DNA was either uniformly distributed in the vesicles or was only localized in the wall-associated compartment. The following reactions can take place in the two compartments:

$$\text{DNA} \xrightarrow{\alpha} \text{mRNA}$$
$$\text{mRNA} + \text{Ribosome} \xrightarrow{k_b} \text{C}$$
$$\text{C} \xrightarrow{k_p} \text{mRNA} + \text{Ribosome} + \text{protein}$$

Ribosomes are exchanged from the wall compartment to the bulk compartment by a rate Γ_{wb} and from the bulk compartment to the wall compartment by a rate Γ_{bw}. The two rates are constrained such that: $\frac{\Gamma_{bw}}{V_{wall}} = \frac{\Gamma_{wb}}{V_{bulk}}$, where V_{wall} and V_{bulk} are the volume of the wall-associated and bulk compartments. The system of ordinary differential equations (ODEs) are solved by using a custom code in Python.

4.4.3 Experimental methods

Spinach2, a plasmid vector coding for mCherry and a downstream fluorescent mRNA aptamer,[123,124] was expressed in order to simultaneously track transcription and translation outputs. The plasmid pRSET-b-mCherry-Spinach2 transcribes from a T7 polymerase promoter to create a transcript with a translated region coding for mCherry, followed by an untranslated aptamer tag which fluoresces after folding and binding with the fluorophore DFHBI-1T23 ((Z)-4-(3,5-difluoro-4-hydroxybenzylidene)-2-methyl-1-(2,2,2-trifluoroethyl)-1H-imidazol-5(4 H)-one, Lucerna, Inc). A commercial cell-free protein synthesis kit (PURExpress, NEB) was used to express the plasmid in the presence of DFHBI-1T and a crowding molecule, Ficoll-70 (Sigma-Aldrich).

Vesicles containing the cell-free expression system and added components (the "Inner Solution" were prepared by a shearing method adapted from Nishimura et al.[121]. In summary, vesicles are prepared by assembling the cell-free reaction mixture, plasmid, DFHBI-1T, sucrose (to aid with visualizing vesicles), and Ficoll-70. Concentrated Ficoll-70 was added at a final concentration from 0-90 mg/mL. The Inner Solution is vortexed in a paraffin oil solution containing phospholipids (POPC, Avanti Polar Lipids) to create a polydisperse population of water-in-oil droplets. This paraffin oil mixture with droplets is layered on to an aqueous "Outer Solution" and

then centrifuged for 20 minutes at 4C at 14k g. The Outer Solution is balanced with the inner solution, containing small molecules found in the PURE system reactions.[129,130] Vesicles are collected by pipetting and are prepared for microscopy by placing 10 μL of vesicles in Outer Solution between two glass coverslips separated by a 2 mm PDMS spacer. Most vesicle diameters range from 5-30 μm.

Vesicles were observed while resting on a coverslip, using a (Zeiss LSM 710 Axio Observer) confocal microscope to image every 5 minutes for 6 hours. A 20x objective (Zeiss Plan Apochromat 20x/0.8 M27) was used for the timescale data, followed by a 63x objective (Zeiss Plan Apochromat 63x/1.40 Oil DIC M27) for a more detailed image of fluorescence distribution at the end of the experiment. The Spinach2-DFHBI-1T signal was measured using a 561 nm laser from 488/536 nm Ex/Em. The mCherry was measured using a 561 nm laser from 561/637 nm Ex/Em. Brightfield images were also acquired contemporaneously. For each timepoint, the vesicles were imaged using a z-stack capture, using 14 images per slice at 2 um increments. The images were analyzed using ImageJ and custom MATLAB code to detect vesicle size and location and to acquire intensity values for Spinach2-DFHBI-1T and mCherry from individual vesicles over time.

To determine spatial DNA distribution in the vesicles, vesicles were prepared as normal with the 0.25 µL of the 200x fluorophore Pico488 (Lumiprobe) in the Inner Solution, instead of DFHBI-1T. These vesicles were imaged using confocal microscopy, using a 63x objective and 561nm laser at 488/536 Ex/Em. Ficoll-70 was added at a final concentration at 0, 10, 20, 30, 40, 60, and 90 mg/mL. A control reaction containing no DNA was also performed. Z-stack renderings and cross-sections in the middle of vesicles were used to characterize DNA distribution within vesicles.

Cell-free protein synthesis experiments were performed for each Ficoll-70 crowder concentration of 0, 10, 40, 60, and 90 mg/mL. Built-in functions in ImageJ and custom MATLAB code were used to identify the boundaries of vesicles in a brightfield view, select regions of interest around each vesicle, and extract fluorescence information

from each ROI. For an individual vesicle in each experiment, mRNA and protein abundance was extracted at the last timepoint for the detected vesicles.

Chapter 5

Conclusions

The presence of macromolecules such as proteins and ribosomes can significantly crowd the intracellular environment. Large volume fractions of crowding molecules can result in depletion interactions that can affect the conformations and spatial organization of biopolymers. In this thesis, we used computer simulations to study impact of crowding on polymer-polymer and polymer-wall interactions. We also studied how crowding can be used to spatially organize gene expression in cell-free systems and studied the role of crowding-induced spatial correlations on gene expression noise.

We first studied a flexible ring polymer in the presence of spherical crowding particles and observed that crowding could lead to compaction of the ring polymer and weak aggregation between two ring polymers at high crowding. In the presence of a flat confining surface, the polymer was partially adsorbed onto the wall at intermediate crowding and fully adsorbed at high levels of crowding. We calculated the potential of mean force (PMF) for polymer-polymer and polymer-wall interactions as a function of crowding fraction and observed that the polymer-wall interactions were much stronger than polymer-polymer interactions. We also observed, both from PMF calculations and unbiased simulations, that the attractive polymer-wall

interactions emerged at much smaller crowding fractions as compared to the polymer-polymer interactions. Our work has implications in understanding the role of depletion interactions on spatial organization and conformations of a flexible polymer in the crowded cellular environment.

We also observed that crowding resulted in different conformations of the polymer depending on the presence/absence of confining wall. Crowding in the presence of a flat wall resulted in adsorption and flattening of the polymer onto the wall, and an extension of the polymer chain. In contrast, crowding in the absence of a confining surface resulted in compaction of the polymer chain. Thus, crowded environment can lead to different conformations in the bulk vs the confining surface and that can result in different reaction kinetics by limiting/promoting access of reactants to the polymer. For instance, DNA plasmids compacted via the polycation spermine showed no transcription activity while the DNA in extended conformations adsorbed on lipid vesicles showed transcriptional activity similar to that in aqueous solutions.[101]

In this work, we only considered excluded volume interactions between the polymer beads but it would be interesting to study how crowding would affect polymer-polymer and polymer-wall interactions for polymers with "sticky" interactions. Presumably, it would favor the polymer-polymer interactions over polymer-wall interactions. In some cases with weak "sticky" interactions between the two polymers, polymers may remain as a dimer/multimer in the bulk but crowding-induced adsorption to the wall might result in demixing of the polymer chains. Another interesting avenue for future work would be on understanding the role of semiflexibility of polymers on crowding-induced depletion interactions. While we have studied the role of bending stiffness on polymer adsorption to wall in Chapter 3, it would also be interesting to study how bending stiffness would affect polymer-polymer interactions in a crowded environment.

In light of our results, it is imperative to ask why does a bacterial chromosome condense in the midcell and not adsorb on the cell membrane. The answer to that question might lie in the fact that a cellular environment is not just crowded

by macromolecules but also has proteins modulating interactions between different segments of the chromosome polymer. Different nucleoid-associated proteins (NAPs) can act as DNA-bridging proteins and have been implicated in playing a role in condensing the chromosome polymer.[32] In order to accurately understand the role of crowding on conformations of chromosome inside cells, future studies studying role of crowding on chromosome organization should also incorporate the role of NAP-mediated intra-chromosome interactions.

The cellular environment is replete with polymers of varying persistence lengths: for example, actin has a persistence length of 17.7 μm[131] and DNA has a persistence length of $\sim$ 55 nm. We studied the role of bending stiffness on crowding-induced adsorption of a semiflexible linear polymer. We observed that the adsorption of a semiflexible polymer to a flat surface was promoted by stiffer polymers, smaller crowding particles, and larger volume fractions of crowders. The transition from non-adsorbed to adsorbed states was facilitated by an increase in bending stiffness, and a sharper transition occurred with small changes in crowding for stiffer polymers.

In our studies in chapters 2 & 3, we only focused on the role of monodisperse spherical crowders on polymer-polymer and polymer-wall interactions. In contrast, cellular environment has crowding molecules that span from globular proteins and ribosomes to proteins with highly assymetric shapes and intrinsically disordered proteins. Hence, it would be interesting to study how polydispersity in crowder shapes and sizes would affect depletion interactions between polymers and between a polymer and a wall. In addition, there are proteins in the cellular environment that can act as DNA-bending proteins. It would be interesting to study how the DNA-bending proteins modulate bending stiffness of a polymer and in turn what role that would play on crowding-induced polymer-wall interactions. Depending on whether the DNA-bending proteins associate with the DNA in a sequence specific way or in a non-specific manner, different local stiffness effects are likely to be observed. Computer simulations can be utilized to address the role of DNA-bending proteins on intra-polymer, polymer-polymer and polymer-wall interactions in a crowded environment.

Crowding in cells has been implicated in many cellular processes such as gene expression bursting. It is difficult to study the role of crowding on these processes in live cells due to the inherent difficulty in modulating crowding in live cells. Due to their open nature and ability to manipulate physical environments, cell-free protein synthesis (CFPS) systems are being used to study gene expression. A major limitation of the cell-free paradigm in studying cellular behavior is the inability to control spatial organization of gene expression components in synthetic systems. We used computational modeling to guide the design of a cell-free experimental platform capable of spatially organizing DNA and ribosomes akin to a prokaryotic cell. We carried out Langevin dynamics simulations of a coarse-grained DNA plasmid and crowder Ficoll-70 to show that crowding-induced depletion interactions could lead to adsorption of the DNA plasmid to the confining surface. Experimentally, we observed that the DNA is uniformly distributed throughout the vesicle at low crowding but localized near the vesicle walls at high crowding. In contrast, the ribosomes remained uniformly distributed at all crowding levels creating spatial segregation of DNA and ribosomes at high crowding. We further analyzed the effects of this spatial segregation on protein abundance, by using a two-compartment reaction kinetics model. We observed that the segregation of DNA and ribosomes along with altered diffusion lead to a decrease in protein abundance, consistent with the experimental observations. Our work sheds light on the role of spatial organization and resource availability on gene expression.

The design of an artificial cell has been a long-standing goal of the synthetic biology community. The ability to control the production and the spatial organization of desired protein product in an artificial cell would be a huge engineering feat. As one of the initial steps in that direction, our work here provides an experimental platform with the ability to control the spatial organization of gene expression. It is quite exciting to speculate on the more advanced cell-free platforms that can be created by building on our work. These advanced cell-free systems can either take inspiration from the natural world and mimic For instance, future works can study

the role of spatial segregation of two plasmid species by using crowding to spatially organize one plasmid species near the vesicle membrane while the other species can remain uniformly distributed throughout the vesicle. Our results in Chapter 3 show that crowding-induced adsorption to a confining surface is dependent on the bending stiffness of the polymer and hence the two plasmid species might be spatially segregated by changing the bending stiffness of one of the plasmid species (for example, by subjecting it to DNA-bending proteins such as HP1).

We also studied the role of crowding on gene expression noise by using a computational model to understand CFPS experiments carried out in 15μL reaction volumes. We developed a phenomeonological model to understand how crowding in cell-free systems affects gene expression noise. We observed that the crowding-induced spatial correlations and altered diffusion affected gene expression noise, with the exclusion and colocalization of translation factors leading to an increase in gene expression noise. The exclusion of reactants due to crowding lead to a decrease in burst frequency while rapid rebinding due to colocalization of reactants lead to an increase in burst size. Thus, cell-free platforms in combination with computational simulations can help to understand the role of crowding on gene expression kinetics and noise in cells.

In conclusion, work in this thesis would help to understand the role of crowding on the cellular and cell-free organization as well as understanding gene expression kinetics in cells.

Bibliography

[1] Remco Tuinier and Henk NW Lekkerkerker. *Colloids and the Depletion Interaction*. Springer Netherlands, 2011. xi, 6, 7, 9, 10, 11, 42

[2] R John Ellis. Macromolecular crowding: an important but neglected aspect of the intracellular environment. *Curr. Opin. Struct. Biol.*, 11(1):114–119, 2001. 1, 16, 42

[3] Huan-Xiang Zhou, Germán Rivas, and Allen P Minton. Macromolecular crowding and confinement: biochemical, biophysical, and potential physiological consequences. *Annu. Rev. Biophys.*, 37:375–397, 2008. 2, 3, 16, 42

[4] Steven B Zimmerman and Stefan O Trach. Estimation of macromolecule concentrations and excluded volume effects for the cytoplasm of escherichia coli. *Journal of molecular biology*, 222(3):599–620, 1991. 1

[5] Ron Milo and Rob Phillips. *Cell biology by the numbers*. Garland Science, 2015. 1

[6] Hans Bremer and Patrick P Dennis. Modulation of chemical composition and other parameters of the cell at different exponential growth rates. *EcoSal Plus*, 3(1), 2008. 1

[7] Morgan Delarue, Gregory P Brittingham, Stefan Pfeffer, IV Surovtsev, S Pinglay, KJ Kennedy, M Schaffer, JI Gutierrez, D Sang, G Poterewicz,

et al. mtorc1 controls phase separation and the biophysical properties of the cytoplasm by tuning crowding. *Cell*, 174(2):338–349, 2018. 1, 2, 3, 16, 39, 42

[8] Jacek T Mika and Bert Poolman. Macromolecule diffusion and confinement in prokaryotic cells. *Current opinion in biotechnology*, 22(1):117–126, 2011. 1

[9] R Swaminathan, Cathy P Hoang, and AS Verkman. Photobleaching recovery and anisotropy decay of green fluorescent protein gfp-s65t in solution and cells: cytoplasmic viscosity probed by green fluorescent protein translational and rotational diffusion. *Biophysical journal*, 72(4):1900–1907, 1997. 1

[10] Jonas Van Den Berg, Arnold J Boersma, and Bert Poolman. Microorganisms maintain crowding homeostasis. *Nature Reviews Microbiology*, 15(5):309–318, 2017. 1

[11] Daiki Shibata, Shinji Kajimoto, and Takakazu Nakabayashi. Label-free tracking of intracellular molecular crowding with cell-cycle progression using raman microscopy. *Chemical Physics Letters*, page 138843, 2021. 1

[12] Davide Marenduzzo, Cristian Micheletti, and Peter R Cook. Entropy-driven genome organization. *Biophys. J.*, 90(10):3712–3721, 2006. 2, 42

[13] James Pelletier, Ken Halvorsen, Bae-Yeun Ha, Raffaella Paparcone, Steven J Sandler, Conrad L Woldringh, Wesley P Wong, and Suckjoon Jun. Physical manipulation of the escherichia coli chromosome reveals its soft nature. *Proc. Natl. Acad. Sci. U.S.A.*, 109(40):E2649–E2656, 2012. 2, 16, 71

[14] Omar L Kantidze and Sergey V Razin. Weak interactions in higher-order chromatin organization. *Nucleic Acids Res.*, 48(9):4614–4626, 2020.

[15] Chanil Jeon, Youngkyun Jung, and Bae-Yeun Ha. A ring-polymer model shows how macromolecular crowding controls chromosome-arm organization in escherichia coli. *Sci. Rep.*, 7(1):1–10, 2017. 2, 14, 16, 17, 42

[16] Argyris Papantonis and Peter R Cook. Transcription factories: genome organization and gene regulation. *Chem. Rev.*, 113(11):8683–8705, 2013. 2, 42

[17] Davide Marenduzzo, Kieran Finan, and Peter R Cook. The depletion attraction: an underappreciated force driving cellular organization. *J. Cell. Biol.*, 175(5): 681–686, 2006. 2, 3, 16, 39, 42, 43, 71

[18] Margaret S Cheung, Dmitri Klimov, and D Thirumalai. Molecular crowding enhances native state stability and refolding rates of globular proteins. *Proc. Natl. Acad. Sci. U.S.A.*, 102(13):4753–4758, 2005. 2, 16

[19] Noga Kozer, Yosef Yehuda Kuttner, Gilad Haran, and Gideon Schreiber. Protein-protein association in polymer solutions: from dilute to semidilute to concentrated. *Biophys. J.*, 92(6):2139–2149, 2007. 2, 16

[20] Yu-Ling Zhou, Jun-Ming Liao, Jie Chen, and Yi Liang. Macromolecular crowding enhances the binding of superoxide dismutase to xanthine oxidase: implications for protein–protein interactions in intracellular environments. *Int. J. Biochem. Cell Biol.*, 38(11):1986–1994, 2006. 2, 16

[21] Warren M Mardoum, Stephanie M Gorczyca, Kathryn E Regan, Tsai-Chin Wu, and Rae M Robertson-Anderson. Crowding induces entropically-driven changes to dna dynamics that depend on crowder structure and ionic conditions. *Frontiers in physics*, 6:53, 2018. 2, 68

[22] LS Lerman. A transition to a compact form of dna in polymer solutions. *Proc. Natl. Acad. Sci. U.S.A.*, 68(8):1886–1890, 1971. 17

[23] Amar Nath Gupta and Johan RC van der Maarel. Compaction of plasmid dna by macromolecular crowding. *Macromolecules*, 50(4):1666–1671, 2017. 2, 17

[24] Anatoly Zinchenko, Qinming Chen, Nikolay V Berezhnoy, Sai Wang, and Lars Nordenskiöld. Compaction and self-association of megabase-sized chromatin

are induced by anionic protein crowding. *Soft matter*, 16(18):4366–4372, 2020. 2

[25] David Pastré, Loïc Hamon, Alain Mechulam, Isabelle Sorel, Sonia Baconnais, Patrick A Curmi, Eric Le Cam, and Olivier Piétrement. Atomic force microscopy imaging of dna under macromolecular crowding conditions. *Biomacromolecules*, 8(12):3712–3717, 2007. 2, 17

[26] Ronald Hancock. Self-association of polynucleosome chains by macromolecular crowding. *Eur. Biophys. J.*, 37(6):1059–1064, 2008. 2, 17

[27] AWC Lau, A Prasad, and Z Dogic. Condensation of isolated semi-flexible filaments driven by depletion interactions. *Europhys. Lett.*, 87(4):48006, 2009. 2, 43

[28] Martijn S Luijsterburg, Malcolm F White, Roel van Driel, and Remus Th Dame. The major architects of chromatin: architectural proteins in bacteria, archaea and eukaryotes. *Critical reviews in biochemistry and molecular biology*, 43(6): 393–418, 2008. 2

[29] Tyler N Shendruk, Martin Bertrand, Hendrick W de Haan, James L Harden, and Gary W Slater. Simulating the entropic collapse of coarse-grained chromosomes. *Biophys. J.*, 108(4):810–820, 2015. 2, 13, 17, 39, 43

[30] Sónia Cunha, Conrad L Woldringh, and Theo Odijk. Polymer-mediated compaction and internal dynamics of isolated escherichia coli nucleoids. *Journal of structural biology*, 136(1):53–66, 2001. 2

[31] Theo Odijk. Osmotic compaction of supercoiled dna into a bacterial nucleoid. *Biophysical chemistry*, 73(1-2):23–29, 1998. 2

[32] Suckjoon Jun. Chromosome, cell cycle, and entropy. *Biophysical journal*, 108 (4):785, 2015. 2, 89

[33] Pilong Li, Sudeep Banjade, Hui-Chun Cheng, Soyeon Kim, Baoyu Chen, Liang Guo, Marc Llaguno, Javoris V Hollingsworth, David S King, Salman F Banani, et al. Phase transitions in the assembly of multivalent signalling proteins. *Nature*, 483(7389):336, 2012. 3

[34] Amandine Molliex, Jamshid Temirov, Jihun Lee, Maura Coughlin, Anderson P Kanagaraj, Hong Joo Kim, Tanja Mittag, and J Paul Taylor. Phase separation by low complexity domains promotes stress granule assembly and drives pathological fibrillization. *Cell*, 163(1):123–133, 2015. 3

[35] Simon Alberti and Serena Carra. Quality control of membraneless organelles. *Journal of molecular biology*, 430(23):4711–4729, 2018. 3

[36] Jeffrey B Woodruff, Beatriz Ferreira Gomes, Per O Widlund, Julia Mahamid, Alf Honigmann, and Anthony A Hyman. The centrosome is a selective condensate that nucleates microtubules by concentrating tubulin. *Cell*, 169 (6):1066–1077, 2017. 3

[37] Taranpreet Kaur, Ibraheem Alshareedah, Wei Wang, Jason Ngo, Mahdi Muhammad Moosa, and Priya R Banerjee. Molecular crowding tunes material states of ribonucleoprotein condensates. *Biomolecules*, 9(2):71, 2019. 3, 16, 39, 42

[38] Sarah Elizabeth Norred, Rosemary M Dabbs, Gaurav Chauhan, Patrick M Caveney, Charles Patrick Collier, Steven M Abel, and Michael L Simpson. Synergistic interactions between confinement and macromolecular crowding spatially order transcription and translation in cell-free expression. *bioRxiv*, page 445544, 2018. 3, 18, 39, 41, 43

[39] Nupur Biswas, Masatoshi Ichikawa, Alokmay Datta, Yuko T Sato, Miho Yanagisawa, and Kenichi Yoshikawa. Phase separation in crowded microspheroids: Dna–peg system. *Chem. Phys. Lett.*, 539:157–162, 2012. 3, 18, 43

[40] David Welch, MP Lettinga, Marisol Ripoll, Zvonimir Dogic, and Gerard A Vliegenthart. Trains, tails and loops of partially adsorbed semi-flexible filaments. *Soft matter*, 11(38):7507–7514, 2015. 3, 10, 15, 43, 44, 47, 51, 67

[41] Travis Hoppe and Allen P Minton. An equilibrium model for the combined effect of macromolecular crowding and surface adsorption on the formation of linear protein fibrils. *Biophys. J.*, 108(4):957–966, 2015. 3, 43

[42] Allen P Minton. The cumulative effect of surface adsorption and excluded volume in 2D and 3D on protein fibrillation. *Biophys. J.*, 117(9):1666–1673, 2019. 3, 43

[43] Todd P Silverstein and Kristin Slade. Effects of macromolecular crowding on biochemical systems. *Journal of Chemical Education*, 96(11):2476–2487, 2019. 3

[44] Emmanuel Dauty and AS Verkman. Molecular crowding reduces to a similar extent the diffusion of small solutes and macromolecules: measurement by fluorescence correlation spectroscopy. *Journal of molecular recognition*, 17(5): 441–447, 2004. 3, 76

[45] Mahesh A Vibhute, Mark H Schaap, Roel JM Maas, Frank HT Nelissen, Evan Spruijt, Hans A Heus, Maike MK Hansen, and Wilhelm TS Huck. Transcription and translation in cytomimetic protocells perform most efficiently at distinct macromolecular crowding conditions. *ACS synthetic biology*, 9(10):2797–2807, 2020. 4, 79

[46] Hiroaki Matsuda, Gregory Garbes Putzel, Vadim Backman, and Igal Szleifer. Macromolecular crowding as a regulator of gene transcription. *Biophysical journal*, 106(8):1801–1810, 2014. 4

[47] Maike MK Hansen, Lenny HH Meijer, Evan Spruijt, Roel JM Maas, Marta Ventosa Rosquelles, Joost Groen, Hans A Heus, and Wilhelm TS Huck. Macromolecular crowding creates heterogeneous environments of gene expression in picolitre droplets. *Nat. Nanotechnol.*, 11(2):191, 2016. 4, 18, 39, 41, 71, 80

[48] Sho Asakura and Fumio Oosawa. On interaction between two bodies immersed in a solution of macromolecules. *J. Chem. Phys.*, 22(7):1255–1256, 1954. 5, 42, 58, 67

[49] Kurt Binder, Peter Virnau, and Antonia Statt. Perspective: The Asakura Oosawa model: A colloid prototype for bulk and interfacial phase behavior. *J. Chem. Phys.*, 141(14):559, 2014. 10, 42

[50] Kevin J Mutch, Jeroen S van Duijneveldt, and Julian Eastoe. Colloid–polymer mixtures in the protein limit. *Soft Matter*, 3(2):155–167, 2007. 10

[51] Manolis Doxastakis, Y-L Chen, and Juan José de Pablo. Potential of mean force between two nanometer-scale particles in a polymer solution. *The Journal of chemical physics*, 123(3):034901, 2005. 10

[52] Peter G Bolhuis, Evert Jan Meijer, and Ard A Louis. Colloid-polymer mixtures in the protein limit. *Physical review letters*, 90(6):068304, 2003. 10

[53] Wei Kang Lim and Alan R Denton. Polymer crowding and shape distributions in polymer-nanoparticle mixtures. *J. Chem. Phys.*, 141(11):114909, 2014. 39

[54] Wei Kang Lim and Alan R Denton. Influence of polymer shape on depletion potentials and crowding in colloid–polymer mixtures. *Soft Matter*, 12(8):2247–2252, 2016. 10

[55] Margaret S Cheung. Where soft matter meets living matter—protein structure, stability, and folding in the cell. *Current opinion in structural biology*, 23(2): 212–217, 2013. 10

[56] Harold P Erickson. Size and shape of protein molecules at the nanometer level determined by sedimentation, gel filtration, and electron microscopy. *Biological procedures online*, 11(1):32–51, 2009. 10

[57] Liang Dai, Jeremy J Jones, Johan RC van der Maarel, and Patrick S Doyle. A systematic study of DNA conformation in slitlike confinement. *Soft Matter*, 8 (10):2972–2982, 2012. 10, 47

[58] Liang Dai, C Benjamin Renner, and Patrick S Doyle. The polymer physics of single dna confined in nanochannels. *Advances in colloid and interface science*, 232:80–100, 2016. 10

[59] Jonathan K Armstrong, Rosalinda B Wenby, Herbert J Meiselman, and Timothy C Fisher. The hydrodynamic radii of macromolecules and their effect on red blood cell aggregation. *Biophys. J.*, 87(6):4259–4270, 2004. 10, 47

[60] Steve Plimpton, A Thompson, P Crozier, and A Kohlmeyer. Lammps molecular dynamics simulator. *URL http://lammps. sandia. gov*, 2011. 12, 20, 47

[61] Hongsuk Kang, Philip A Pincus, Changbong Hyeon, and D Thirumalai. Effects of macromolecular crowding on the collapse of biopolymers. *Phys. Rev. Lett.*, 114(6):068303, 2015. 13, 17, 27, 39, 43, 50, 54

[62] Anpu Chen and Nanrong Zhao. Comparative study of the crowding-induced collapse effect in hard-sphere, flexible polymer and rod-like polymer systems. *Phys. Chem. Chem. Phys.*, 21(23):12335–12345, 2019. 13, 17, 68

[63] Youngkyun Jung and Bae-Yeun Ha. Collapse transition of a heterogeneous polymer in a crowded medium. *The Journal of Chemical Physics*, 155(5):054902, 2021. 13

[64] Hongsuk Kang, Ngo Minh Toan, Changbong Hyeon, and D Thirumalai. Unexpected swelling of stiff DNA in a polydisperse crowded environment. *J. Am. Chem. Soc.*, 137(34):10970–10978, 2015. 14, 17, 43, 68

[65] PG De Gennes. Polymers at an interface; a simplified view. *Adv. Colloid Interface Sci.*, 27(3-4):189–209, 1987. 14, 43

[66] Roland R Netz and David Andelman. Neutral and charged polymers at interfaces. *Phys. Rep.*, 380(1-2):1–95, 2003.

[67] Jörg Baschnagel, Hendrik Meyer, Joachim Wittmer, Igor Kulić, Hervé Mohrbach, Falko Ziebert, Gi-Moon Nam, Nam-Kyung Lee, and Albert Johner. Semiflexible chains at surfaces: Worm-like chains and beyond. *Polymers*, 8(8): 286, 2016. 14, 43

[68] Juin Kim, Chanil Jeon, Hawoong Jeong, Youngkyun Jung, and Bae-Yeun Ha. A polymer in a crowded and confined space: effects of crowder size and polydispersity. *Soft Matter*, 11(10):1877–1888, 2015. 14, 17

[69] Andrey Milchev and Kurt Binder. Linear dimensions of adsorbed semiflexible polymers: What can be learned about their persistence length? *Phys. Rev. Lett.*, 123(12):128003, 2019. 15, 43, 44, 58, 67

[70] Chwen-Yang Shew and Kenichi Yoshikawa. A toy model for nucleus-sized crowding confinement. *J. Phys. Condens. Matter*, 27(6):064118, 2015. 14, 17

[71] Robert Simha, HL Frisch, and FR Eirich. The adsorption of flexible macromolecules. *J. Phys. Chem.*, 57(6):584–589, 1953. 14, 43

[72] Andrey Milchev and Kurt Binder. Static and dynamic properties of adsorbed chains at surfaces: Monte carlo simulation of a bead-spring model. *Macromolecules*, 29(1):343–354, 1996.

[73] E Eisenriegler, K Kremer, and K Binder. Adsorption of polymer chains at surfaces: Scaling and monte carlo analyses. *J. Chem. Phys.*, 77(12):6296–6320, 1982. 14, 43

[74] Tomàs Sintes, K Sumithra, and E Straube. Adsorption of semiflexible polymers on flat, homogeneous surfaces. *Macromolecules*, 34(5):1352–1357, 2001. 15, 44, 67

[75] J Kierfeld. Force-induced desorption and unzipping of semiflexible polymers. *Phys. Rev. Lett.*, 97(5):058302, 2006.

[76] Jan Kierfeld and Reinhard Lipowsky. Unbundling and desorption of semiflexible polymers. *Europhys. Lett.*, 62(2):285, 2003. 15, 44

[77] Tyler N Shendruk, Martin Bertrand, James L Harden, Gary W Slater, and Hendrick W de Haan. Coarse-grained molecular dynamics simulations of depletion-induced interactions for soft matter systems. *J. Chem. Phys.*, 141 (24):244910, 2014. 15, 58, 68

[78] Sho Asakura and Fumio Oosawa. Interaction between particles suspended in solutions of macromolecules. *J. Polym. Sci.*, 33(126):183–192, 1958. 16

[79] Pinaki Swain, Bela M Mulder, and Debasish Chaudhuri. Confinement and crowding control the morphology and dynamics of a model bacterial chromosome. *Soft Matter*, 15(12):2677–2687, 2019. 16

[80] Ronald Hancock. Structure of metaphase chromosomes: a role for effects of macromolecular crowding. *PLOS One*, 7(4):e36045, 2012. 16

[81] Ce Zhang, Pei Ge Shao, Jeroen A van Kan, and Johan RC van der Maarel. Macromolecular crowding induced elongation and compaction of single dna molecules confined in a nanochannel. *Proc. Natl. Acad. Sci. U.S.A.*, 106(39): 16651–16656, 2009. 17

[82] Jaeoh Shin, Andrey G Cherstvy, and Ralf Metzler. Mixing and segregation of ring polymers: spatial confinement and molecular crowding effects. *New J. Phys.*, 16(5):053047, 2014. 17

[83] Adam D Silverman, Ashty S Karim, and Michael C Jewett. Cell-free gene expression: an expanded repertoire of applications. *Nat. Rev. Genet.*, pages 1–20, 2019. 17

[84] S Elizabeth Norred, Patrick M Caveney, Gaurav Chauhan, Lauren K Collier, C Patrick Collier, Steven M Abel, and Michael L Simpson. Macromolecular crowding induces spatial correlations that control gene expression bursting patterns. *ACS Synth. Biol.*, 7(5):1251–1258, 2018. 18, 39, 41, 42, 71, 79, 80

[85] Robert Byron Bird, Robert Calvin Armstrong, and Ole Hassager. *Dynamics of polymeric liquids. Vol. 1: Fluid mechanics*. Wiley, 1987. 18

[86] John D Weeks, David Chandler, and Hans C Andersen. Role of repulsive forces in determining the equilibrium structure of simple liquids. *J. Chem. Phys.*, 54 (12):5237–5247, 1971. 19, 46

[87] William Arthur Steele. *The interaction of gases with solid surfaces*, volume 3. Pergamon, 1974. 19

[88] Steve Plimpton. Fast parallel algorithms for short-range molecular dynamics. Technical report, Sandia National Labs., Albuquerque, NM (United States), 1993. 20, 47

[89] Alexander Stukowski. Visualization and analysis of atomistic simulation data with ovito–the open visualization tool. *Model. Simul. Mater. Sci. Eng.*, 18(1): 015012, 2009. 20, 47

[90] Giacomo Fiorin, Michael L Klein, and Jérôme Hénin. Using collective variables to drive molecular dynamics simulations. *Mol. Phys.*, 111(22-23):3345–3362, 2013. 20

[91] Shankar Kumar, John M Rosenberg, Djamal Bouzida, Robert H Swendsen, and Peter A Kollman. Multidimensional free-energy calculations using the weighted histogram analysis method. *J. Comput. Chem.*, 16(11):1339–1350, 1995. 20

[92] Alan Grossfield. Wham: the weighted histogram analysis method, version 2.0.10. *"WHAM: an implementation of the weighted histogram analysis method", http://membrane.urmc.rochester.edu/content/wham. Accessed July*, 2020. 20, 25

[93] Daniel Trzesniak, Anna-Pitschna E Kunz, and Wilfred F van Gunsteren. A comparison of methods to compute the potential of mean force. *ChemPhysChem*, 8(1):162–169, 2007. 20

[94] Handan Arkın and Wolfhard Janke. Gyration tensor based analysis of the shapes of polymer chains in an attractive spherical cage. *J. Chem. Phys.*, 138 (5):054904, 2013. 27

[95] Bing Li and Steven M. Abel. Shaping membrane vesicles by adsorption of a semiflexible polymer. *Soft Matter*, 14:185–193, 2018. 27, 44, 68

[96] Arturo Narros, Angel J Moreno, and Christos N Likos. Influence of topology on effective potentials: coarse-graining ring polymers. *Soft Matter*, 6(11):2435–2441, 2010. 27

[97] Iurii Chubak, Emanuele Locatelli, and Christos N Likos. Ring polymers are much stronger depleting agents than linear ones. *Mol. Phys.*, 116(21-22):2911–2926, 2018. 35

[98] Da Yang, Jaana Männik, Scott T Retterer, and Jaan Männik. The effects of polydisperse crowders on the compaction of the escherichia coli nucleoid. *Mol. Microbiol.*, 113(5):1022–1037, 2020. 39

[99] Lisa M Dominak and Christine D Keating. Macromolecular crowding improves polymer encapsulation within giant lipid vesicles. *Langmuir*, 24(23):13565–13571, 2008. 39

[100] Anthony A Hyman, Christoph A Weber, and Frank Jülicher. Liquid-liquid phase separation in biology. *Annu. Rev. Cell Dev. Biol.*, 30:39–58, 2014. 40

[101] Akihiko Tsuji and Kenichi Yoshikawa. On- off switching of transcriptional activity of large dna through a conformational transition in cooperation with phospholipid membrane. *J. Am. Chem. Soc.*, 132(35):12464–12471, 2010. 40, 88

[102] Gaurav Chauhan, Michael L Simpson, and Steven M Abel. Crowding-induced interactions of ring polymers. *Soft Matter*, 17(1):16–23, 2021. 43, 48, 50, 62, 73, 74

[103] Jian Jiang. Nonmonotonic adsorption behavior of semiflexible polymers. *J. Chem. Phys.*, 153(3):034902, 2020. 44, 67

[104] Tobias A Kampmann, Horst-Holger Boltz, and Jan Kierfeld. Controlling adsorption of semiflexible polymers on planar and curved substrates. *J. Chem. Phys.*, 139(3):034903, 2013. 44, 46

[105] Wei Chien and Yeng-Long Chen. Confinement, curvature, and attractive interaction effects on polymer surface adsorption. *J. Chem. Phys.*, 147(6): 064901, 2017.

[106] Xiaolin Zhou, Fuchen Guo, Ke Li, Linli He, and Linxi Zhang. Entropy-induced separation of binary semiflexible ring polymer mixtures in spherical confinement. *Polymers*, 11(12):1992, 2019. 44

[107] A Milchev and K Binder. How does stiffness of polymer chains affect their adsorption transition? *J. Chem. Phys.*, 152(6):064901, 2020. 44, 58

[108] AN Semenov. Adsorption of a semiflexible wormlike chain. *Eur. Phys. J. E.*, 9 (4):353–363, 2002. 44

[109] Theo Odijk. The statistics and dynamics of confined or entangled stiff polymers. *Macromolecules*, 16(8):1340–1344, 1983. 44

[110] Tobias A Kampmann and Jan Kierfeld. Adsorption of finite semiflexible polymers and their loop and tail distributions. *J. Chem. Phys.*, 147(1):014901, 2017. 44, 51, 56

[111] Jing-Zi Zhang, Xiang-Yao Peng, Shan Liu, Bang-Ping Jiang, Shi-Chen Ji, and Xing-Can Shen. The persistence length of semiflexible polymers in lattice Monte Carlo simulations. *Polymers*, 11(2):295, 2019. 46

[112] Petra Gutjahr, Reinhard Lipowsky, and Jan Kierfeld. Persistence length of semiflexible polymers and bending rigidity renormalization. *Europhys. Lett.*, 76 (6):994, 2006. 46

[113] Sina Mirzaeifard and Steven M Abel. Confined semiflexible polymers suppress fluctuations of soft membrane tubes. *Soft Matter*, 12(6):1783–1790, 2016. 60

[114] Somenath Bakshi, Albert Siryaporn, Mark Goulian, and James C Weisshaar. Superresolution imaging of ribosomes and rna polymerase in live escherichia coli cells. *Mol. Microbiol.*, 85(1):21–38, 2012. 70, 71

[115] Paula Montero Llopis, Audrey F Jackson, Oleksii Sliusarenko, Ivan Surovtsev, Jennifer Heinritz, Thierry Emonet, and Christine Jacobs-Wagner. Spatial organization of the flow of genetic information in bacteria. *Nature*, 466(7302): 77, 2010. 71

[116] Mathew Stracy, Christian Lesterlin, Federico Garza De Leon, Stephan Uphoff, Pawel Zawadzki, and Achillefs N Kapanidis. Live-cell superresolution microscopy reveals the organization of rna polymerase in the bacterial nucleoid. *Proc. Natl. Acad. Sci. U.S.A.*, 112(32):E4390–E4399, 2015. 70, 71

[117] Maike MK Hansen, Sabine Paffenholz, David Foschepoth, Hans A Heus, Julian Thiele, and Wilhelm TS Huck. Cell-like nanostructured environments alter diffusion and reaction kinetics in cell-free gene expression. *ChemBioChem*, 17 (3):228–232, 2016. 71

[118] Gaurav Chauhan, Michael L. Simpson, and Steven M. Abel. Adsorption of semiflexible polymers in crowded environments. *The Journal of Chemical Physics*, 155(3):034904, 2021. doi: 10.1063/5.0054797. URL https://doi.org/10.1063/5.0054797. 73, 74

[119] Adedayo A Fodeke and Allen P Minton. Quantitative characterization of polymer- polymer, protein- protein, and polymer- protein interaction via tracer sedimentation equilibrium. *The Journal of Physical Chemistry B*, 114(33): 10876–10880, 2010. 73, 83

[120] Peter N Lavrenko, Olga I Mikriukova, and Olga V Okatova. On the separation ability of various ficoll gradient solutions in zonal centrifugation. *Analytical biochemistry*, 166(2):287–297, 1987. 73, 83

[121] Kazuya Nishimura, Saburo Tsuru, Hiroaki Suzuki, and Tetsuya Yomo. Stochasticity in gene expression in a cell-sized compartment. *ACS synthetic biology*, 4(5):566–576, 2015. 74, 79, 84

[122] Pauline van Nies, Zohreh Nourian, Maurits Kok, Roeland van Wijk, Jonne Moeskops, Ilja Westerlaken, Jos M Poolman, Rienk Eelkema, Jan H van Esch, Yutetsu Kuruma, et al. Unbiased tracking of the progression of mrna and

protein synthesis in bulk and in liposome-confined reactions. *ChemBioChem*, 14(15):1963–1966, 2013. 79

[123] Georgios Pothoulakis, Francesca Ceroni, Benjamin Reeve, and Tom Ellis. The spinach rna aptamer as a characterization tool for synthetic biology. *ACS synthetic biology*, 3(3):182–187, 2014. 84

[124] Georgios Pothoulakis and Tom Ellis. Using spinach aptamer to correlate mrna and protein levels in escherichia coli. *Methods in enzymology*, 550:173–185, 2015. 79, 84

[125] Rita L Strack, Matthew D Disney, and Samie R Jaffrey. A superfolding spinach2 reveals the dynamic nature of trinucleotide repeat–containing rna. *Nature methods*, 10(12):1219–1224, 2013. 79

[126] Elke Hebisch, Johannes Knebel, Janek Landsberg, Erwin Frey, and Madeleine Leisner. High variation of fluorescence protein maturation times in closely related escherichia coli strains. *PloS one*, 8(10):e75991, 2013. 79

[127] Koji Nishimura, Tomoaki Matsuura, Kazuya Nishimura, Takeshi Sunami, Hiroaki Suzuki, and Tetsuya Yomo. Cell-free protein synthesis inside giant unilamellar vesicles analyzed by flow cytometry. *Langmuir*, 28(22):8426–8432, 2012. 80

[128] Aidan Tinafar, Katariina Jaenes, and Keith Pardee. Synthetic biology goes cell-free. *BMC biology*, 17(1):1–14, 2019. 80

[129] Yoshihiro Shimizu, Akio Inoue, Yukihide Tomari, Tsutomu Suzuki, Takashi Yokogawa, Kazuya Nishikawa, and Takuya Ueda. Cell-free translation reconstituted with purified components. *Nature biotechnology*, 19(8):751–755, 2001. 85

[130] Yoshihiro Shimizu, Takashi Kanamori, and Takuya Ueda. Protein synthesis by pure translation systems. *Methods*, 36(3):299–304, 2005. 85

[131] Frederick Gittes, Brian Mickey, Jilda Nettleton, and Jonathon Howard. Flexural rigidity of microtubules and actin filaments measured from thermal fluctuations in shape. *J. Cell. Biol.*, 120(4):923–934, 1993. 89

Vita

Gaurav Chauhan was born and brought up in Haridwar, Uttarakhand in the foothills of the mighty Himalayas. After graduating from St. Mary's Sr. Secondary school, he graduated with a Bachelor of Technology (B.Tech.) degree from the Indian Institute of Technology (IIT) Dhanbad in 2015. He briefly worked in the research group of Prof. Prateek Jha at the Indian Institute of Technology Roorkee in 2015 before joining the doctoral program in the Department of Chemical and Biomolecular Engineering at the University of Tennessee Knoxville. He graduated with a PhD in Chemical and Biomolecular Engineering in December 2021. His doctoral research focused on studying the effects of crowding on spatial organization of biopolymers and the resultant effect on gene expression.